SYNTHESIS AND CHARACTERIZATION OF RESPONSIVE NANOPOROUS MATERIALS

by

Alexis Elizabeth Abelow

A dissertation submitted to the faculty of
The University of Utah
in partial fulfillment of the requirements for the degree of

Doctor of Philosophy

Department of Chemistry

The University of Utah

December 2011

The University of Utah Graduate School

STATEMENT OF DISSERTATION APPROVAL

The dissertation of **Alexis Elizabeth Abelow**

has been approved by the following supervisory committee members:

Ilya Zharov	, Chair	**8-22-2011** Date Approved
Jon D. Rainier	, Member	**8-22-2011** Date Approved
Peter J. Stang	, Member	**8-22-2011** Date Approved
Jennifer Shumaker-Parry	, Member	Date Approved
Patrick F. Kiser	, Member	Date Approved

and by **Henry S. White**, Chair of the Department of **Chemistry**

and by Charles A. Wight, Dean of The Graduate School.

ABSTRACT

This thesis describes the synthesis and properties of polymer or oligonucleotide-modified nanoporous membranes and nanopores which exhibit a response to external stimuli, synthesized with the intention of mimicking biological protein channels. The responsiveness of these systems arises as a function of the polymer or oligonucleotide modifier, which exhibit a change in conformation with exposure to temperature, pH, introduction of a small molecule, or electric potential.

First, the transport of ions through supported silica colloidal films modified with poly(L-alanine) on platinum electrodes was studied using cyclic voltammetry. By monitoring the flux of a redox species through the polymer-modified colloidal film it is demonstrated that the polymer expands and contracts when the temperature was increased and decreased, respectively. We also observed an expansion and contraction as the pH was increased and decreased, respectively. Transport of a neutral dye molecule through free-standing silica colloidal films modified with poly(L-alanine) was also studied. As noted previously, the polymer expands and contracts as the pH is increased and decreased, respectively.

Next, the transport was monitored through both silica colloidal film-modified Pt microelectrodes and Pt single nanopore electrodes as an oligonucleotide-based binder, or aptamer, was attached. The aptamer is

responsive to a small molecule, cocaine where, in the absence of cocaine, only one “arm” of the aptamer is folded in on itself, leaving the rest of the chain partially unfolded, blocking the nanopores. However, when the cocaine molecule is introduced into solution, the aptamer folds completely in on itself, forming a three-armed structure with the small molecule encapsulated in the middle. This change in conformation is monitored by observing the change in transport of a redox species through the pores as cocaine is introduced into the system. We observed an increase rate of transport as the aptamer bound to cocaine in both systems, consistent with previous reports of aptamer behavior.

Next, two types of electro-active polymers, polypyrrole (PPy) or poly(3,4-ethylene-dioxythiophene) (PEDOT), were vapor-phase polymerized onto the surface of a commercially available aluminum oxide nanoporous membrane, or Anodisc. These polymers expand in the reduced state and contract in the oxidized state to produce a responsive membrane.

TABLE OF CONTENTS

LIST OF FIGURES

LIST OF TABLES

LIST OF ABBREVIATIONS

µg, mg, g	Microgram, Milligram, Gram
µM, mM, M	Micromolar, Millimolar, Molar
µmol, mmol, mol	Micromole, Millimole, Mole
CH_3CN	Acetonitrile
NH_3	Ammonia
APTES	3-(Aminopropyl) triethoxysilane
ATRP	Atom Transfer Radical Polymerization
Boc	*Tert*-Butyl Carbonate
C	Concentration
$CDCl_3$	Deutrochloroform
CH_2Cl_2	Dichloromethane
Cl	Chlorine
DMSO	Dimethylsulfoxide
D	Diffusion Coefficient
D_{sol}	Diffusion Coefficient of the Diffusing Species in Solution
R_D	Diffusion Rate
DMF	N, N-Dimethylformamide
EtOH	Ethanol
Et_2O	Diethyl Ether
Et_3N	Triethylamine

eq.	Equivalents
F	Faraday's Constant
Fcc	Face Centered Cubic
Fc	Ferrocene
$Fc(CH_2OH)_2$	1, 1'-Ferrocenedimethanol
$FeCl_3$	Iron (III) Chloride
FeTs	Iron (III) Tosylate
h	Hour
H	Proton
H_20	Water
Hz	Hertz
i	Current
i_{lim}	Limiting Current
J	Flux
J_{opal}	Flux Through and Opal
KCl	Potassium Chloride
L	Membrane Thickness
MeOH	Methanol
min	Minute
MW	Molecular Weight
NaCl	Sodium Chloride
NMR	Nuclear Magnetic Resonnance
PPy	Polypyrrole
PEDOT	Poly(3,4-ethylene-dioxythiophene)
$Ru(NH_3)Cl_3$	Hexaammineruthenium (III) Chloride

$Ru(NH_3)_6^{3+}$	Hexaammineruthenium (III) Chloride
RAFT	Reversible Addition-Fragmentation Chain Transfer
RT	Room Temperature
SEM	Scanning Electron Microscopy
SiO_2	Silica
TEOS	Tetraethyl Orthosilicate
TGA	Thermogravimetric Analysis
UV	Ultraviolet
Vis	Visible
wt%	Weight Percent
δ	Chemical Shift
ΔC	Concentration Gradient
E	Void Fraction
τ	Tortuosity

ACKNOWLEDGMENTS

I wish to thank my advisor, Dr. Ilya Zharov, for his guidance and patience and for giving me a chance to work in his lab. I would also like to thank my co-workers who have been there through all of the late nights, difficult projects, and broken equipment. Best wishes to you all and thank you for keeping things light.

I would also like to express my heartfelt gratitude to my family for all of their love and support throughout my studies: My parents, Mary and Stephen Abelow, for all of their love and encouragement, and my brother, Nicholas, and my sister, Camille, for all of their support.

CHAPTER 1

INTRODUCTION

Background and Significance

Controlled transport of small molecules and ions through nanoporous films, membranes, and electrodes have gained interest in fundamental research and technology in recent years. [1,2,3] With these materials, molecular transport can be controlled at the nanoscale by controlling the nanopore size and surface functional groups as well as the number of nanopores in the system. The ability to easily control transport through the nanopores has great potential in the development of separation, controlled drug release, and sensing devices. Nanoporous materials focused on in this thesis range from having one single nanopore to multiple nanopores with pore sizes of less than 100 nm in diameter.

Nanoporous membranes have been synthesized and used in a variety of applications. These applications include separations of biomacromolecules[4] and drug molecules,[5] controlled release and drug delivery[6,7] and chemical sensors[8] and are based on the ability to control the molecular transport through the nanopores by modifying their surfaces with moieties that are capable of electrostatic[9] and noncovalent[10] interactions with the diffusing species.

Alternatively, selectivity can be achieved by modifying the nanopore surfaces with polymer molecules that respond to environmental stimuli.[11]

Many types of nanoporous membranes have been prepared using polymers,[12] carbon nanotubes,[13-15] zeolites,[16] and alumina.[17,18] These materials, however, have a number of limitations. The most significant include low molecular flux due to low porosity, and the inability to accurately control the pore size of the membrane. For this reason, we use silica colloidal crystals that possess high molecular flux and easily and accurately controllable nanopore size as well as surface chemistry that is facile and has been well developed.[19]

To study transport at the single nanopore, we employ single nanopore electrodes. These electrodes are advantageous in that their fabrication is simple and reproducible, molecular transport through the pore is easily monitored, and they are portable and mechanically robust.[20,21,22,23]

Diffusion through Nanoporous Membranes

For free-standing nanoporous membranes used in this thesis, the porous membrane is placed between a reservoir containing a solution of a probe molecule and a reservoir with pure solvent. The solute will diffuse from high concentration to low concentration through the membrane (diffusion is defined as a spontaneous process of movement of molecules from higher chemical potential to lower chemical potential where chemical potential is represented by a change in concentration).[24] The amount that flows through the unit area per unit time, or flux, through the membrane can thus be represented by Fick's Law.

$$-J = D\frac{dc_1}{dz} \tag{1.1}$$

Solving Fix's Law gives flux through a porous material to be:

$$J = \frac{D}{L}(c_a - c_b) \tag{1.2}$$

where *J* is the flux through a membrane, D is the diffusion coefficient of the solute, L is the thickness of the membrane, c_a is the concentration of feed solution and c_b is the concentration of the reservoir solution. In the diffusion measurements performed using this experimental set-up $c_a >> c_b$ so the equation can be written as:

$$J = \frac{\Delta C}{L}D \tag{1.3}$$

where ΔC is the concentration gradient or the concentration of the solute in the feed solution. Equation 1.3 is the basic flux equation used in this thesis to determine the diffusion rate of molecules.

This thesis will also focus on the diffusion through the nanopores in silica colloidal crystals. To describe the molecular flux in a colloidal crystal, geometric characteristics of the system have to be taken into account because the pores in the colloidal crystal are not cylindrical. Such geometrical characteristics include void fraction ε and tortuosity τ. Both ε and τ are the intrinsic properties of the colloidal crystals and 0.26 and 3.0, respectively.[25] The void fraction, ε, is the ratio of the volume taken up by air spaces (the voids) to the total volume of a material

in the colloidal membrane. Tortuosity, τ, is the path diffusing molecules take through the colloidal membrane. These values are independent of the size of the silica sphere and are the cause of the high molecular transport rate through the colloidal membrane compared to other membranes of the same thickness.[26]

The molecular flux, $J_{colloid}$ $(mol/cm^2 \cdot s)$, through a colloidal membrane is described by equation 1.4,[25]

$$J_{colloid} = \frac{\Delta C}{L} \cdot \frac{\varepsilon}{\tau} \cdot D_{sol} \tag{1.4}$$

where ΔC is the concentration gradient, L is the thickness of the membrane, ε is the void fraction, τ is the tortuosity and D_{sol} is the diffusion coefficient of the diffusing species in solution. As a result of having constant porosity regardless of the nanopore size, molecular transport through the colloidal crystal is significant even as the pore size is reduced to the nanoscale.

Nanoporous Membranes with Controlled Molecular Transport

Anodized Alumina

Anodized alumina is a widely used nanoporous material (Figure 1.1. a.). The formation of nanoporous alumina is performed by anodizing aluminum foil under a bias of 10-100 V in aqueous polyprotic acidic media.[27] This process produces highly ordered pores with columnar structure. Variation in the electrochemical and etching conditions provide control over the pore density and pore diameter, with available pore sizes between 10 and 200 nm. Porous

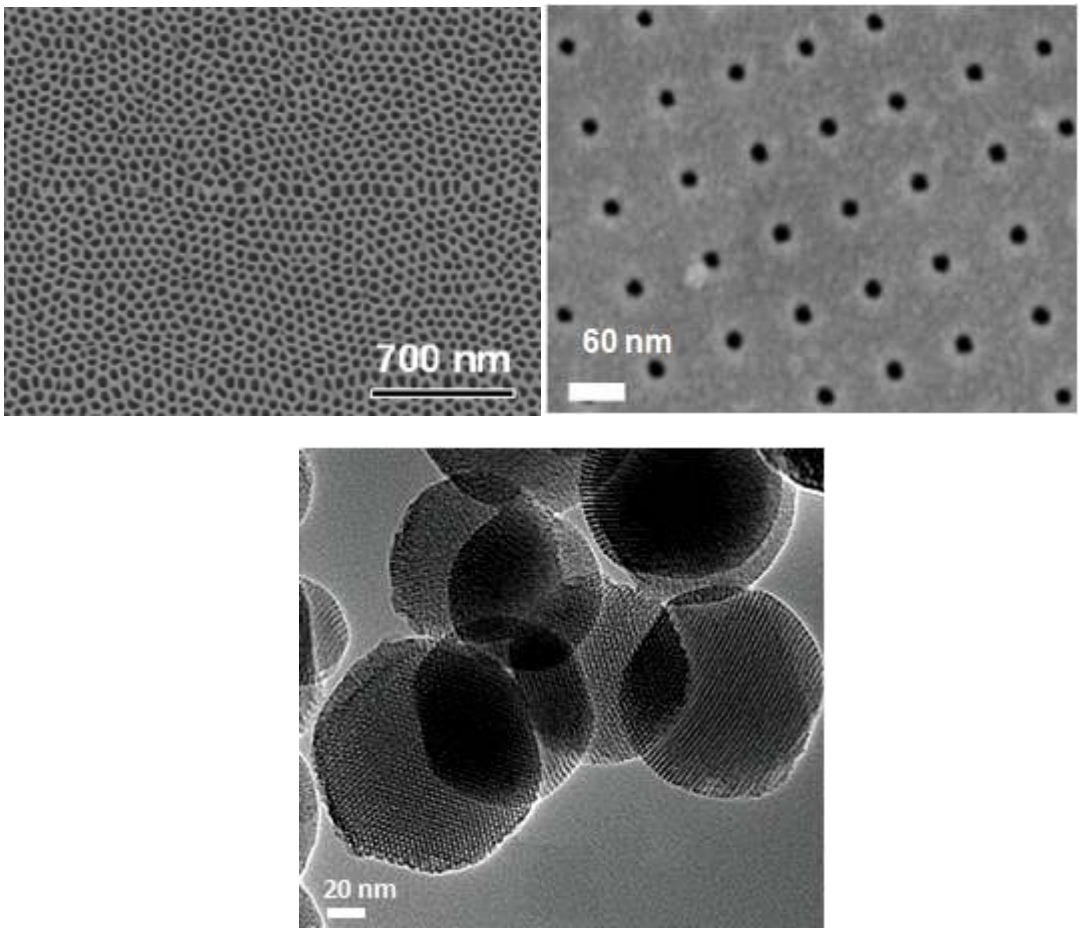

Figure 1.1. SEM images of conventional nanoporous materials: (A) anodized alumina; (B) silicon nitride; (C); mesoporous silica.

alumina has micron film thickness, resulting in long pores (longer than 60 μm in length), and low molecular flux through the membrane.

Molecular transport through nanoporous alumina has been controlled either by controlling the pore size or by chemical modification of the alumina surface.[28,29,30,31] For example, changing the pore size in alumina from 20 nm to 50 nm in diameter caused the transport rate for crystal violet to increase from 1 $\mu g \cdot day^{-1}$ to 3 $\mu g \cdot day^{-1}$.[27] The surface of alumina can be modified with siloxanes.[30,32,31] Siloxane modification is used to produce a membrane capable of enantioseperations as these siloxane-modified surfaces are further modified

with antibodies capable of selectively binding to a chiral enantiomer of the drug 4-[3-(4-fluorophenyl)-2-hydroxy-1- [1,2,4]triazol-1-yl-propyl]-benzonitrile, an inhibitor of aromatase enzyme activity to the surface of silane-modified alumina pores.[30]

Surface modification of Alumina anodisc membranes has also been used to produce a selectively permeable membrane useful in bioseparations. Membranes modified with an aminosilane are further modified with a glutaraldehyde linker that binds to the 5'-aminated DNA. This produces a membrane that will bind a specific target ss-DNA while allowing noncomplementary ss-DNA to pass through the membrane.[33] Another example demonstrates that surface modification with siloxanes and then PEG monolayers produces a membrane that shows a 50 % decrease in ovalbumin diffusivity compared to unmodified membranes, thus producing a selective membrane.[34]

Anodisc membranes have also been used as stimuli-responsive gates by pore gating using nanoparticles, electrically active polymers, and temperature responsive polymers. The first system has been demonstrated by Li and coworkers who were able to modify the surface of the anodisc with the amino acid cysteine. Cysteine has an isoelectric point of ~6.2, and is positively charged in acid and negatively charged in alkali. This polymer-modified membrane is then combined with negatively charged Au nanoparticles. When the solution is alkaline, the nanoparticles are repelled from the surface, opening the pores. When the system in acidic, the nanoparticles will be attracted to the surface, blocking the nanopores.[35] The second system, based on an electrically active

polymer was recently developed by Kim and coworkers and utilizes a nanoporous membrane, modified with a thin gold layer, and then polypyrrole doped with dodecylbenzenesulfonate anion (PPy/DBS) electropolymerized on the top of anodized aluminum oxide membrane. This polymer exhibits a volume change (up to 35 %) depending on the electrical state, with swelling (decrease of pore size, pore size 140 nm measured by AFM) upon reduction from the oxidized state (increase of pore size, pore size 190 nm measured by AFM). This allowed for a pulsatile release of a model drug (FITC-BSA) molecule.[36] The third study described utilizes a switchable membrane made from an anodized aluminum oxide membrane coated with a temperature responsive polymer, poly(N-isopropylacrylamide) (PNIPAM), which is in the extended state below the LCST (25º C) and the collapsed state above the LCST (40º C), effectively closing and opening the pores, respectively.[37,38]

The anodiscs used in this thesis are commercially available (Whatman) with a thickness of 60 μm and a pore diameter of 200 nm.

Silicon Nitride

Silicon nitride is another type of multipore nanoporous membrane (Figure 1.1.B). Nanopores are created in silicon nitride using microfabrication techniques, including photolithography and e-beam lithography on a membrane with a thickness of 20 - 50 nm. This allows for a high molecular flux through the membrane. Arrays of nanopores have been made in thin films of silicon nitride, but at this time, these membranes have not yet been used for selective

separations.[39] A single nanopore in silicon nitride has been used as a sensor for DNA and small molecules.[40,41] Recently, silicon nitride nanopores have been modified using siloxanes, similar to the chemistry used to modify anodized alumina.[42] Despite the impressive advances in the field of nanoporous membrane materials, silicon nitride for use as a membrane is still problematic. First, construction of all of these nanoporous membranes is expensive, time consuming, and requires specialized equipment, such as track-etching[43] or photolithography.[44] Second, these nanoporous membranes contain very long pores and/or low porosity. This results in slow molecular transport through such membranes, 10^{-12} mol·s^{-1}·cm^{-2},[45] and makes them impractical in separations and controlled transport applications. The flux through these nanoporous membranes can be increased using pressure[46] or electro-osmotic transport,[47] but these techniques introduce new problems as well.

Mesoporous Silica

Mesoporous silica nanoparticles (MSNs) are solid materials, which contain hundreds of empty channels (mesopores) arranged in a 2D network of honeycomb-like porous structure (Figure 1.1 C). These silica-based nanoparticles offer several unique and advantageous structural properties, such as high surface area (>700 m^2 g^{-1}), pore volume (>1 cm^3 g^{-1}), stable mesostructure, tunable pore diameter (2–10 nm), two functional surfaces (exterior particle and interior pore faces), and modifiable morphology (controllable particle shape and size).[48] Typically, these materials are

synthesized by self-assembly of silica-surfactant (typically cetyltrimethyl-ammonium bromide, CTAB) in which inorganic species simultaneously condense, giving rise to mesoscopically ordered composites formation.[49] In contrast to the low biocompatibility of other amorphous silica materials, recent studies have shown that MSNs exhibit superior biocompatibility at concentrations adequate for pharmacological applications.[50,51]

Mesoporous silica nanoparticles as nanovalves. These nanoparticles can be used as nanovalves for use in drug delivery applications as their surfaces can be easily functionalized in order to control the nanopore openings.[52] For example, Zink and coworkers have synthesized a redox-controllable molecular nanovalve using two bistable [2]rotaxanes with different spacer lengths between their recognition sites as the gatekeepers. The silica nanopores can be closed and opened by moving the mechanically interlocked ring component of the bistable [2]rotaxane closer to and away from the pores' orifices, respectively, a process which allows the luminescent probe molecules, coumarins, tris(2-phenylpyridine)iridium, and rhodamine B, to be loaded into or released from the mesoporous silica substrate on demand.[53]

Polymers-modified mesoporous silica. Various responsive polymers have been used to modify the surface of mesoporous silica nanoparticles. These polymers can be used as capping agents to control transport from the silica mesopores as they have the ability to open and close the pores of the silica nanoparticles when subjected to various external stimuli such as temperature, light, and pH as described below. Poly(N-isopropyl acrylamide (PNIPAM) has

been used by López and coworkers to modulate the transport of aqueous solutes due to the temperature-dependant nature of the polymer, which is hydrated and extended at low temperature (room temperature), and collapsed in a hydrophobic state at high temperature (50º C).[54] An analog of (PNIPAM) modified with 2-nitrobenzyl acrylate, which is photolysed upon UV irradiation, is used to create a light responsive nanogated ensemble where the polymer is collapsed until UV light is shone on the nanoparticles and the hydrophobic 2-nitrobenzyl acrylate is photolysed into hydrophilic acrylate that leads to an increase in the LCST (usually 37 ºC) and opens the gate, allowing the entrapped molecules to escape.[55] Another example of photochemical nanogating is with spiropyran which changes from a charged to neutral form in visible light and a neutral to positively charged form in darkness. The positively charged form of spiropyran, covalently linked to the surface of the nanopores, binds to generation 1.5 poly(amidoamine) dendrimers in solution, effectively blocking the pores and allowing the release of the payload, in this case the dye $Ru(bipy)_3^{2+}$.

pH-responsive polymers have been used on the surface of mesoporous silica as responsive nanocarriers for controlled release. The effect of attaching a stimuli-responsive polypeptide chain, poly(L-glutamic acid) which undergoes a helix-coil transition triggered by pH change (from helical conformation at low pH to random coil conformation as pH is increased) to mesoporous silica which will regulate the flow of a molecule out of the pores has been modeled.[56] Feng and coworkers have grafted poly(4-vinyl pyridine) (PVP) to the surface of mesoporous silica nanoparticles which, at high pH, is deprotonated and produces

a hydrophobic shrunken state, inhibiting the release of trapped molecules. The swollen state of the protonated PVP at low pH is permeable to molecule transport, leading to the pH-controlled release.[57]

Mesoporous silica nanoparticles modified with responsive molecules. Nanopore openings have also been modified with responsive molecules such as azobenzene, a light responsive polymer that isomerizes from trans to cis (350 nm) and from cis to trans (450 nm). Mesoporous silica nanoparticles modified with azobenzene released a dye molecule or Cs^+ and Na^+ ions when stimulated with 457 nm excitation beam, indicating that the particle holds the guest molecule and expels them when stimulated.[58]

The nanoparticles in this thesis differ from mesoporous silica nanoparticles in that they are nonporous throughout their interior.

Single Glass Nanopores

Recently, single glass nanopores have been developed as a structurally simple and reliable platform for investigating molecular transport through orifices of nanoscale dimensions. These single synthetic nanopores are of interest as potential mimics of biological pores such as gated ion channels. The single glass nanopore electrodes consist of a Pt microdisk electrode embedded at the bottom of a conical pore made in glass, with the circular orifice of the pore having a diameter ranging from 5 to 100 nm (Figure 1.2). In contrast to free-standing membranes, a nanopore electrode is open to solution though a single orifice. This characteristic imparts the following advantages: (1) simplicity and

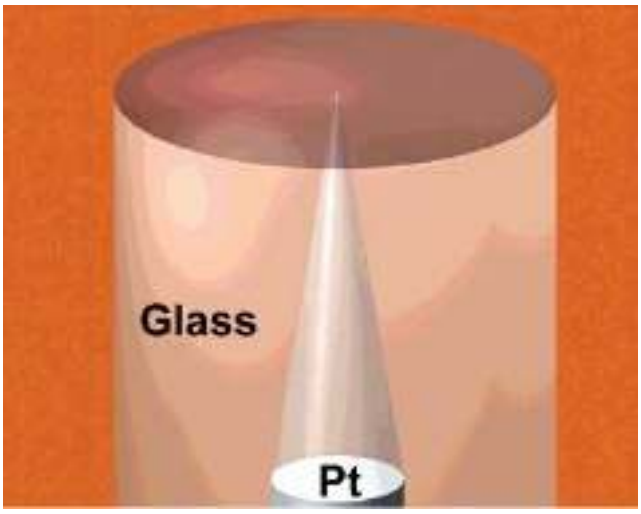

Figure 1.2. Schematic representation of a glass nanopore electrode

reproducibility of fabrication; (2) a built-in signal transduction element (the Pt electrode) for monitoring molecular transport through the pore; and (3) the portability and mechanical robustness of the solid electrode.[59] Controlled transport through these synthetic pores can be achieved by integrating polymers responsive to chemical or physical stimuli.[60] Stimuli reported to date include pH,[61] ionic strength,[62] temperature,[63] UV light as well as recognition of an ion,[64] a small molecule,[65] or a protein.[66] The responsive components in the system can exhibit a single or a combination of several responses to the environmental conditions, such as changes in charge and conformation of surface-bound macromolecules For example, previous work from our laboratories demonstrated that it is possible to functionalize the interior of the nanopore with amine groups followed by spiropyran moieties , which control the flux of a redox molecule through the orifice by acting as a photoswitch, in which a small number of photons, absorbed by spiropyran moieties in the pore orifice, induce reversible

gating of the steady-state flow of charged species through the pore orifice demonstrating that the flux through glass nanopore can be controlled by an external physical stimulus.[67,68]

Colloidal Crystals

A colloidal crystal is a highly ordered array of self-assembled spherical nanoparticles (Figure 1.3). Synthetic colloidal crystals are made from either polystyrene spheres[69] or silica spheres.[70,71] While polystyrene spheres are used to form colloidal crystals, silica colloidal crystals are more advantageous as they are mechanically and thermally robust and the surface of the silica colloidal crystals can be modified using well defined siloxane chemistry.[72] Colloidal crystals have been modified to produce a change in transport by varying the pH, and ionic strength,[73,74] addition of chiral molecules [75] and light.[76] In all these studies molecular transport has been successfully controlled either by electrostatics or molecular recognition. Another way to achieve controlled transport of molecules is by sterics or size selection of the diffusing molecule.

This thesis will focus on using polymer -modified silica colloidal crystals as a multipore nanoporous membrane to control the molecular transport of molecules and ions sterically and via molecular recognition. These colloidal membranes will be modified with environmentally-responsive macromolecules such as polypeptides and oligonucleotide-based binders that undergo conformational changes in response to external stimuli such as temperature, pH, and response to a small molecule.

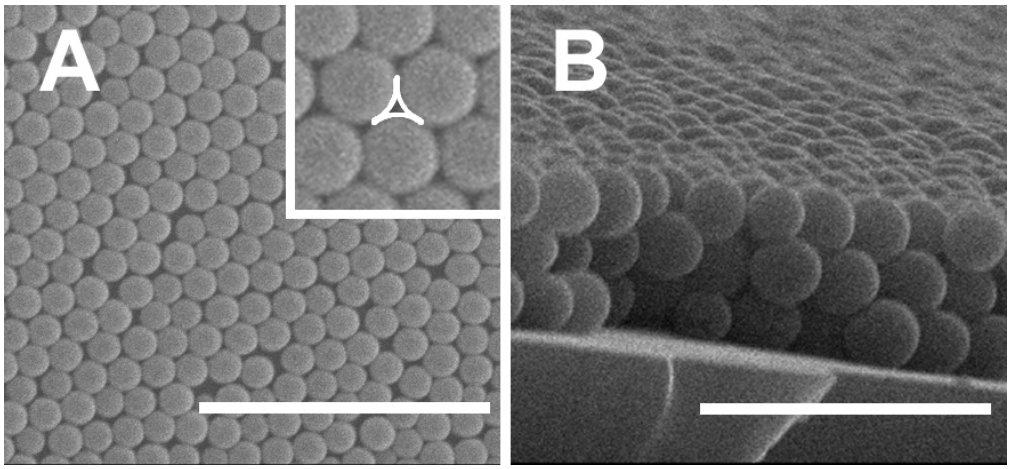

Figure 1.3. SEM images of a colloidal crystal prepared from 440 nm diameter silica spheres. (A) top view (size bar 4 μm); and (B) side view (size bar 2 μm). The geometric projection of a pore observed from the (111) plane is outlined in the inset in (A).

This novel nanoporous material has the potential to be used in several applications, including separations of biomacromolecules, such as DNA, peptides and proteins, and in the separations of ions and small molecules in microfluidic systems.

Self-assembled colloidal crystals are attractive because they allow a simple, powerful and cost effective approach to membranes with high porosity, molecular flux, as well as easily controllable nanopore size in the 5-100 nm range. The silica surface of the nanopores can be modified to contain a variety of functionalities, and solution characterization techniques can be used to confirm surface modification. Another important advantage of colloidal membranes is that the nanopores are tortuous and have high surface area allowing diffusing molecules to interact with surface functionalities more effectively. This results in higher selectivity compared to nanoporous materials with cylindrical pores.[77]

One disadvantage of the colloidal membranes is that they cannot be used under highly basic conditions (pH >10) because silica can be dissolved under such conditions.

Silica Colloidal Crystal Formation and Properties

Colloidal Crystal Formaiton

Monodisperse silica nanoparticles are used to create opals. Silica colloidal crystals are formed via self-assembly of silica nanoparticles into a close-packed face-centered cubic (fcc) lattice.[78] They contain ordered arrays of three-dimensional interconnected nanopores whose size can be controlled by varying the sphere size of silica spheres in the solution used to prepare the membrane (the distance from the center of the pore to the nearest silica sphere surface is ca. 15% of the sphere diameter).[79] The pores are formed between the silica spheres as highlighted in Figure 1.4.

To create silica nanoparticles, the most common and prefered method is one developed by Stöber.[80] This method produces silica spheres with size polydespersity of less than 10%, ideal for the formation of colloidal films.[81] In this synthesis, tetraethylorthosilicate is mixed with ammonia and water in absolute ethanol to produce silica nanospheres (Figure 1.5). The mechanism of this process includes two steps: hydrolysis of tetraethylorthosilicate and condensation (polymerization) of hydrolyzed silica species. The overall rate of the particle growth is limited by the first-order hydrolysis rate of tetraethylorthosilicate. The

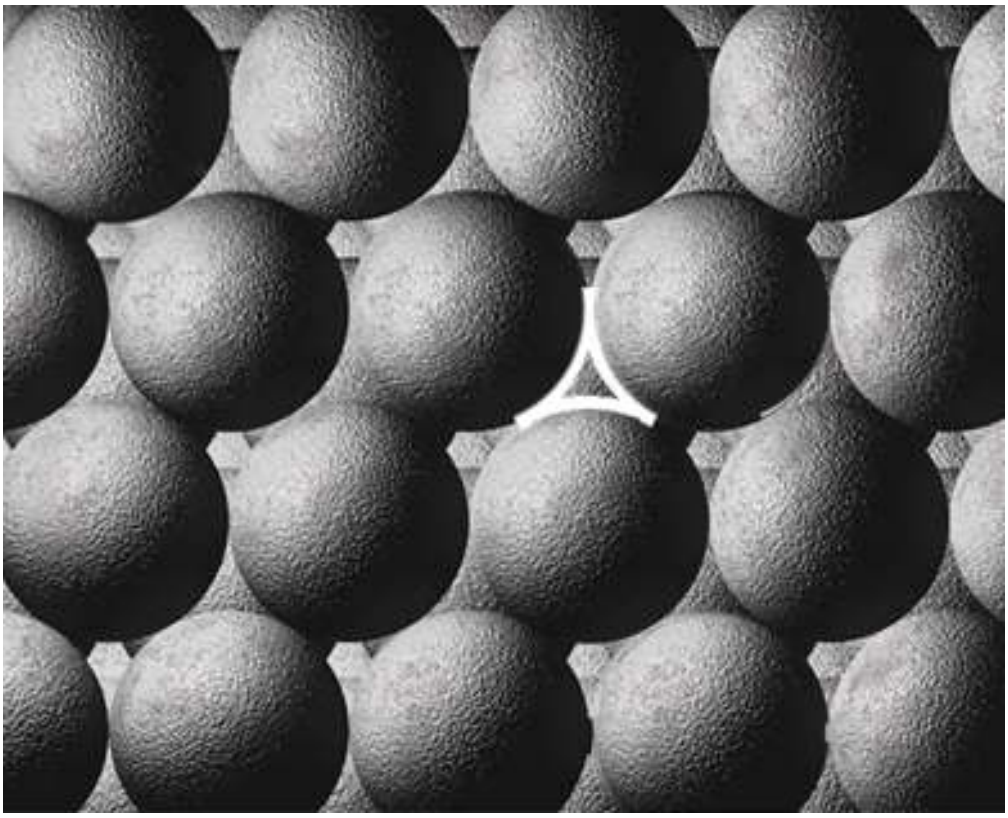

Figure 1.4. Schematic of silica spheres assembled in an fcc(111) orientation producing a colloidal crystal. The pore created by three packed silica spheres is outlined in white. The spheres used to make colloidal crystal can range from 20 to 2000 nm.

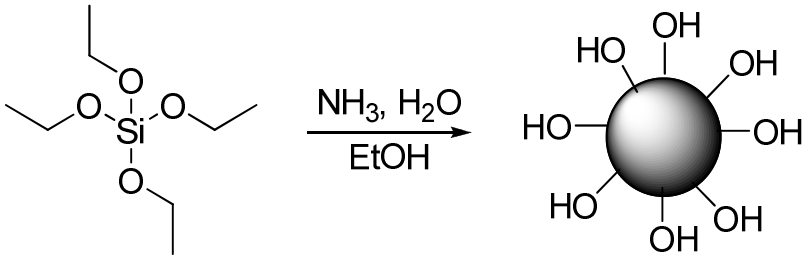

Figure 1.5. Basic synthetic scheme used to create monodisperse silica spheres.

size of the spheres is dependent on the concentration of ammonia and water used to create the spheres. The higher concentration of ammonia in the reaction mixture the larger the silica spheres that are produced. The following explanation for this phenomenon has been proposed. Under more basic conditions the surface of the forming silica particles is highly negatively charged and unstable causing the particles to react with tetraethylorthosilicate and silica aggregates and the particles grow faster.[82] The particles grow until the overall surface charge neutralizes allowing the particle to become stable and precipitate out of solution. After the reaction has gone to completion, usually anywhere from 15 to 120 min, the spheres' size and dispersity will not change with time. The size of the silica spheres prepared using the general procedure developed by Stöber. range from 20 nm to 10 μm in diameter, with a size dispersity of 10% or lower.

After silica nanoparticles have been synthesized, they can be used to form a colloidal crystal via self-assembly. Self-assembly is a spontaneous aggregation of particles into thermodynamically stable, structurally well-defined arrays. During self-assembly the silica particles interact with each other through

van der Waals forces and hydrogen bonding. The two most common techniques used to assemble a colloidal crystal are sedimentation[83] and vertical deposition.[84,85]

In sedimentation, a colloidal solution of silica spheres settles on the bottom of a container. A slowly evaporating solvent, usually water, is used to disperse the spheres and, as they settle, they self-assemble into the lowest energy arrangement, which is the fcc packing.[86] There are some disadvantages of this technique. First, the colloidal crystals contain a lot of defects. Second, the thickness of the colloidal film can be difficult to control and thin films are hard to produce. The third and probably the biggest drawback is that this process is very slow and can take weeks to months to produce a colloidal film, making this assembly technique impractical.

Vertical deposition is also used to create opal films without the drawbacks of sedimentation.[71,85] In this technique, a substrate, usually a glass slide or electrode, is placed vertically into a colloidal solution of silica spheres, usually 1-25 weight percent (wt%) in water or ethanol. For silica colloidal crystals the solvent must be polar, ethanol is preferred, to allow good solvation of negatively charged silica particles resulting in well-dispersed and a stable colloidal suspension. The solvent is then allowed to evaporate in a vibration free environment producing a colloidal film on the substrate surface. Figure 1.6 schematically represents this technique. This technique is preferred as it is reproducible and results in the rapid formation of colloidal crystals that are relatively defect free.

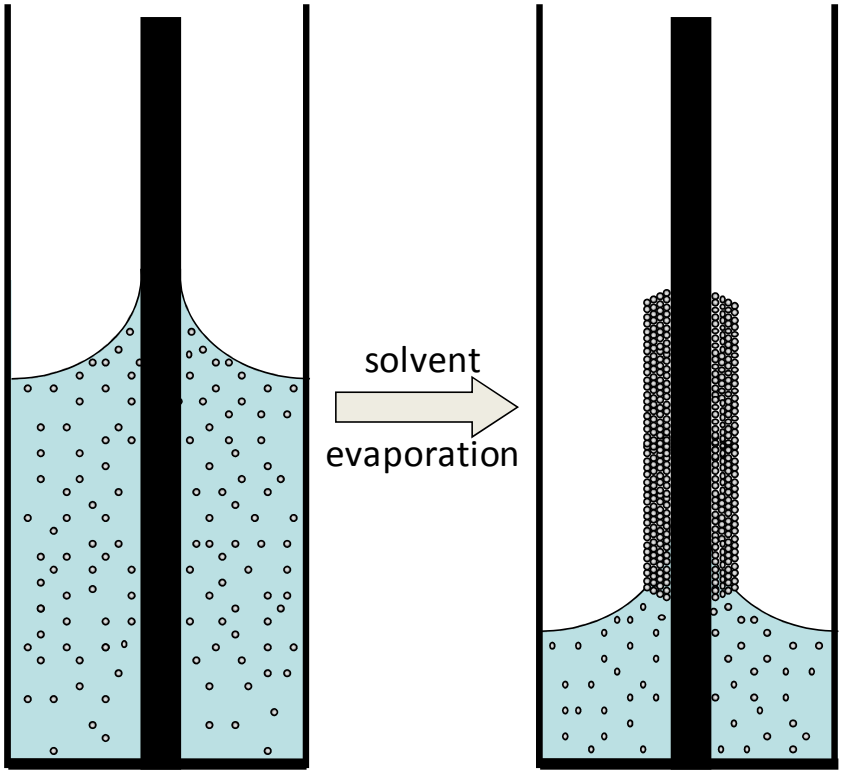

Figure 1.6. Scheme of the vertical deposition process used to self-assemble opals. Not drawn to scale.

The self-assembly of silica spheres into a colloidal crystal is driven by capillary forces in the solvent meniscus (Figure 1.7). After the silica spheres are brought to the surface of the substrate, they assemble into close-packed fcc lattice.[71,87,88]

The thickness of colloidal films can be easily controlled in the vertical deposition technique by varying the concentration (wt%), the size of spheres in the colloidal solution, and the solvent used. At higher wt% of the colloidal suspension more spheres are drawn up the meniscus forming a thicker film. Jiang. studied the dependence of the volume percent of 300 nm silica spheres on the number of spherical layers in a colloidal film. As the volume percent increased from 1 - 3% the colloidal film thickness increased from 20 to 50 layers.[71] The size of the particles influences the thickness in that as the size of the silica particles decreases, the thickness of the colloidal film increases for the same wt% colloidal solutions.

Larger particles settle out of solution quicker than smaller particles because larger silica particles are heavier than smaller ones.[71] That results in the formation of thinner colloidal film. Also, for the same wt% the number of smaller particles is higher in a colloidal solution than number of the larger particles, allowing for a thicker film. For example, our group has shown that 1.5 wt% solutions of silica spheres 440±11 nm and 170±14 nm produce colloidal films with thickness of 1.2 and 3.2 μm, respectively.[89]

Solvent volatility can affect colloidal crystal thickness in that a more volatile solvent gives a thicker colloidal film. This is due to the silica

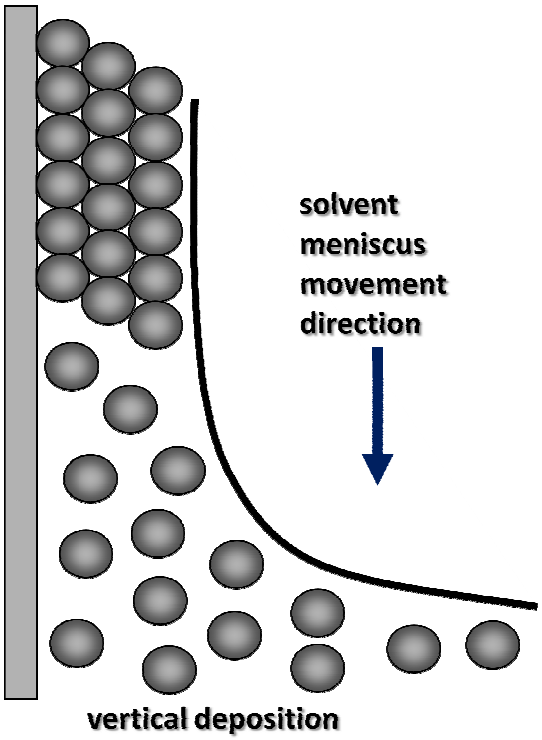

Figure 1.7. The mechanism of colloidal film formation on a solid substrate. The spheres are drawn up the meniscus by capillary action. As the solvent evaporates the meniscus lowers on the substrate creating a film on the substrate. Not drawn to scale.

particles having less time to settle out of solution, allowing more particles to be taken up by the meniscus. By changing solvent to a less volatile one, evaporation rate is decreased resulting in a thinner colloidal film. For example, colloidal solutions in ethanol give thicker films than colloidal solutions in water since ethanol evaporates more quickly than water.

Because vertical deposition is a fast, reproducible, and simple way to create high-quality silica colloidal crystals of with controlled thickness, it will be utilized in this thesis.

Polymer Modified Surfaces and Nanoporous Materials

Environmentally Responsive Modified Surfaces

In recent years, significant attention has been paid to the functionalization of surfaces with polymer brushes to create “smart” surfaces with switchable adaptive-responsive properties. The chain conformation as well as physical and chemical properties of polymer brushes can be manipulated with the environmental stimuli including pH, temperature, small molecule binding, etc. For example, polymers synthesized from amino acids can be tuned to be sensitive to a variety of stimuli such as pH and Ionic strength, solvent polarity, temperature, or response to electrochemical stimuli.[90]

Small Molecule Responsive Modified Surfaces

Aptamers can be selected for affinity to small molecules, biopolymers, surfaces, or even whole cells, and can be of use in the preparation of nanoporous materials whose function mimics that of protein channels in gating

the transport of a small molecule across a cell membrane. Specifically, these aptamers should provide the ability to control molecular transport through a nanoporous colloidal film by utilizing conformational changes in a biopolymer in response to small molecule binding. The secondary structure for the 32-base cocaine aptamer possesses a three-way junction, in the middle of which there is a cavity which binds the target molecule In the absence of a target, however, the aptamer is thought to remain partially unfolded, with only one of the three junctions folded.[91]

In this thesis, we use a cocaine-sensing aptamer which will experience a conformational change of the oligonucleotide inside the nanopores in the presence of cocaine, causing a reversible increase in the rate of diffusion through the nanopore.

Electrically Active Polymer Modified Surfaces

Conducting polymers can be attached to a surface via chemical or electrochemical polymerization.[92] Modification of a surface with these polymers allows for electrochemical control of the surface energy and topography. For example, surface switches have been synthesized using both polypyrrole (PPy) and poly(3,4-ethylene-dioxythiophene) (PEDOT) polymers (Figure 1.8). Polypyrrole and poly(3,4-ethylene-dioxythiophene) are conducting polymers which, due to their biocompatibility and biostability, are used in various electrochemical devices particularly targeting applications in biology. These polymers exhibit a change in conformation via swelling and hydrophobic

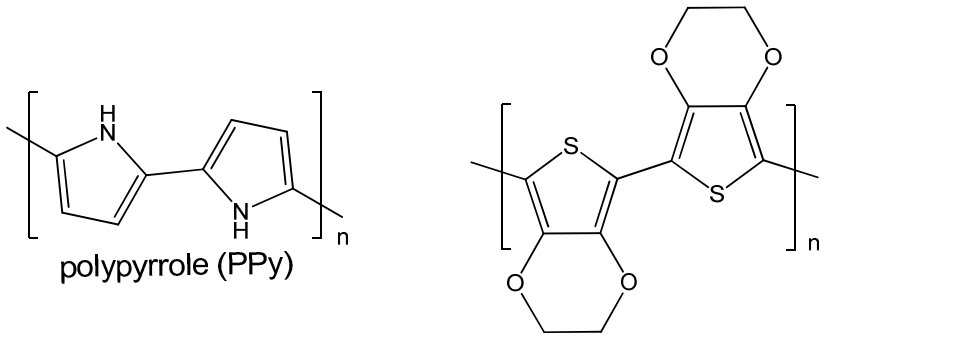

Figure 1.8. Structures of polypyrrole and poly(3,4-ethylene-dioxythiophene).

interactions. As the oxidation state of PPy is altered, it exhibits a volume change, making it an ideal polymer for use as an electrochemical actuator,[93] or as a membrane for the controlled release of anionic drugs.[94,95] It has been shown[96] that volume changes in conjugated polymers result from ionic movement into and out of the polymer due to oxidation and reduction. For the films of such polymers, expansion in the reduced state is observed for polymers doped with large immobile anions in contact with an electrolyte containing small mobile cations. In this case, cations are inserted upon reduction to maintain electroneutrality and thus the polymers expand when a negative potential is applied. For polymers doped with small, mobile anions in contact with an electrolyte containing both mobile cations and anions, expansion in oxidized state is observed due to anions that are inserted upon oxidation to maintain electroneutrality.

Electrodes of PPy combined with a common electrolyte can be reversibly oxidized and reduced. Upon reduction of the polymer from the oxidized state to

the neutral state, it exhibits a volume increas and its chemical character is altered.[97] The increase of thickness in thin PPy films can be as large as 40% upon the first reduction switch, whereas repeated switching typically provides a 20% reversible change of the volume.[98] It also exhibits a change in wetability as a result of oxidation state.[99] PEDOT, in a similar manner, undergoes a conformational change as it is reduced or oxidized.[100]

Synthesis of Polymer Brushes

There are two techniques used to covalently attach polymer chains to a surface, namely "grafting to" or "grafting from." In the "grafting to" method, fully formed polymer chains possessing a suitable end-functionalized group are reacted with the surface to obtain the desired brush. For example, the surfaces of silica and gold both possess functionalities that can react with polymer chains containing thiol, hydroxyl, and carboxyl groups. This technique allows for the synthesis of polymer chains possessing narrow molecular weight distributions and uniform brush thickness. This method, however, has drawbacks, which include limited surface grafting density due to the increasing size of the grafted chains. This limits the diffusion of large polymer chains to the reactive sites on the surface resulting in low brush thickness.[101]

To circumvent this problem, the "grafting from" technique is used. In this technique, polymer brushes are generated in situ by using a monolayer of surface-attached initiators to perform a surface-initiated polymerization. In this method, monomer units (rather than fully formed polymer chains) migrate to the

growing polymer brush layer allowing higher grafting density and brush thickness. Polymerization techniques used for surface-initiated polymerization include ring-opening, ring-opening metathesis, radical, ionic, or controlled radical polymerization, such as RAFT (reversible addition fragmentation transfer), NMP (nitroxide-mediated polymerization), and ATRP (atom transfer radical polymerization), which allow the polymerization of wide range of monomers.

This thesis will focus on utilizing both the "grafting to" and the "grafting from" techniques.

Polymer-modified Nanoporous Materials for Controlled Transport of Molecules

Switchable polymer brushes have been utilized to create "smart" synthetic nanopores that can mimic gating behavior of biological nanopores and control molecular transport. Such "smart" nanopores have been applied in chemical and biochemical sensors,[102] novel medical devices,[103] and separation of biomacromolecules and pharmaceuticals.[104] The idea of using polymer brushes in confined spaces as a gate to control molecular flow has been explored both theoretically[105] and experimentally.

Ito and coworkers demonstrated that transport selectivity can be introduced into porous materials using grafted macromolecules that respond to environmental stimuli, such as pH[106] and synthetic polyelectrolytes,[107] light-responsive spirobenzopyran-containing copolymers,[108] and ion-responsive polymers.[109]

One of the major drawbacks of existing polymer-based responsive membranes made using “grafting from” method or conventional radical polymerization on the surface is the lack of control in polymer length and surface coverage as well as limitations in surface modification and characterization of interior nanopore surfaces, and low molecular transport rate.

This thesis focuses on developing polymer-modified colloidal crystals and single nanopores as new responsive nanoporous membranes with controlled gating behavior. High porosity of colloidal crystal allows reagents to easily diffuse inside the film to react with the nanopore surface, allowing for uniform polymer brush growth with high surface coverage inside the nanopores. Another important advantage of colloidal crystals is that any surface modification and characterization can be performed in a colloidal solution of silica spheres in order to model the processes that can take place inside the nanopores.

Surface Modification and Characterization of Colloidal Crystals

Surface Modification of Colloidal Crystals

After the colloidal film has been assembled, the surface of the nanopores can be chemically modified in order to impart the desired transport selectivity. The silica surface contains hydroxyl groups which can be functionalized by reacting them with siloxanes.[110] In this reaction a covalent silicon-oxygen-silicon bond is formed as a result of substitution of the hydroxyl groups on the silica surface by the alkoxy groups in the siloxanes . Siloxane chemistry can be used

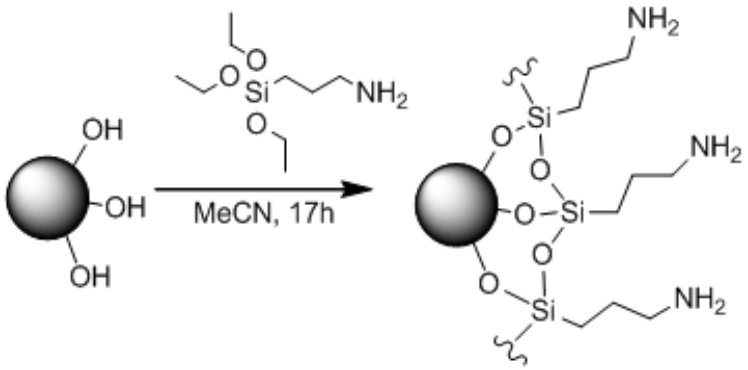

Figure 1.9. Modification of silica surface with 3-(Aminopropyl)triethoxysilane).

to aminate the silica surface using 3-aminopropyltriethoxysilane (Figure 1.9).[111] Amine-modified silica surfaces have been used in our group to attach a wide range of functional groups to the surface including small molecules and polymers.

Polymers can be attached to the surface of amine modified colloidal films using either the “grafting to” or “grafting from” method as previously discussed.

Characterization of Colloidal Crystals

One of the advantages of using silica colloidal crystals is that the surface chemistry of silica can be studied in a colloidal solution. Because the colloidal films are assembled from silica spheres the chemistry is presumed to be the same under the same modification conditions used for the colloidal films. Modified silica spheres are dispersed in a solvent and solution characterization techniques can be used which include dynamic light scattering (DLS), infrared

spectroscopy (IR), UV/Vis spectroscopy and nuclear magnetic resonance (NMR) and scanning electron microscopy (SEM).

Thesis Overview

Chapter 2 describes the preparation of poly(L-alanine)-modified silica colloidal films and diffusion studies of molecules as a function polymer bush length, pH, and temperature. Chapter 3 describes the preparation of poly(L-alanine)-modified free-standing colloidal films or “nanofrits” and the diffusion studies of a dye as a function of pH. Chapter 4 describes the modification of silica colloidal films with oligonucleotide-based binders, or aptamers, and examines the transport through these films as a function of small molecule binding. Chapter 5 highlights the preparation of aptamer-modified single nanopore electrodes and their ability to be used for molecular recognition. Finally, Chapter 6 describes the proof-of-principal preparation of electrically active, free-standing alumina anodiscs, and the diffusion of a dye as the potential is varied.

References

1. Tanev, P. T.; Butruille, J. R.; Pinnavaia, T. J , ed.; Interrante L. V.; Hampden-Smith, M. J. Wiley-VCH, New York, N. Y, 1998, p. 329.

2. Davis, M. E., *Nature*, **2002**, *417*, 813–821.

3. Bayley, H.; Martin, C.R. *Chem. Rev*., **2000**, *100*, 2575–2594.

4. Yu, S.; Lee, S. B.; Kang, M.; Martin, C. R. *Nano Lett.* **2001**, *1*, 495-498.

5. Schlenoff, J. B.; Ramaile, H.H.; *J. Am. Chem. Soc.*, 125, **2003**, 6602-6603.

6. Desai, T. A.; Hansford, D. J.; Kulinsky, L.; Nashat, A. H.; Rasi, G.; Tu, J.; Wang, Y.; Zhang, M.; Ferrari, M. *Biomed. Microdev.* **1999**, *2*, 11-40.

7. Sershen, S.; West, J. *Adv. Drug Delivery Rev*. **2002**, *54*, 1225-1235.

8. Bayley, H.; Martin, C. R. *Chem.Rev*. **2000**, *100*, 2575-2594.

9. Nishizawa, M.; Menon, V. P.; Martin, C. R. *Science* **1995**, *268*, 700-702.

10. Pirkle, W. H.; Pochapsky, T. C. *Chem. Rev.* **1989**, *89*, 347-362.

11. Ito, Y.; Park, Y. S. *Polym. Adv. Technol*. **2000**, *11*, 136-144.

12. Ulbricht, M. *Polymer.* **2006**, *47*, 2217-2262.

13. Hinds, B. J.; Chopra, N.; Rantell, T.; Andrews, R.; Gavalas, V.; Bachas, L. G. *Science* **2004**, *303*, 62-65.

14. Miller, S. A.; Martin, C. R. *J. Am. Chem. Soc*. **2004**, *126*, 6226-6227.

15. Sun, L.; Crooks, R. M. *J. Am. Chem. Soc*. **2002**, *122*, 12340-12345.

16. Kallus, S.; Condre, J.-M.; Hahn, A.; Golemme, G.; Algieri, C.; Dieudonne, P.; Timmins, P.; Ramsay, J. D. F. *J. Mat. Chem.* **2002**, *12*, 3343-3350.

17. Toh, C.-S.; Kayes, B. M.; Nemanick, E. J.; Lewis, N. S. *Nano Lett.* **2004**, *4*, 767-770.

18. Yamaguchi, A.; Uejo, F.; Yoda, T.; Uchida, T.; Tanamura, Y.; Yamashita, T.; Teramae, N. *Nature Mat.* **2004**, *3*, 337-341.

19. Hanai, T. Adv. Chrom. **2000**, *40*, 315-357.

20. Zhang, B.; Zhang, Y.; White, H. S. *Anal. Chem.* ***2004*****,** 76, 6229-6238.

21. Wang, G.; Bohaty, A. K.; Zharov, I.; White, H. S. *J. Am. Chem. Soc.* **2006**, *128*, 13553-13558.

22. Zhang, B.; Zhang, Y.; White, H. S. *Anal. Chem.* **2006,** *78*, 477-483.

23. Shim, J. H.; Kim, J.; Cha, G. S.; Nam, H.; White, R. J.; White, H. S.; Brown, R. B. *Anal. Chem*. **2007,** *79*, 3568

24. Cussler, E. L. *Diffusion: Mass Transfer in Fluid Systems,* 2nd ed.; Cambridge University Press: New York, 1997.

25. Newton, M. R.; Morey, K. A.; Zhang, Y.; Snow, R. J.; Diwekar, M.; Shi, J.; White, H. S. *Nano Lett.* **2004**, *4*, 875.

26. Lee, S. B.; Mitchell, D. T.; Trofin, L.; Nevanen, T. K.; Söderlund, H.; Martin, C. R. *Science* **2002**, *296*, 2198.

27. Kipke, S.; Schmid, G. *Adv. Funct. Mater.* **2004**, *14*, 1184.

28. Yamaguchi, A.; Uejo, F.; Yoda, T.; Uchida, T.; Tanamura, Y.; Yamashit, T.; Teramae, N. *Nature Mat.* **2004**, *3*, 337.

29. Kipke, S.; Schmid, G. *Adv. Funct. Mater.* **2004**, *14*, 1184.

30. Lee, S. B.; Mitchell, D. T.; Trofin, L.; Nevanen, T. K.; Söderlund, H.; Martin, C. R. *Science* **2002**, *296*, 2198.

31. Vlassiouk, I.; Krasnoslobodtsev, A.; Smirnov, S.; Germann, M. *Langmuir* **2004**, *20*, 9913.

32. Lee, S. W.; Shang, H.; Haasch, R. T.; Petrova, V.; Lee, G. U. N*anotechnology* **2005**, *16*, 1335.

33. Vlassiouk, I.; Krasnoslobodtsev, A.; Smirnov, S.; Germann, M. *Langmuir* **2004**, *20*, 9913.

34. Lee, S. W.; Shang, H.; Haasch, R. T.; Petrova, V.; Lee, G. U. *Nanotechnology*. **2005**, *16*, 1335.

35. Zhu, X.; Liu, Y.; Huang, J.; Li, Genxi. *Chem. Eur. J*. **2010**, *16*, 1441 .

36. Jeon, G.; Yang, S. Y.; Byun, J.; Kim, J. K. *Nano Lett*. **2011**, *11*, 1284.

37. Li, P. F.; Jiang, J. C.; Meng, T.; Yang, M.; Ju, X. J.; Yang, L.; Chu, L. Y. *Journal of Membrane Science*, **2009,** *337*, 310.

38. Fu, Q.; Rao, R.; Basame, S. B.; Keller, D. J.; Artyushkova, K.; Fulghum, J. E.; Lopez, G. P. *J. Am. Chem. Soc*. **2004**, *126*, 8904.

39. Yen, B. K.; White, R. L.; Waltman, R. J.; Dai, Q.; Miller, D. C.; Kellock, A. J.; Marchon, B.; Kasai, P. H.; Toney, M. F.; York, B. R.; Deng, H.; Xiao, Q.-F.; Raman, V. *J. Vac. Sci. Tech.* **2003**, *A21*, 1895.

40. Chang, H.; Kosari, F.; Andreadakis, K. G.; Alam, M. A.; Vasmatzis, G.; Bashir, R. *Nano Lett.* **2004**, *4*, 1551.

41. Zhao, Q.; Sigalov, G.; Dimitrov, V.; Dorvel, B.; Mirsaidov, U.; Sligar, S.; Aksimentiev, A.; Timp, G. *Nano Lett.* **2007**, *7*, 1680.

42. Wanunu, M.; Meller, A. *Nano Lett.* **2007**, *7*, 1580.

43. Apel, P. *Rad. Measur.* **2001**, *34*, 559.

44. van Rijn, C. J. M.; Veldhuis, J.; Kuiper, S. *Nanotechnology* **1998**, *9*, 343.

45. Martin, C. R.; Nishizawa, M.; Jirage, K.; Kange, M.; Lee, S. B. *Adv. Mater.* **2001**, *13*, 1351.

46. Yu, S.; Lee, S. B.; Kang, M.; Martin, C. R. *Nano Lett.* **2001**, *1*, 495.

47. Miller, S. A.; Martin, C. R. *J. Am. Chem. Soc*. **2004**, *126*, 6226.

48. Vivero-Escoto, J.; Slowing, I.; Trewyn, B. G.; Lin, V. S.-Y. *Small,* **2010**, *6,* 1952.

49. Vallet,-Regi, M.; Ramila, A.; de Real, R. P.; Perez-Pariente, J. *Chem. Mater*, **2001,** *13*, 308.

50 . Descalzo, A. B.; Martinez-Manez, R.; Sancenon, F.; Hoffmann, K.; Rurack, K.; *Angew. Chem., Int. Ed.* **2006** , *45* , 5924 .

51. Trewyn, B. G.; Slowing, I. I.; Giri, S.; Chen, H. T.; Lin, V. S. Y. *Acc.Chem. Res.* **2007** , *40* , 846.

52. (a) Vinu, A.; Hossain, K. Z.; Ariga, K. *J. Nanosci. Nanotechnol*. **2005***, 5* 347. (b) Oye, G.; Sjoblom, J.; Stocker, M. *Adv. Colloid Interface Sci*. **2001**, *89–90*, 439. (c) Corma, A. *Chem. Rev*. **1997**, *97,* 2373.

53. Nguyen, T. D.; Liu, Y.; Saha, S.; Leung, K. C.-F.; Stoddart, J. D.; Zink, J. I. *J. Am. Chem. Soc.* **2007**, *129*, 626.

54. (a) Fu, Q.; Rao, R. G. V.; Ista, L. K.; Wu, Y.; Andrzejewski, B. P; Sklar, L. A.; Ward, T. L.; López, G. P. *Adv. Mater*. **2003,** *15*, 1262. (b) Fu, Q.; Rao, R.; Ward, T. L.; Lu, Y.; López, G. P. *Langmuir*, **2007**, *23*, 170. (c) Rao, R. G. V.; López, G. P. *Adv. Mater.* **2000**, *12*, 1692.

55. Lai, J.; Mu, X.; Wu, X.; Wu, C.; Li, C.; Chen, J.; Zhao, Y. *Chem. Commun*., **2010**, *46*, 7370.

56. Adiga, S. P.; Brenner, D. W. *Macromolecules,* **2007**, *40*, 1342.

57. Liu, R.; Liao, P.; Liu, J.; Feng, P. *Langmuir,* **2011**, *27*, 3095.

58. (a) Sierocki, P.; Maas, H.; Dragut, P.; Richardt, G.; Vogtle, F.; Cola, L. D.; Brouwer, F. (A.M.); Zink, J. *J. Phys. Chem. B*, **2006**, *110*, 24390. (b) Angelos, S.; Choi, E; Vogtle, F.; Cola, L. D.; Zink, J*. J. Phys. Chem. C,* **2007**, *111*,6589. (c) Liu, N.; Chen, Z.; Dunphy, D. R.; Jiang, Y. B.; Assink, R.. A.; Brinker, C. J. *Angew. Chem. Int*. *Ed*. **2003**, *42*, 1731 – 1734. (d) Jiang, X.; Liu, N.; Assink, R. A.; Jiang, Y.; Brinker, C. J. *J. Nanomaterials*, **2011**, *2011*, 1.

59. Zhang, B.; Zhang, Y.; White, H. S. *Anal. Chem*. **2004,** *76*, 6229.

60. (a) Harrell, C. C.; Kohli, P.; Ziwy, Z.; Martin, C. R., *J. Am. Chem. Soc*., **2004**, *126*, 15646; (b) Heins, E. A.; Siwy, Z. S.; Baker, L. A.; Martin, C. R., *Nano Lett*., **2005**, *5*, 1824; (c) Siwy, Z.; Heins, E.; Harrell, C. C.; kohli, P.; Martin, C. R., *J. Am. Chem. Soc.*, **2004**, *126*, 10850.

61. (a) Xia, F.; Guo, X.; Mao, Y.; Hou, X.; Xue, J.; Xia, H. Wang, J.; Song, Y.; Ji, H.; Quyang, Q.; Wang, Y.; Jiang, L, *J. Am. Chem. Soc*., **2008**, *130*, 8345; (b) Yameen, B.; Ali, M.; Neumann, R.; Ensinger, W.; Knoll, W.; Azzaroni, O., *Nano Lett*., **2009**, *9*, 2788; (c) Yameen, B.; Ali, M.; Neumann, R.; Ensinger, W.; Knoll, W.; Azzaroni, O., *J. Am. Chem. Soc*., **2009**, *131*, 2070. (d) Zhang, L. X.; Cao, X. –H.; Zheng, Y. –B.; Li, Y. –Q. *Electrochem. Commun*. **2010**, *12*, 1249.

62. (a) Fologea, D.; Gershow, M.; Ledden, B.; McNabb, D. S.; Golovchenko, J. A.; Li, J., *Nano Lett*., **2005**, *5*, 1905; (b) Fologea, D.; Gershow, M.; Uplinger, J.; Thomas, B.; McNabb, D. S.; Li, J., *Nano Lett*., **2005**, *5*, 1734; (c) Chen P.; Gu, J.; Brandin, E.; Kin, Y. R.; Wang, Q.; Branton, D., *Nano Lett*., **2004**, *4*, 2293; (d) Storm, A. J.; Chen, J. H.; Ling, X. S.; Zanbergen, H. W.; Dekker, C., *Nat. Mater.*, **2003**, *2*, 537; (e) Ali, M.; Yameen, B.; Neumann,

R.; Ensinger, W.; Knoll, W.; Azzaroni, O., *J. Am. Chem. Soc*., **2008***, 130*, 16351.

63. (a) Ito, T.; Sun, L.; Crooks, R. M. *Anal. Chem*., **2003**, *75*, 2399; (b) Ito, T.; Sun, L.; Henriquez, R. R.; Crooks, R. M. *Acc. Chem. Res*., **2004**, *37*, 937; (c) Yameen, B.; Ali, M.; Neumann, R.; Ensinger, W.; Knoll, W.; Azzaroni, O. *Small*, **2009**, *5*, 1287.

64. Tian, Y.; Hou, X.; Wen, L.; Guo, W.; Song, Y.; Sun, H.; Wang, Y.; Jiang, L.; Zhu, D. *Chem. Commun*., **2010**, *46*, 1682.

65. Abelow, A. E; Schepelina, O.; White, R. J.; Vallée-Bélisle, A.; Plaxco, K. W.; Zharov, I. *Chem. Commun*., **2010**, *46*, 7948.

66. Ding, S.; Gao, C.; Gu, L. Q. *Anal. Chem*., **2009**, *81*, 6649.

67. Wang, G.; Zhang, B.; Wayment, J. R.; Harris, J. M.; White, H. S. *J. Am. Chem. Soc.* **2006**, *128*, 7679.

68. Wang, G.; Bohaty, A. K.; Zharov, I. Z.; White, H. S. *J. Am. Chem. Soc.* **2006**, *128*, 13553.

69. Kamp, U.; Kitaev, V.; von Freymann, G.; Ozin, G. A. *Adv. Mater.* **2005**, *17*, 438.

70. Zhang, H.; Wirth, M. J. *Anal. Chem.* **2005**, *77*, 1237.

71. Zheng, S.; Ross, E.; Legg, M. A.; Wirth, M. J. *J. Am. Chem. Soc.* **2006**, *128*, 9016.

72. Zheng, S.; Ross, E.; Legg, M. A.; Wirth, M. J. *J. Am. Chem. Soc.* **2006**, *128*, 9016.

73. Newton, M. R.; Bohaty, A. K.; Zhang, Y.; White, H. S.; Zharov, I. *Langmuir* **2006**, *22*, 4429.

74. Smith, J.; Zharov, I. *Langmuir* **2008**, *24*, 2650.

75. Cichelli, J.; Zhukov, A.; Antipin, I. S.; Stoikov, I. I.; Zharov, I. Unpublished results

76. Bohaty, A.; Zharov, I. *J. Porous Mat*er. **2009**, submitted.

77. Park, J.; Lee, D.; Kim, W.; Horiike, S.; Nishimoto, T.; Lee, S. H.; Ahn, C. H. *Anal. Chem.* **2007,** *79*, 3214.

78. Wong, S.; Kitaev, V.; Ozin, G. A. *J. Am. Chem. Soc.* **2003**, *125*, 15589.

79. Jiang, P.; Bertone, J. F.; Hwang, K. S.; Colvin, V. L. *Chem. Mater.* **1999**, *11*, 2132.

80. Stober, W.; Fink, A.; Bohn, E. J. *Colloid. Interface Sci,* **1968**, *26*, 62.

81. Jiang, P.; Bertone, J. F.; Hwang, K. S.; Colvin, V. L. *Chem. Mater.* **1999**, *11*, 2132.

82. van Blaaderen, A.; van Geest, J.; Vrij, A. *J. Colloid Interface Sci.* **1992**, *154*, 481.

83. Pieranski, P. *Contemp. Phys.* **1983**, *24*, 25.

84. Jiang, P.; Bertone, J. F.; Hwang, K. S.; Colvin, V. L. *Chem. Mater.* **1999**, *11*, 2132.

85. Wong, S.; Kitaev, V.; Ozin, G. A. *J. Am. Chem. Soc.* **2003**, *125*, 15589.

86. Okubo, T. *Langmuir.* **1994**, *10*, 1695.

87. Leger, L.; Raphael, E.; Hervert, H. *Adv. Polym. Sci*. **1999**, *138*, 186.

88. Joanny, J.-H. *Langmuir.* **2001**, *17*, 388.

89. Bohaty, A. K. *Studies of Diffusion of Molecules and Ions Through Nanoporous Opal Films and Membranes*. University of Utah, Utah, 2008.

90. Mart, R. J.; Osborne, R. D.; Stevens, M. M.; Ulijn, R. V. *Soft Matter,* **2006**, *2*, 822.

91. Stojanovic M. N., Prada P., Landry D. W.: *J. Am. Chem. Soc.* **2001**, *123*, 4928.

92. Heinze, J., *Top. Curr. Chem.*, 1990, **152**, 2.

93. (a) Jager, E. W. H.; Inganas, O.; Lundstrom, I. *Science* **2000**, *288*, 2335; (b) Jager, E. W. H.; Smela, E.; Inganas, O. *Science* **2000**, *290*, 1540.

94. Kontturi, K.; Murtomaeki, L.; Pentti, P.; Sundholm, G. *Synth. Meta* **1998**, *92*, 179.

95. Wallace, G. G.; Adeloju, S. B.; Shaw, S. J. In *Electroassembly of Smart Polymer Structures (Role of Polyelectrolytes)*; SPIE: Bellingham, WA, 1997.

96. Jager, E. W. H.; Smela, E.; Inganas, O. *Science*, **2000,** *290*, 1540.

97. Pei, Q. B.; Ingana¨s, O. *J. Phys. Chem.* **1992**, *96*, 10507.

98. Smela, E.; Gadegaard, N. *Ad*V*. Mater.* **1999**, *11*, 953.

99. Wang, X.; Berggren, M.; Inganas, O., *Langmuir,* **2008,** *24,* 5942.

100. Isaksson, J.; Kjäll, P.; Nilsson, D.; Robinson, N. D.; Berggren, M.; Richter-Dahlfors, R., Nature Materials, 2007, 6, 673.

101. Advincula, R. A. *Polymer brushes: Synthesis, Characterization, Applications.* Ed. Wiley-VCH Verlag, 2004.

102. Choi, Y.; Baker, L. A.; Hillebrenner, H.; Martin, C. R. *Phys. Chem. Chem. Phys*. **2006**, *8*, 4976.

103. Leoni, L.; Desai, T. A. *Adv. Drug Delivery Rev.* **2004**, *56*, 211.

104. Yu, S.; Lee, S. B.; Kang, M.; Martin, C. *Nano Lett.* **2001**, *1*, 495.

105. Israels, R.; Gersapper, D.; Fasolka, M.; Roberts, V.A.; Balazs, A.C. *Macromolecules* **1994**, *27*, 5285.

106. Ito, Y.; Park, Y. S.; Imahishi, Y. *Langmuir* **2000**, *16*, 5376.

107. Ito, Y.; Park, Y. S.; Imanishi, Y. *J. Am. Chem. Soc.* **1997**, *119*, 2739.

108. Ito, Y.; Park, Y. S.; Imahishi, Y. *Macromol.* **1998**, *31*, 2606.

109. Yamaguchi, T.; Ito, T. *J. Am. Chem. Soc.* **2004**, *126*, 6202.

110. Flink, S.; van Veggel, F. C. J. M.; Reinhoudt, D. N. *J. Phys. Org. Chem.* **2001**, *14*, 407.

111. Halliwell, C. M.; Cass, A. E. G. *Anal. Chem.* **2001**, *73*, 2476.

CHAPTER 2

POLY(L-ALANINE)-MODIFIED NANOPOROUS COLLOIDAL FILMS

Introduction

This chapter focuses on modifying the surface of silica nanoparticles and colloidal films with a polypeptide brush which will impart a pH and temperature dependent permselectivity based on electrostatic interactions between the polypeptide chains. The mechanism of this observed permselectivity will be elucidated by measuring the molecular flux of a neutral redox molecule through the bare, initiator modified, and polypeptide-modified colloidal film as a function of temperature and pH.

Experimental Section

Materials

Chemicals. (3-Aminopropyl) triethoxysilane (99%, Aldrich), phosphorus trichloride (99%, Aldrich), tetraethoxysilane, TEOS (99.999+%, Aldrich), N-(tert-Butoxycarbonyl)-Lalanine (>99%, Fluca), Hexaammineruthenium(III) chloride, [Ru(NH3)6]Cl3 (99%, Strem Chemicals), 1,1'-ferrocenedimethanol, Fc(CH2OH)2 (98%, Aldrich), and potassium chloride (99%, Mallinckrodt) were used as received. N,N-Dimethylformamide, DMF (99.9%, Fisher Scientific) was dried

over molecular sieves. Acetonitrile (Mallinckrodt) was distilled before using. 18 MΩ cm water was obtained from a Barnsted ‘‘E-pure’’ water purification system.

Instrumentation. Dynamic light scattering (Brookhaven ZetaPALS) was employed to measure size of unmodified and polymer-modified silica spheres. To characterize the surface composition of silica spheres, thermogravimetric analysis (TGA) (TGA Q500, TA Instruments) was performed. Scanning electron microscopy (Hitachi S3000-N) was used to image unmodified and polymer-modified silica nanoparticles. NMR spectra were recorded on Varian VXL-300MHz at 300 MHz. A Branson 1510 sonicator (50-60 Hz) was used for all sonications.

Methods

Preparation and modification of ~200 nm silica spheres in solution. All glassware was cleaned with 18 MΩ·cm water. Silica nanoparticles were prepared following the literature procedure.[1] A solution of tetraethoxysilane (TEOS) in absolute ethanol was rapidly poured into a stirred mixture of ammonia and water in absolute ethanol at room temperature. The final concentrations of the reagents were 0.2 M TEOS, 0.4 M ammonia and 17 M water. The reaction mixture was covered and stirred for 18 h. The silica spheres were isolated by repeated centrifugation and resuspension in 15 mL centrifuge tubes (Corning) for 10 min at 1163 g. After the spheres were collected from the original reaction mixture, the supernant was removed and the spheres were dispersed in absolute ethanol by sonication for 30 min. The diameter of the spheres was found to be 218 ± 27 nm using scanning electron microscopy (SEM) and 255 ± 26 nm using

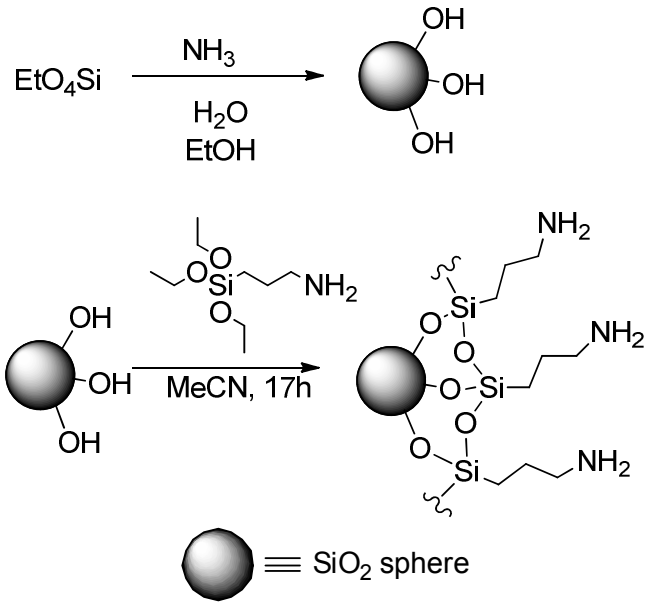

Figure 2.1. Silica sphere preparation and amination of silica spheres.

dynamic light scattering (DLS). The size difference can be attributed to swelling as spheres are suspended in aqueous media for DLS measurements. A general scheme of silica sphere preparation is shown in Figure 2.1 and Figure 2.2. Amine functionalization of silica spheres (Figure 2.1) was achieved by treatment with a solution of 0.20 mL (0.85mmol, 0.056 M) (3-aminopropyl) triethoxysilane in 15 mL of dry acetonitrile under nitrogen in a dry 20 mL scintillation vial at room temperature for 17 h followed by centrifugation for 10 min at 1163g followed by resuspension in acetonitrile. The presence of amino groups was confirmed by treating the silica spheres with dansyl chloride, followed by fluorescence measurements, as previously described.[2]

Preparation and modification of 50 nm silica spheres. All glassware was cleaned with 18 MΩ·cm water. Silica nanoparticles 50 nm in diameter were synthesized following a literature procedure.[3] Tetraethyl orthosilicate (25 mmol)

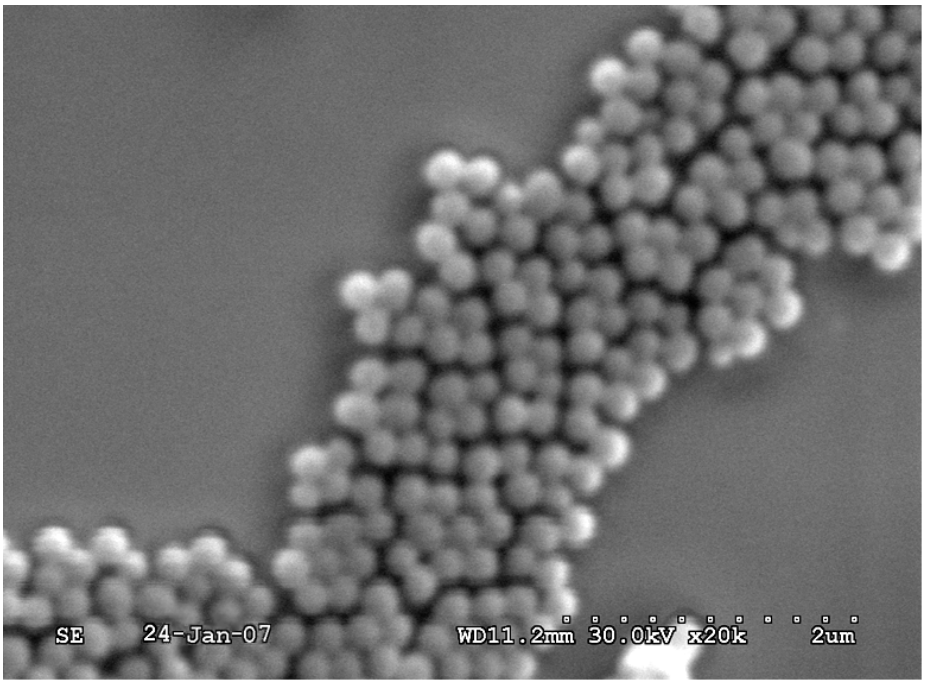

Figure 2.2. Scanning electron microscopy (SEM) image of 218 ± 27 nm diameter silica spheres.

was added to a mixture of 5.7 mL of concentrated aqueous ammonium hydroxide and 114 mL of ethanol with stirring. The solution was covered and stirred for 18 h. A 50 mL aliquot of the resulting SiO_2 colloidal dispersion was removed and used for amine functionalization. Amine functionalization of the silica nanoparticles was achieved by adding 1.0 mL of (3- aminopropyl) triethoxysilane to the colloidal suspension. This solution was stirred overnight at room temperature during which the opaqueness of the solution increased noticeably. The colloidal silica was isolated by centrifugation and washed with three portions of 50 mL of ethanol and dried under vacuum to afford a white powder of amine functionalized colloidal silica spheres. The dried powder could be dispersed in

water to give clear solutions of the functionalized silica spheres. The diameter of the amine functionalized colloidal spheres was found to be 57 ± 3 nm using DLS.

Preparation of L-alanine NCA[4] N-tert-butyloxycarbonyl alanine (0.005 mol, 0.95g) was dissolved in methylene chloride (25 mL) under a nitrogen atmosphere and cooled to 0˚C in an ice bath. Phosphorus trichloride (0.006 mol, 0.524 mL) was added to the solution. The reaction mixture was stirred for 4 hours at 0˚C, the solvent was removed under reduced pressure and the residue washed with 20 mL of carbon tetrachloride three times to afford the N-carboxy amino acid anhydride (Figure 2.3). ^{1}H NMR (300 MHz, $CDCl_3$): δ: 5.83 (s, 1H), 4.44-4.40 (m, 1H), 1.58 (d, 3H).

Poly(L-alanine)-modified silica nanoparticles. Polymer modification of silica nanoparticles was conducted using the reaction shown in Figure 2.4. Silica spheres (0.1 g) were suspended in 100 mL of *N*,*N*-dimethylformamide (DMF) with the L-alanine N-carboxy amino acid anhydride (0.001 g). The colloidal solution was stirred and 10 mL aliquots were taken at intervals ranging from 15 min to 6 h. After an aliquot was isolated, polymer-modified spheres were isolated and purified by repeated washing and centrifugation in E-pure water.

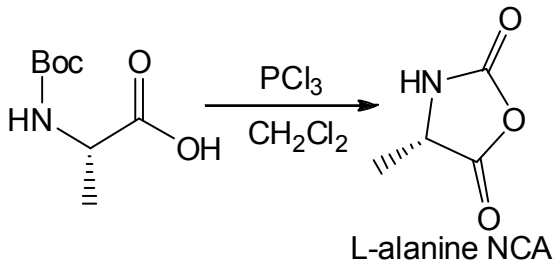

Figure 2.3. Preparation of L-alanine N-carboxyanhydride.

Colloidal film-modified platinum microdisc electrodes. Platinum microdisc electrodes (25 μm in diameter) shrouded in glass were prepared by first attaching a 1.0 mm diameter Cu wire (99.95%, Alfa Aesar) to a 25 μm diameter Pt wire using Ag paint (DuPont). The silver paste was allowed to cure for 2 h in a 150˚C oven before the wire was flame sealed in a glass capillary. The capillary was bent into a U-shape, and the middle was cut orthogonal to the length of the capillary with a diamond saw to expose the Pt disc. The open end of the electrodes was sealed with epoxy (Loctite 0150, Hysol). The resulting electrodes were polished with Microcut Paper discs (Buehler), from 240 to 1200 grit in succession, until the surface was free from visible defects. The electrodes were then polished using 0.005 micron deagglomerated gamma alumina (Buehler) on a microcloth polishing pad (Beuhler). The colloidal films were deposited onto the Pt and the glass shroud by placing the electrodes vertically into 1.5 wt% colloidal solution of silica spheres in ethanol. The electrodes were elevated off the bottom of the vials by wrapping a piece of copper wire around to top of the vial and electrode. The vials were placed under a crystallization dish which was elevated 6 cm off the bench using four 20 mL scintillation vials with caps and the solutions were allowed to evaporate for 3 days in an environment free from any major vibrations. Colloidal films were formed via vertical deposition[5,6,7] onto the face of the electrode (Figures 2.4 and 2.5).

Graft polymerization of L-alanine NCA in colloidal films.[8] First, amine modification of the colloidal films was achieved by immersing the platinum microelectrode in a dry scintillation vial containing 15 mL of dry acetonitrile and

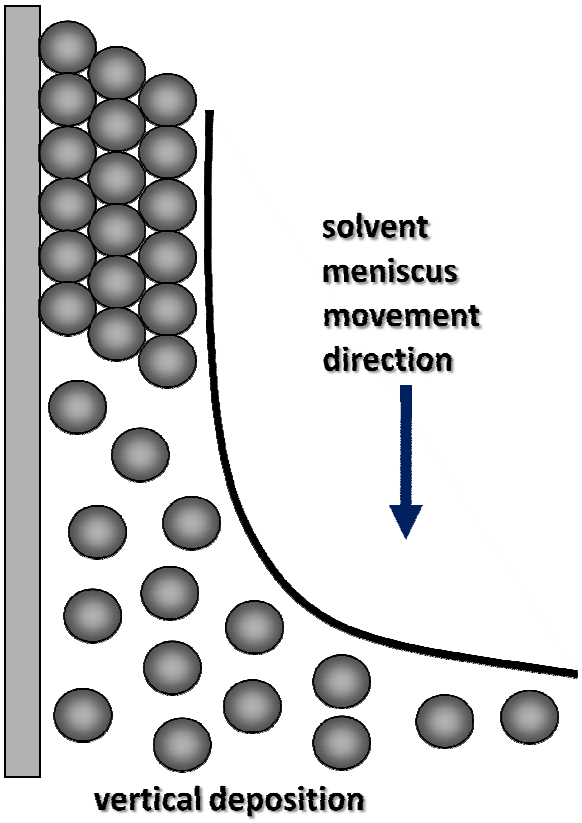

Figure 2.4. Mechanism of nanoporous opal film formation via vertical deposition.[5,6,7]

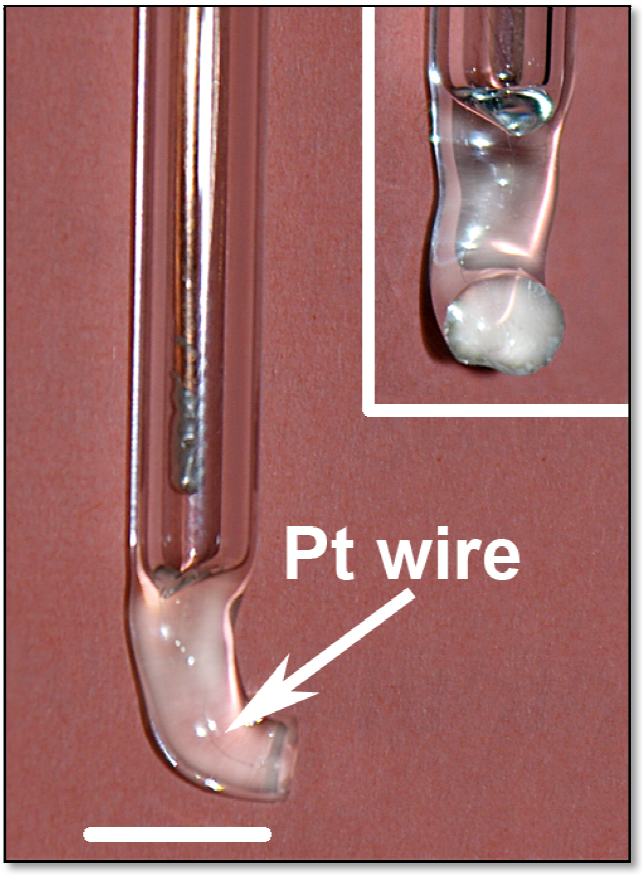

Figure 2.5. Photograph of a Pt microdisk electrode after opal film assembly using a 1.5 wt% colloidal solution of 218 ± 27 nm silica spheres.

0.20 mL (0.85 mmol, 0.056 M) of 3-aminopropyltriethoxysilane for 17 h at room temperature. The opening in the vial was wrapped in parafilm and placed in a fume hood for 17 h without stirring. The electrodes were then soaked in 15 mL of dry acetonitrile for 1 h three times. Next, the surface of the colloidal films on the Pt electrodes was modified with poly(L-alanine) by immersing the amine-modified electrodes vertically into a stirred solution of DMF containing L-alanine NCA (0.0047 M) under a nitrogen atmosphere. Polymerization time was varied from 15 min to 6 h after which the electrodes were rinsed in E-pure water (Figure 2.6).

Voltammetric measurements. The flux of permeants across the colloidal film was measured voltammetrically using a 2-electrode cell and a silver/silver chloride reference/counter electrode. A par Model 175 Universal Programmer and Dagan Cornerstone Chem-Clamp potentiostat were used to conduct the measurements. Data were recorded with a PC using programs written in LabView. Aqueous solutions were prepared using 18 MΩ·cm water obtained from a Barnstead “E-pure” water purification system. All solutions were purged with nitrogen to remove dissolve oxygen. The pH was adjusted by the addition of hydrochloric acid and sodium hydroxide. The following concentrations of redox species used were 1.6mM $Fc(CH_2OH)_2$.

Temperature and pH-responsive behavior measurements. The temperature-response measurements at temperatures ranging from 20–80˚C were performed using an immersion circulator with a temperature controller (VWR). The circulator was connected to an external jacketed beaker. To measure the temperature-response for poly(L-alanine) modified nanoporous

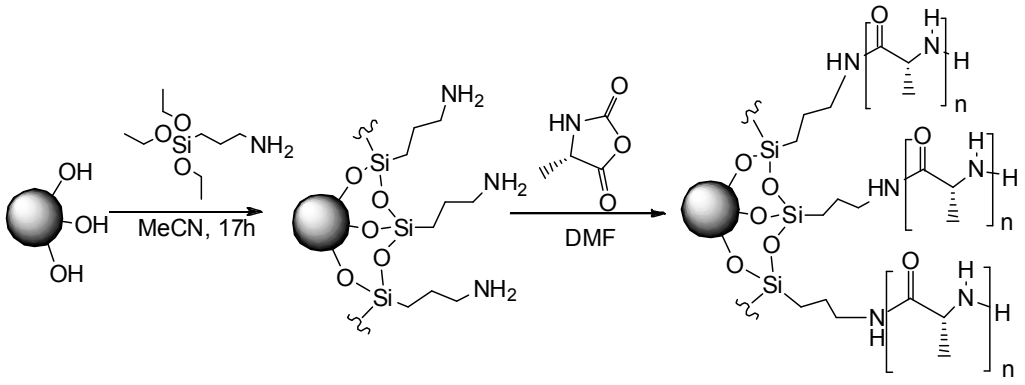

Figure 2.6. Preparation of Poly(L-alanine)-modified Silica Nanoparticles.

colloidal films, a solution of the redox species was placed into the beaker and maintained at a constant temperature during the electrochemical measurements. DLS measurements were conducted at 25˚C. Aqueous colloidal solutions of poly(L-alanine)-modified nanoparticles were prepared using either HCl or NaOH to achieve the desired pH, which ranged from pH 3 to pH 11. To measure the pH response on poly(L-alanine)-modified nanoporous colloidal films, HCl or NaOH was added to a solution of the redox species and CV measurements were conducted at pH 3, 6, and 8.

SEM imaging. Silica spheres were imaged by making a 0.1 wt% colloidal solution in ethanol and placing a drop of the colloidal solution onto a piece of silicon wafer. The solvent was allowed to evaporate, leaving the spheres distributed on the surface of the wafer. All SEM images were taken using a Hitachi S3000N after sputtering gold for 60 s onto the surface of the substrates.

Results and Discussion

Poly (L-alanine)-Modified Silica Nanoparticles and Colloidal Films

Surface-initiated polymerization on silica spheres in solution. In order to demonstrate that the polymerization can be performed on the surface of silica spheres, we modified 218 nm silica spheres in solution with initiator molecules followed by treatment with L-alanine NCA in DMF solution. The polymer growth as a function of polymerization time was monitored by dynamic light scattering (DLS) for the silica spheres in their colloidal solution, and the corona thickness was calculated. The results of these measurements are shown in Table 2.1. The polymer brush thickness increases linearly at first and reaches the saturation thickness of ca. 35 nm after 2 h of polymerization without significantly changing after longer polymerization times. The graft density of polymer brushes was calculated using thermogravimetric analysis (TGA). TGA was run on polymer-grafted spheres (35 nm brush thickness determined by DLS in the colloidal

Table 2.1. Silica sphere diameter (d) and poly(L-alanine) corona thickness (Δr) as a function of polymerization time calculated from DLS measurements.

Polymerization time/ min	d, nm	Δr, nm
0	255±26	0
15	270±15	7.5
30	296±32	20.5
45	310±46	27.5
60	314±35	29.5
90	320±47	32.5
120	323±42	34
360	325±38	35

$$Poly(L-alanine)(nm^{-2}) = \frac{WL*N_A}{MW_{(poly(L-alanine)*\left(\frac{SA}{v*d}\right)}} \quad \text{Equation 2.1.}$$

aqueous solution) and is shown in Figure 2.7. Based on these results we estimate the grafting density as 0.61 chains per nm^2, using equation 2.1. where WL is the weight loss to the poly(L-alanine) groups between 200 – 700 ˚C, after accounting for the weight loss due to the drying of silica spheres, N_A is Avogadro's number, $MW_{Poly(L\text{-}alanine)}$ is the molecular weight of the poly(L-alanine) group, SA is the surface area of the spheres ($4\pi r^2$), v is the volume of the spheres ($4/3\pi r^3$), and d is the density of the spheres (1.9 g/cm^3). This estimated graft density is well below the maximum grafting density that can be achieved for the silica surface (~4-6 groups/nm^2 density of hydroxyl groups on surface).[9]

The poly(L-alanine)-modified nanoparticles were washed with 1M and 2M triflouroacetic acid and then with water by repeated centrifugation and re-suspension. This was done in order to remove any free poly(L-alanine) oligomers not covalently attached to the surface. No change in the diameter of the poly- (L-

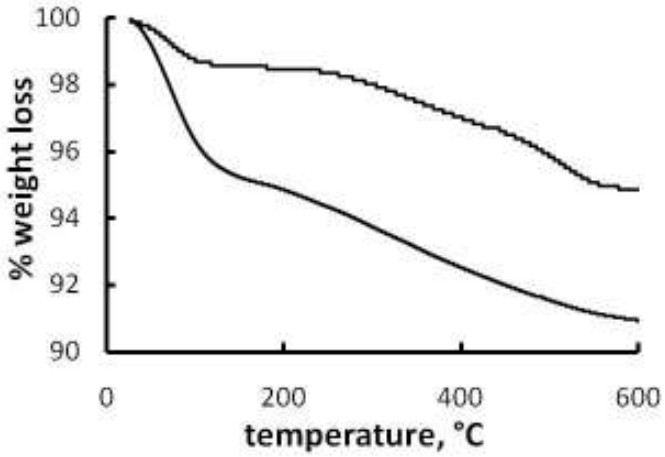

Figure 2.7. Thermogravimetric analysis (TGA) plots for unmodified (top line) and poly(L-alanine)-modified (bottom line, polymerization time 3 h, brush thickness 35 nm) silica spheres.

alanine)-modified silica nanoparticles was observed using DLS after these washes indicating that the change in diameter is due purely to covalently attached polymer brushes on the surfaces of the nanoparticles. We observed complete cleavage of the polymer from the nanoparticles only when a high (5 M) concentration of triflouroacetic acid was used as the observed diameter returned to that of the unmodified silica nanoparticles.

In order to investigate the conformation of poly(L-alanine) brushes on the surface of the poly(L-alanine)-modified 255 nm silica spheres in solution, circular dichroism measurements were performed. No α-helical conformation was observed for poly- (L-alanine) brushes of any length. In order to confirm that these results were not a function of multiple light scattering of the silica nanoparticles, smaller (ca. 50 nm) silica nanoparticles were modified with poly(L-alanine). CD measurements for these nanoparticles also showed no evidence of α-helical structures, in agreement with the previous reports where β-form was found for poly(L-alanine) on a silica surface.[10,11]

Graft polymerization inside colloidal films. The colloidal films were assembled on the surface of Pt microelectrodes shrouded in glass using 1.5 wt% solution of 218 nm silica spheres. The surfaces were modified with initiator moieties, and polymerization was performed on the modified colloidal film electrodes in DMF solutions. The electrodes were removed from the solution after different periods of time ranging from 15 min to 6 hours. The limiting current of $Ru(NH3)_6^{3+}$ was then measured for these polymer-modified electrodes and compared to the limiting current before the polymerization. The voltametric

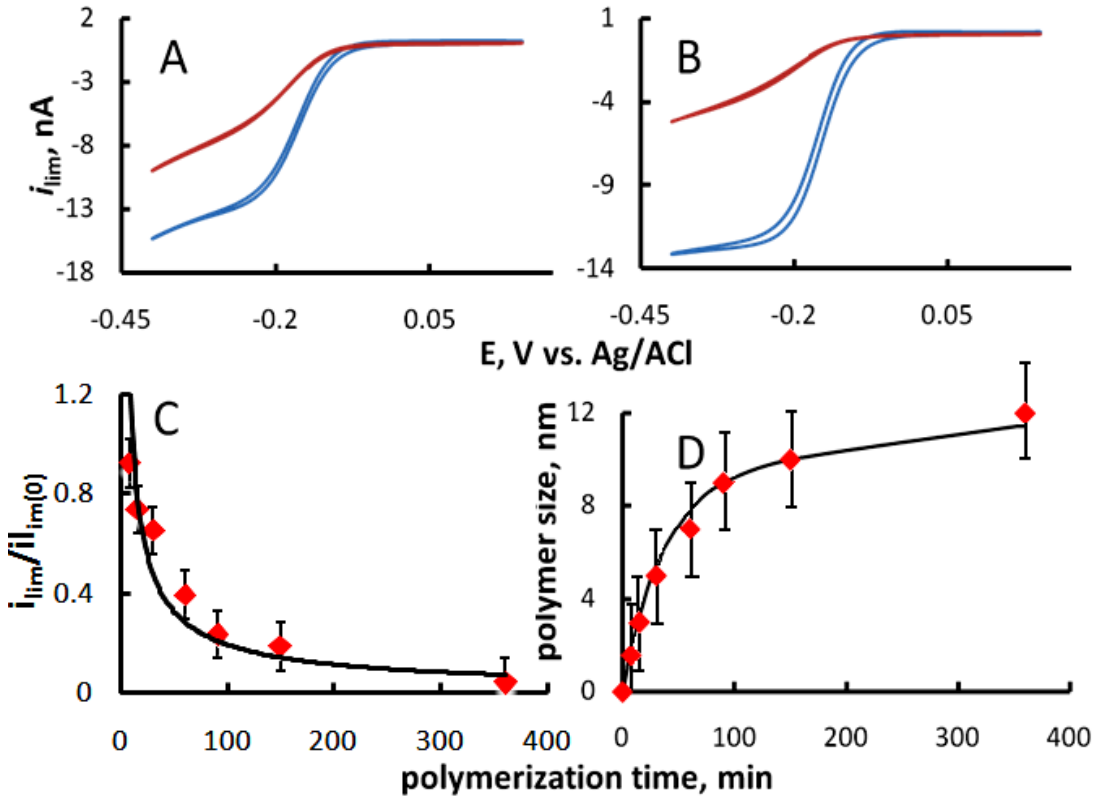

Figure 2.8. ($Ru(NH)_6^{3+}$) voltammetric responses for colloidal film Pt electrodes before (top line) and after (bottom line) polymerization for (A) 30 min and for (B) 1 hour. (C) Plot of relative limiting current as a function of polymerization time. (D) Plot of the poly(L-alanine) brush thickness inside the colloidal nanopores as a function of polymerization time.

responses for a bare electrode in $Ru(NH3)_6^{3+}$ showed a sigmoidal shape, characteristic of the near steady-state radial diffusion of the redox species to a microelectrode.[12] Following deposition of the thin silica colloidal film onto the electrodes, a near steady-state radial diffusion with a reduction in the limiting current (i_{lim}) was observed. This effect is also present for polymer-modified colloidal films. For instance, as shown in Figure 2.8, the limiting current measured for the electrodes after a short polymerization time (30 min) decreased by 34%, which suggests that a polymer brush has been formed inside the nanopores. Similarly, a 60% drop in the limiting current was observed for a longer polymerization time (1 h). The relative limiting current for colloidal film electrodes decreased logarithmically with increasing polymerization time (Figure 2.8). Using a formula obtained earlier,[13] the thickness of the polymer brush was calculated (Table 2.2 and Fig. 2.8). The poly(L-alanine) brush thickness inside the colloidal nanopores increased with the polymerization time and reached ca. 10 nm after 2 h. To directly measure the molecular weights of poly(L-alanine) prepared inside the colloidal nanopores we cleaved the polymers from the silica surface using KOH. However, the amount of the polymeric material obtained this way was not sufficient for GPC studies.

Temperature-responsive behavior of the poly(L-alanine)-modified colloidal films. The temperature-response for poly(L-alanine)- modified colloidal films was investigated using cyclic voltammetry. To exclude the possibility that the observed changes in the molecular transport would result from electrostatic

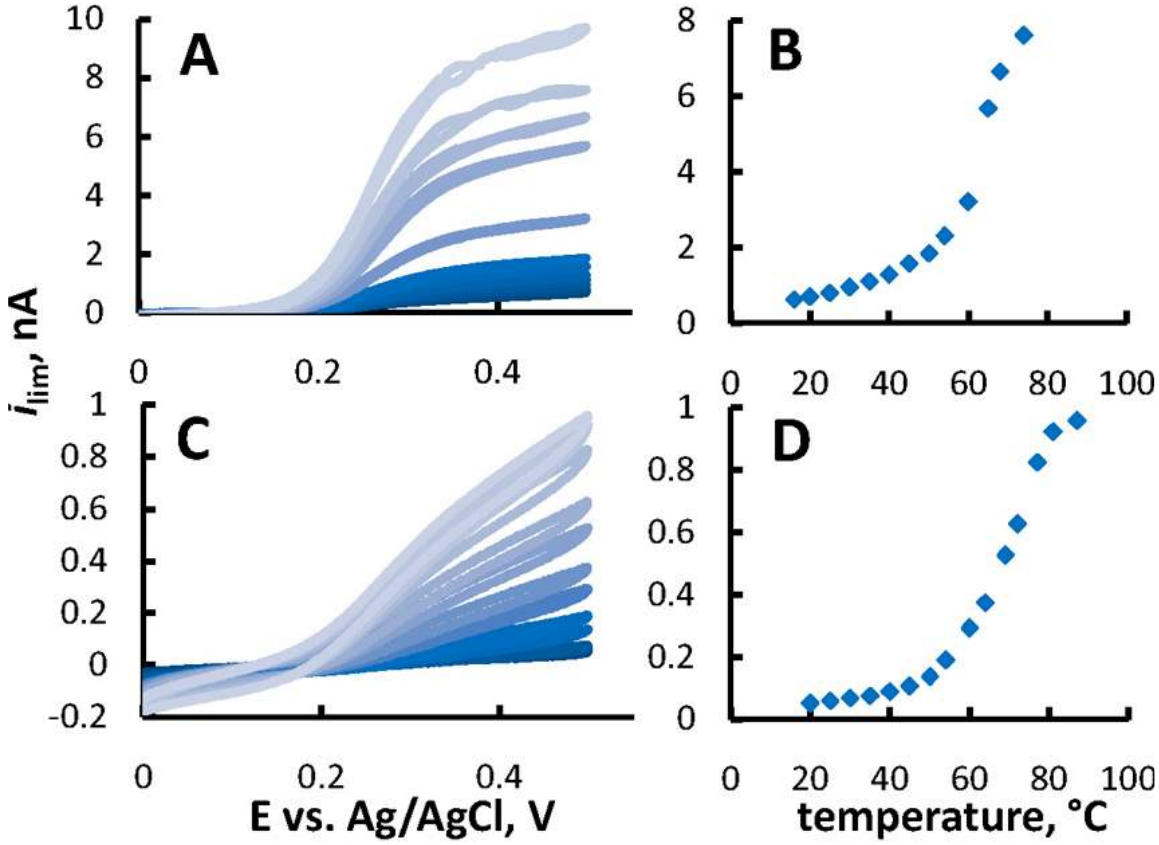

Figure 2.9. (A-C) Representative voltammetric responses, and (B-D) plots of $Fc(CH_2OH)_2$ limiting current as a function of temperature for poly(L-alanine)-colloidal film Pt electrodes after polymerization for 1 h and 3 h, respectively.

effects,[14,15] we examined the temperature-response of colloidal film electrodes for a neutral molecule, $Fc(CH_2OH)_2$. As can be seen in Figure 2.9, the limiting current for the modified colloidal film electrodes is affected by temperature. For all colloidal film electrodes the limiting current slightly increased with increasing temperature as a result of increasing diffusion coefficient.[16] We observed temperature effect for both thin and thick polymer brushes. For nanoporous films modified with a thinner polymer brush (polymerization time of 1 h), the limiting current increased with increasing temperature, with a transition temperature of ca. 65 ˚C (Fig. 2.9 A and B). For colloidal films modified with thick polymer brushes (polymerization time of 3 hours) a temperature response was observed at a higher temperature of ca. 75 ˚C (Fig. 2.9 C and D).

This difference in transition temperature has been studied for poly(L-alanine) in solution and on immobilized on a solid surface as well as with molecular dynamics simulations. Poly(L-alanine) has been immobilized onto a gold surface via self-assembly[17] and introduced via polycondensation,[18] in both cases forming α-helical structures, as demonstrated by IR. Poly(L-alanine) has also been grown on the surface of porous silica using NCA polycondensation.[19,20] In this work, IR spectroscopy was used both to confirm the attachment of the polypeptide to the surface and to show that the poly(L-alanine) attained a β-form structure. This is different from the α -helical conformation of the polymer in solution or on the gold surface and is attributed to the polymerization conditions at the silica surface. CD was also used to show the absence of helical conformation for the poly(L-alanine) when grafted onto a silica support. This is

also the case for poly(L-alanine) brushes on the surface of our silica colloidal films as described previously.

Molecular dynamics simulations have been carried out for poly(L-alanine) chain confirmation as a function of temperature. These simulations show that as temperature increases from low to high, polyalanine undergoes a transition to a random coil formation which is more compact other conformations of the polypeptide, for example, the β-form which is observed in our system. This effect is more pronounced for shorter poly(L-alanine) chains as the flexibility of the chain reduces the stability at terminal segments. Thus, the shorter the chain, the more likely it is for the ends to unravel, causing the whole helix to dissolve.[21]

We observe a similar effect in our polymer-modified colloidal films where shorter chains undergo a transition from extended to the more compact random coil at a lower temperature than longer chains. With this system, we are able to produce a temperature-responsive nanoporous colloidal film where the temperature at which the desired response is observed is tuned by changing the polymer brush length.

To verify that the temperature-responsive behavior described above results from the nanopore surface modification, the limiting current for glass-shrouded Pt microelectrodes carrying the unmodified colloidal film was examined. The resulting electrodes did not show a temperature-responsive behavior (except for a small increase in transport rates resulting from the change in the diffusion coefficients[16]).

The temperature-dependent change in the limiting current was reversible for both types of polymer brush. The nanoporous polymer-modified colloidal films could be cycled between low and high temperatures without apparent loss of responsiveness (Fig. 2.10). This indicates that our polymer-modified colloidal film Pt electrode is robust and re-usable as a material that can control molecular transport at the nanoscale by controlling the nanopore size.

pH-responsive behavior of poly(L-alanine)-modified colloidal films. The size of the polymer brush on the poly(L-alanine)-modified silica spheres was examined in aqueous solutions of different pH. Surprisingly, using dynamic light scattering, we found that the thickness of all poly(L-alanine) brushes on silica spheres was pH-dependent, with the polymer apparently extending at pH 3 and contracting at pH 11 and the overall average change in the polymer brush thickness of 7.5 nm from pH 3 to pH 6 and 3.5 nm from pH 6 to pH 11 (Fig. 2.11).

These observations led us to examine the pH response for poly(L-alanine)-modified colloidal films. The response was studied using cyclic voltammetry with $Fc(CH_2OH)_2$ as the redox-active species. As can be seen in Figure 2.12, the limiting current for the modified colloidal film electrodes is affected by pH. For poly(L-alanine)- modified colloidal films the limiting current increases with increasing pH. This suggests that as pH is increased, the polymer brush shrinks, increasing the colloidal pore size. This reverse is also true, as the limiting current decreases for decreasing pH indicating an elongation of the polymer brush. This trend, while smaller for colloidal films carrying thinner

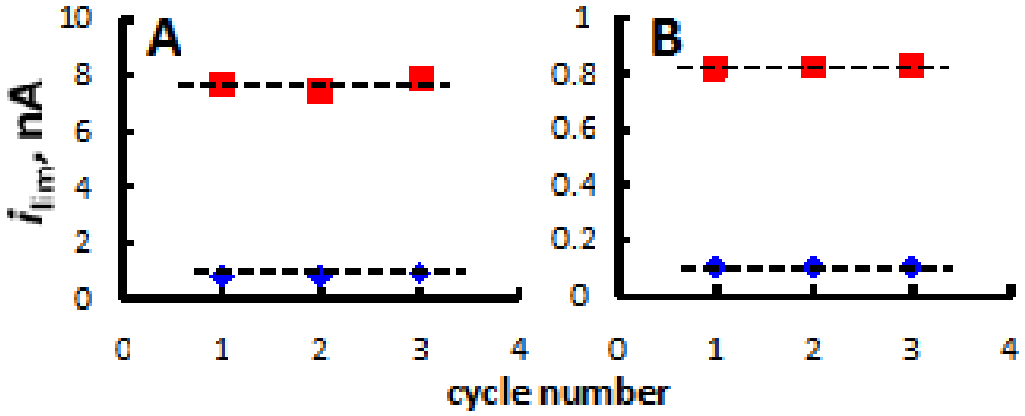

Figure 2.10. Limiting current at low (diamonds) and high (squares) temperature for poly(L-alaniny)-colloidal film Pt electrodes ($Fc(CH_2OH)_2$) after polymerization for (A) 1 h, and (B) 3 h, as a function of temperature cycling.

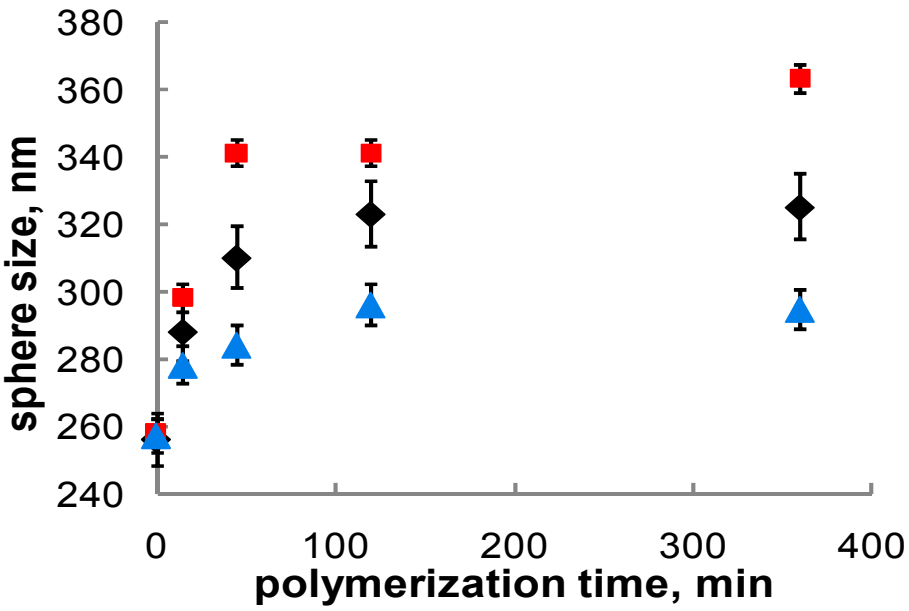

Figure 2.11. DLS measurements of poly(L-alanine)-modified silica nanoparticles in aqueous solution of pH 3 (squares), pH 7 (diamonds), and pH 11 (triangles).

polymer brushes, is consistent for the entire range of polymer brush sizes studied. The pH-dependent change in the limiting current is reversible for polymer brushes of various lengths. The nanoporous polymer-modified colloidal films could be cycled between low and high pH without apparent loss of responsiveness, as shown in Fig. 2.13. The observed pH responsive behavior may originate from the electrostatic interaction between the amine end-groups of the poly(L-alanine) brush and the residual amines on the silica surface in a manner similar to that described earlier for other types of surface-immobilized polymer brushes.[22,23] We speculate that at low pH both types of amine groups become protonated and their mutual repulsion leads to the polymer extension, as described above. Thus, at low pH the polymer brush blocks a larger portion of the nanopore volume. As the pH is increased the electrostatic repulsion decreases and the polymer brush attains a more compact conformation unblocking the nanopores. Such behavior is similar to that observed for the porous membranes modified with poly(L-glutamic acid).[24,25]

Further characterization of the pH response of poly(L-alanine)-modified silica colloidal films can be done by both measuring the surface charge on the surface of poly(L-alanine)-modified colloidal fims as pH is varied and with nanoIR, a combination of AFM and IR, which measures the composition of a sample at the nanoscale. This would help to elucidate the mechanism of the length change as IR can be used to determine the conformation of polyalanine on the surface of colloidal films.

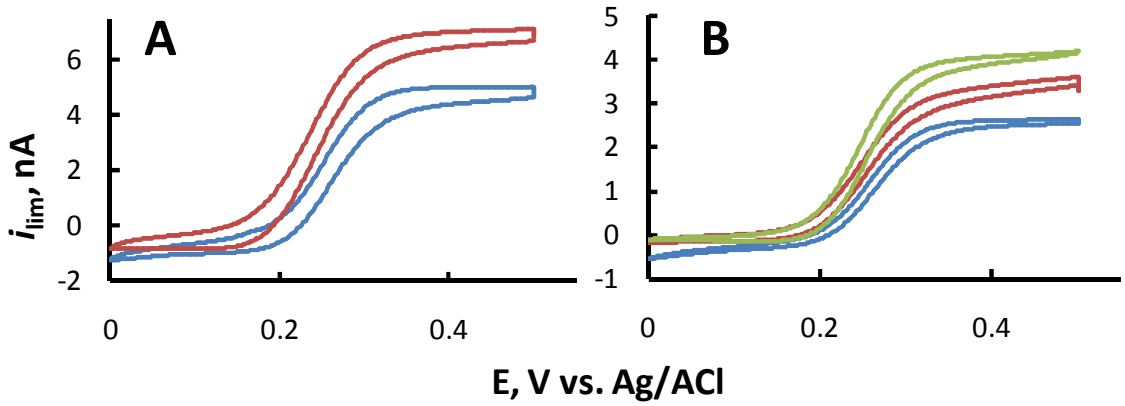

Figure 2.12. ($Fc(CH_2OH)_2$) voltammetric responses for colloidal film Pt electrodes surface-modified with poly-L-alanine for 3 h (A) and 6 h (B) at pH 3 (bottom line), pH 6 (middle line), and pH 8 (top line).

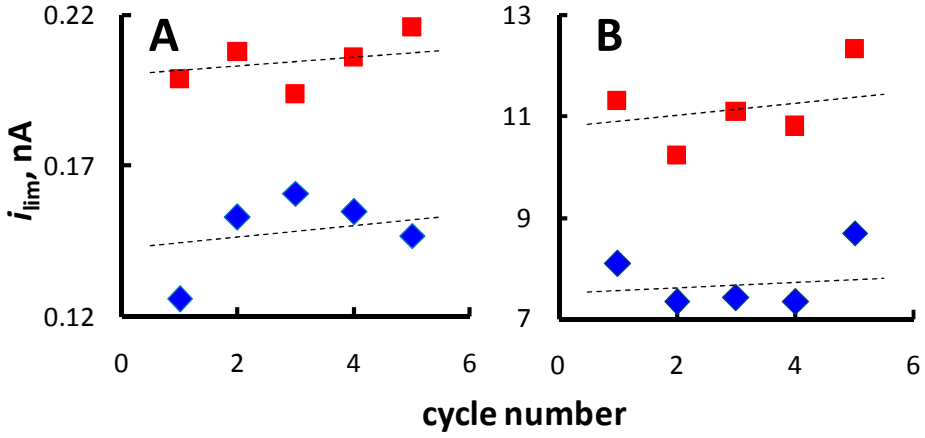

Figure 2.13. Limiting current at pH 3 (diamonds) and pH 11 (squares) poly (L-alanine)-colloidal film Pt electrodes ($Fc(CH_2OH)_2$) after polymerization for (A) 15 min, and (B) 3 h, as a function of pH cycling.

Conclusions

We demonstrated that surface-initiated polycondensation of L-alanine NCA inside colloidal nanopores does not perturb the colloidal lattice and leads to poly(L-alanine)-modified colloidal films. The length of the poly(L-alanine) brushes inside the nanopores can be controlled by the polymerization time. The films show both the temperature-responsive behavior with transition temperature around 60–70 º C depending on the polymer brush length, and a less pronounced pH-responsive behavior for the transport of neutral molecules, both resulting from conformational changes of the polymer inside the nanopores.

Thus, in addition to temperature response, we are able to show that one can vary the size of the nanopores by changing the pH, effectively demonstrating proof of concept that hybrid organic/inorganic systems using silica colloidal crystals as a platform can be used to control the transport of small molecules as they are modified with responsive polymers.

References

1. Stober, W.; Fink, A.; Bohn, E. J. *Colloid. Interface Sci.* **1968***, 26*, 62-69.

2. Newton, M. R.; Bohaty, A. K.; White, H. S.; Zharov, I. Z. *J. Am. Chem. Soc*, **2005**, *127*, 7268–7269.

3. Mahaligam, V.; Onclin, S.; Péter, M.; Ravoo, B. J.; Huskens, J.; Reinhoudt, D. N. *Langmuir*, **2004**, *20*, 11756–11762.

4. Dijk-Wolthuis, W. N. E.; Water, L.; Wetering, P.; Steenbergen, M. J.; Bosch, J. J. K.; Schuyl, W. J. W.; Henninck, W. E. *Macromol. Chem. Phys*., **1997**, *198*, 3893–3906.

5. Jiang, P.; Bertone, J. F.; Hwang, K. S.; Colvin, V. L. *Chem. Mater.* **1999**, *11*, 2132-2140.

6. Norris, D. J.; Arlinghaus, E. G.; Meng, L.; Heiny, R.; Scriven, L. E. *Adv. Mater.* **2004**, *16,* 1393-1399.

7. Meng, L.; Wei, H.; Nagel, A.; Wiley, B. J.; Scriven, L. E.; Norris, D. J. *Nano Lett.* **2006**, *6*, 2249-2253.

8. Dijk-Wolthuis, W. N. E.; Water, L.; Wetering, P.; Stenbergen, M. J.; Boxch, J. J. K.; Schuyl, W. J. W.; Hennick, W. E. *Chem. Phys.,* **1997**, *198,* 3893-3906.

9. Jal, P. K.; Patel, S.; Mishra, B. K. *Talanta,* **2004**, *62,* 1005-1028, and references therein.

10. Shundo, A.; Sakurai, T.; Takafuji, M.; Nagoaka, S.; Ihara, H*. J. Chromatogr. A.* **2005**, *1073*, 169–174.

11. Ihara, H.; Nakanishi, T.; Sagawa, C.; Hirayama, C.; Sakurai, T.; Kinoshita, T.; Tsujita, Y. *Chem. Lett.* **1998**, *27*, 963-964.

12. Bard, A. J.; Faulkner, L. R. Electrochemical Methods: Fundamentals and Applications, 2nd ed.; Wiley: New York, 2001.

13. Wang, J.; Li, Q.; Knoll, W.; Jonas, U. J. *J. Am. Chem. Soc*, **2006**, *128*, 15606–15607.

14. Newton, M. R.; Bohaty, A. K.; White, H. S.; Zharov, I. *J. Am. Chem. Soc.*, **2005**, *127*, 7268–7269.

15. Newton, M. R.; Bohaty, A. K.; Zhang, Y.; White, H. S.; Zharov, I. *Langmuir*, **2006**, *22*, 4429–4432.

16. Cussler, E. L., *Diffusion. Mass Transfer in Fluid Systems*, Cambridge University Press, Cambridge, 2nd edn, 1997.

17. Sek, S.; Tolak, A.; Misicka, A.; Palys, B; Bilewicz, Z. *J. Phys. Chem. B,* **2005**, *109*, 18433–18438.

18. Whitesell, J. K.; Chang, H. K. *Science*, **1993**, *261*, 73–76.

19. Shundo, A.; Sakurai, T.; Takafuji, M.; Nagoaka, S.; Ihara, H. *J. Chromatogr. A*, **2005**, *1073*, 169–174.

20. Ihara, H.; Nakanishi, N.; Sagawa, T.; Hirayama, C.; Sakurai, T.; Kinoshita, T.; Tsujita, Y. *Chem. Lett*, **1998**, *27*, 963–964.

21. (a) Shental-Bechor, D.; Kirca, S.; Ben-Tal, N.; Haliloglu, T. *Biophys. J.,* **2005**, *88*, 2391–2402. (b) Nguyen, H. D.; Marchut, A. J.; Hall, C. K. *Protein Sci*, **2004**, *13*, 2909–2924. (c) Job, G. E.; Kennedy, R. J.; Heitmann, B.; Miller, J. S.; Walker, S. M.; Kemp, D. S. *J. Am. Chem. Soc*, **2006**, *128*, 8227–8233.

22. Ballauff, M.; Borisov, O. *Curr. Op. Colloid and Interface Sci.,* **2006**, *11,* 316-323.

23. Konradi; Rueh, J.; *Macromolecules*, **2005**, *38*, 6140–6151.

24. Smulaec, V.; Butterfield, D. A.; Bhattacharyya, *Chem. Mater.*, **2004**, *16*, 2762–2771.

25. a) Ito, Y.; Park, Y. S.; Imahishi, Y. *Langmuir*, **2000**, *16*, 5376–5381. b) Ito, Y.; Park, Y. S.; Imahishi, Y. *J. Am. Chem. Soc*, **1997**, *119*, 2739–2740.

CHAPTER 3

POLY (L-ALANINE) MODIFIED FREE-STANDING OPAL FRITS

Introduction

This chapter focuses on the preparation of poly (L-alanine) modified, free-standing, nanoporous membranes (opal frits). Opal frits are prepared in a similar manner to colloidal films on the surface of Pt mictodisk electrodes, however, they are much more robust due to increased thickness of the film and due to the sintering process which physically bonds the spheres together as they are heated to >1000 ºC. Previous work in our group has focused on opal frits modified with amines, which impart ion selective transport capabilities on the membrane.[1,2,3,4] In this chapter, I will describe the modification of 0.75 mm thick opal frits with poly (L-alanine) brushes, and my study of the transport of a neutral dye molecule, tannic acid, through the membrane as a function of pH.

Experimental Section

Materials

Chemicals and materials. (3-Aminopropyl) triethoxysilane (99%, Aldrich), phosphorus trichloride (99%, Aldrich), tetraethoxysilane, TEOS (99.999+%,

Aldrich), N-(tert-Butoxycarbonyl)-Lalanine (>99%, Fluca), Tannic acid (Alfa Aesar) and potassium chloride (99%, Mallinckrodt) were used as received. N,N-Dimethylformamide, DMF (99.9%, Fisher Scientific) was dried over molecular sieves. Acetonitrile (Mallinckrodt) was distilled from CaH_2 before using. 18 MΩ cm water was obtained from a Barnsted ‘‘E-pure’’ water purification system. Reagent grade solvents were used except for absolute ethanol and anhydrous MeOH. All ethanol used was 200 proof.

PTFE flat washers (5.16mminner diameter, 14.27 mm outer diameter, and 1.02 mm thickness were purchased from Small Parts, Inc. and used as received. Loctite Hysol 0151 Epoxy was used as received.

Instrumentation. Dynamic light scattering (Brookhaven ZetaPALS) was employed to measure size of unmodified silica spheres. To characterize the surface composition of polymer-modified opal frits, thermogravimetric analysis (TGA) (TGA Q500, TA Instruments) was performed. Scanning electron microscopy (JEOL JSM-6335F) was used to image unmodified and polymer-modified membranes. All samples were coated with gold for use with SEM. A Branson 1510 sonicator (50-60 Hz) was used for all sonications. UV/Vis measurements were performed using an Ocean Optics USB2000 or USB4000 instrument.

Methods

Preparation of ~200 nm silica spheres. Silica spheres were prepared as described in Chapters 2 and 3. All glassware was cleaned with 18 MΩ·cm water.

Silica nanoparticles were prepared following the literature procedure.[5] A solution of tetraethoxysilane (TEOS) in absolute ethanol was rapidly poured into a stirred mixture of ammonia and water in absolute ethanol at room temperature. The final concentrations of the reagents were 0.2 M TEOS, 0.4 M ammonia and 17 M water. The reaction mixture was covered and stirred for 18 h. The silica spheres were isolated by repeated centrifugation and resuspension 15 mL centrifuge tubes (Corning) for 10 min at 1163 g. After the spheres were collected from the original reaction mixture, the supernant was removed and the spheres were dispersed in absolute ethanol by sonication for 30 min. The diameter of the spheres was found to be 218 ± 27 nm using scanning electron microscopy (SEM) and 255 ± 26 nm using dynamic light scattering (DLS). The size difference can be attributed to swelling as spheres are suspended in aqueous media for DLS measurements. A general scheme of silica sphere preparation is shown in Figure 3.1.

Calcination of the silica spheres was achieved by placing them in a Petri dish and crushing any aggregates with a spatula. The Petri dish with the silica sphers was placed in a furnace which heated the spheres for 4 h at 600 ºC.[6,7,8] The furnace was heated at a rate of 20 ºC per minute. After heating, the spheres were allowed to cool to room temperature. SEM images of the spheres were obtained and 100 individual silica spheres were measured to determine the average size of 203 ± 27 nm. SEM images of as made silica nanoparticles and calcinated nanoparticles are shown in Figure 3.2.

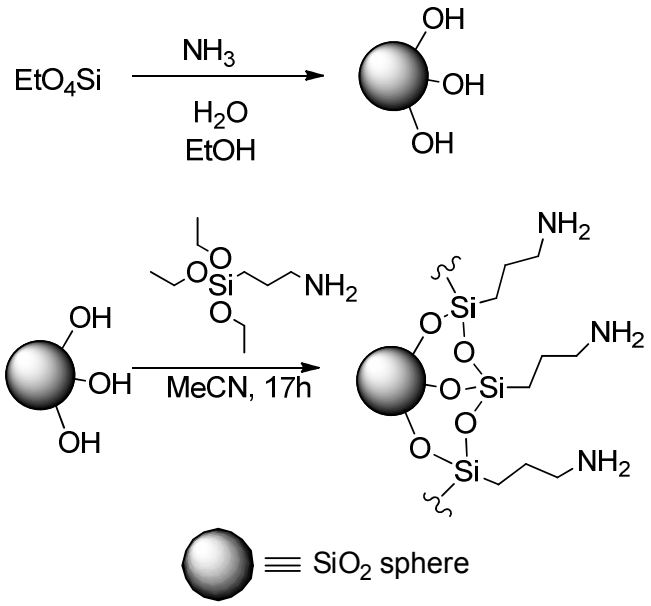

Figure 3.1. Silica sphere preparation and amination of silica spheres.

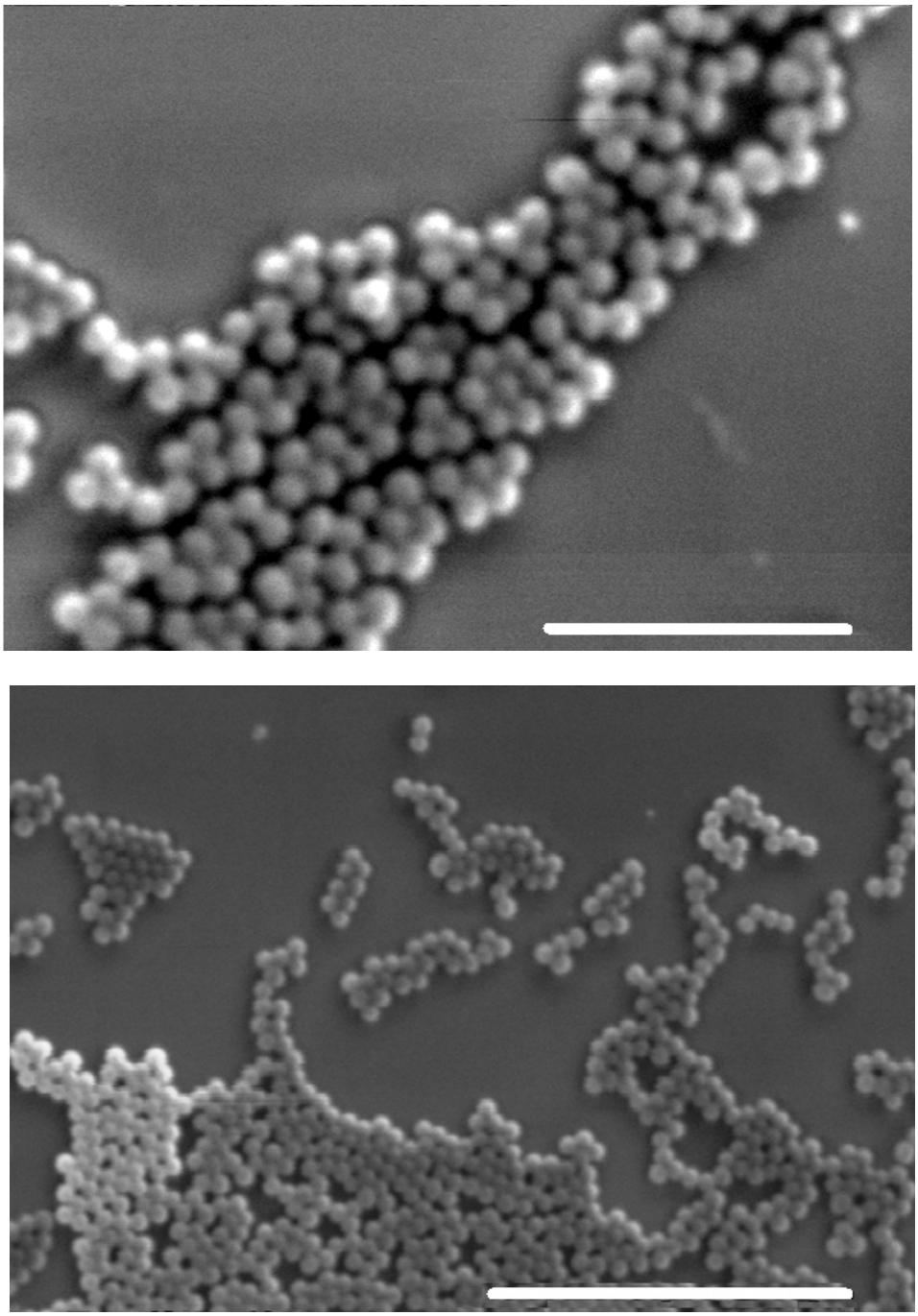

Figure 3.2. SEM images of silica nanoparticles. Top: As made nanoparticles (size bar = 10 μm.) Bottom: calcinated silica nanoparticles (size bar = 50 μm).

Preparation of free-standing colloidal membranes. Colloidal frits were prepared by placing a glass slide vertically into a 50 mL beaker containing ~12 wt% colloidal solution of calcinated silica nanoparticles sonicated in ethanol. The beaker was placed under a crystallization dish elevated 6 cm off the bench in a hood free of any major vibrations and the solvent was allowed to evaporate for 1-2 days. The remaining colloidal film is 200-500 μm thick on the glass slide and beaker sides. The colloidal film was removed from the slide by gently breaking it with a razor. The films were then placed directly on the surface of the furnace and heated to 1050 ºC for 12 h at a rate of 20 ºC per minute to sinter the silica spheres, making the free-standing membrane more robust. After 12 h, the pieces of membrane were allowed to cool to room temperature inside the furnace. The size of the silica nanoparticles after the sintering process is determined by SEM to be 190 ± 16 nm.

Rehydroxylation of colloidal frits. Sintered colloidal membranes were rehydroxylated before further modification by placing the pieces in a 125 mL polyethylene bottle containing 100 mL of a pH 9.5 solution tetrabutylammonium hydroxide in deionized water. The bottle was placed in a 60 ºC oil bath and heated for 24 h.[9] The rehydroxylated pieces were washed with deionized water (2 x 100 mL), 1 M nitric acid (2 x 100 mL), methanol (2 x 100 mL), deionized water (2 x 100 mL), and acetonitrile (2 x 100 mL). The pieces were stored in acetonitrile until further modification.

Modification of colloidal frits with amines. Amine functionalization of silica colloidal frits was achieved in a similar manner as described in Chapter 2. The

frits were placed in a solution of 0.20 mL (0.85mmol, 0.056 M) (3-amino-propyl)triethoxysilane in 15 mL of dry acetonitrile under nitrogen in a dry 20 mL scintillation vial at room temperature for 24 h. After 24 h the pieces were soaked in pure acetonitrile for 2 h (2 x 20 mL) and either used to construct the colloidal frit membrane, further modified with poly (L-ananine), or the amine modification procedure was repeated a second time. In the latter case, the length of time for the APTES modification following the above procedures was 24 h as well. The nanofrit pieces were soaked in pure acetonitrile for 2 h (2 x 20 mL) and used in colloidal frit membrane construction or further modification with poly (L-alanine) was carried out.

Preparation of L-alanine N-carboxyanhydride. L-alanine N-carboxyan-hydride was prepared following the literature procedure as described in Chapter 2.[10] N-tert-butyloxycarbonyl alanine (0.005 mol, 0.95g) was dissolved in methylene chloride (25 mL) under a nitrogen atmosphere and cooled to 0˚C in an ice bath. Phosphorus trichloride (0.006 mol, 0.524 mL) was added to the solution. The reaction mixture was stirred for 4 h at 0˚C, the solvent was removed under reduced pressure and the residue washed with 20 mL of carbon tetrachloride three times to afford the N-carboxy amino acid anhydride (Chapter 2 Figure 2.3). ^{1}H NMR (300 MHz, $CDCl_3$): δ: 5.83 (s, 1H), 4.44-4.40 (m, 1H), 1.58 (d, 3H).

Modification of nanofrits with poly(L-alanine). Polymer modification of silica nanofrits was conducted using the reaction shown in Figure 3.3. Silica nanofrits were soaked in *N*,*N*-dimethylmethanamide (DMF) for 6 h prior to

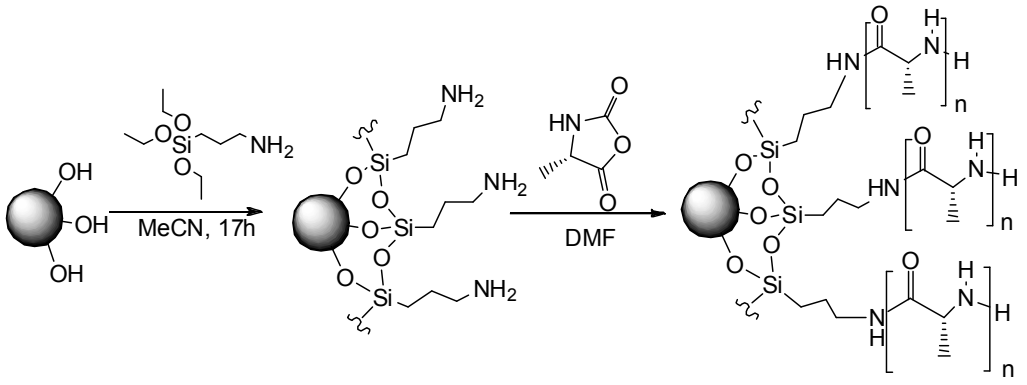

Figure 3.3. Preparation of Poly(L-alanine)-modified Silica Nanoparticles.

modification. The L-alanine N-carboxy amino acid anhydride (0.01 g) was dissolved in fresh DMF (20 mL) and the frits placed into the solution for 20 min, 30 min, 1 h, and 2 h and 1 h two times. After the allotted polymerization time, polymer-modified nanofrits were purified by washing with E-pure water for 1 h (2 x 100 mL). SEM was used to determine the size of the polymer brush on the surface of the nanofrit.

Diffusion measurements through nanofrits. Nanofrit pieces were placed between two PTFE flat washers coated with Loctite Hysol 0151 Epoxy on the inner lip of the washer, so that the epoxy came in contact with the nanofrits. The membranes were allowed to cure for 24 h before any diffusion measurements were performed. Room-temperature diffusion measurements through the colloidal frits were conducted by placing a nanofrit comprised of bare, 1 x amine modified, 2 x amine modified, 1 x amine modified with poly (L-alanine) or 2 x amine modified with poly (L-alanine) silica spheres between two connected 1 cm quartz cuvettes. One of the cuvettes contained 4 mL of either 0.1 M tannic acid at pH 3.0 or 0.1 M tannic acid at pH 6.5 in E-pure water. The other cuvette

contained 4 mL of E-pure water. The nanofrit was placed between two Kalrez o-rings to prevent leaking, and a clamp was used to hold the cuvettes, o-rings, and colloidal membrane in place. Each cuvette contained a stir bar and was covered with Parafilm to prevent evaporation. The cuvette containing the receiving solution was then placed in the cuvette holder between two fiber optic cables, and the solution was blanked. Both solutions were stirred, and the dye diffusion rate was measured by recording the absorbance in the receiving cuvette at a wavelength of 419 nm for at least 18 h while stirring both solutions. Data points were recorded every 150 s with an initial delay of 150 s. All measurements were repeated in triplicate.

Results and Discussion

Poly (L-alanine)-Modified Free-Standing Opal Frits

SEM of sintered and polymer-modified nanofrits. Silica nanoparticles were calcinated to prevent cracks in the nanofrit membrane during the sintering process. This allows solvents (water and ethanol) trapped inside the silica nanoparticles to be released, effectively preshrinking the spheres in preparation for the sintering process. Silica nanofrits are formed via vertical deposition of calcinated nanoparticles, followed by sintering. The resulting frits are free from cracks over a large area, and relatively free from point defects in the lattice which are small and only penetrate the first or second layer when they do occur. An SEM image of the sintered membrane is shown in Figures 3.4. The resulting sintered colloidal membranes are very durable and can be handled and

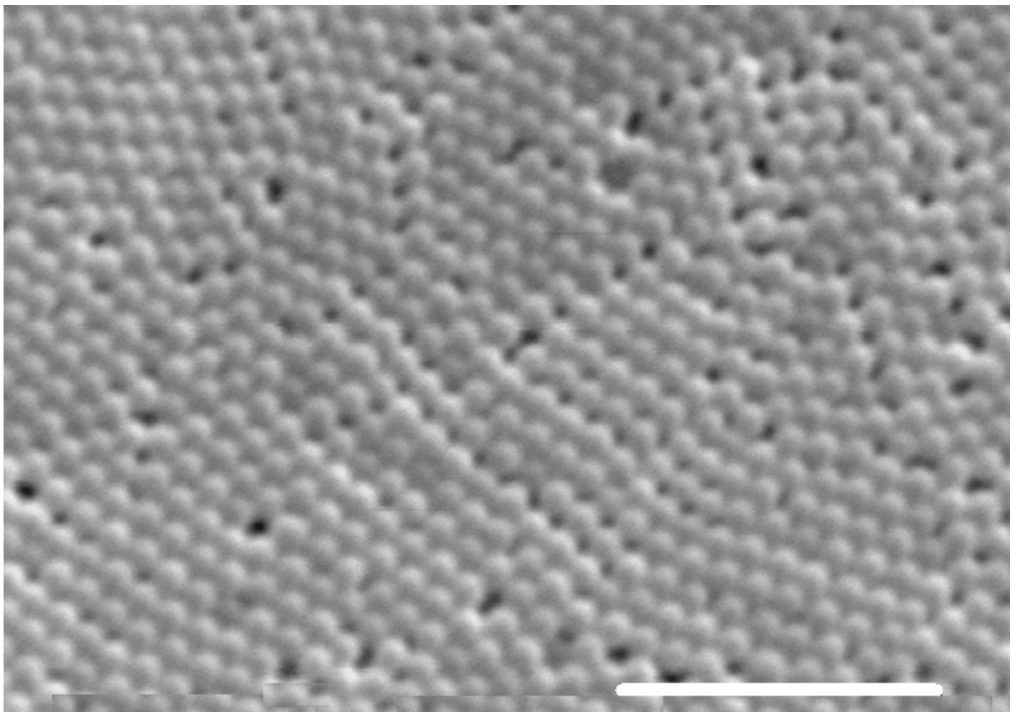

Figure 3.4. SEM image of sintered colloidal frit (scale bar = 10 μm).

sonicated.

In order to model the polymer formation process the size of the polymer-modified nanoparticles was measured by SEM (Table 3.1). Nanofrits modified with amine moieties followed by poly(L-alanine) modification showed increased size by 23 nm. An SEM image of a silica nanofrit modified with amines followed by poly(L-alanine for 20 minutes is shown in Figure 3.5. As described in Chapter 1, pore size is ca. 15% of the nanopore diameter. Thus, for 190 nm silica nanoparticles, the pore size is ~29 nm, indicating that polymerization for 20 min produces a polymer that sufficiently blocks the nanopores of the free-standing nanofrit. This observation also indicates that polymer grows longer on nanoparticles on the surface of free-standing nanofrits than inside the nanopores. We observed that polymer-modified nanofrits generally exhibit a greater amount of disorder than unmodified membranes which is most likely the result of repeated immersion in reaction solutions that may perturb the surface layers, however these defects only extend one or two layers.

Thermogravametric analysis of unmodified and polymer-modified colloidal membranes. Thermogravametric analysis produced results as shown in Figure 3.6. For bare nanofrits, we observe a smooth weight loss of ~0.07 % continuing to 500 ºC, likely due to surface water. Amine-modified and polymer-modified colloidal membranes also undergo a weight loss at above 150 ºC. For amine-modified membranes, a 0.09% weight loss above 150 ºC is observed. This weight loss is used to calculate the number of amines/ nm^2 on the surface of the colloidal membrane, which is 0.46 initiator moieties/nm^2. The number of

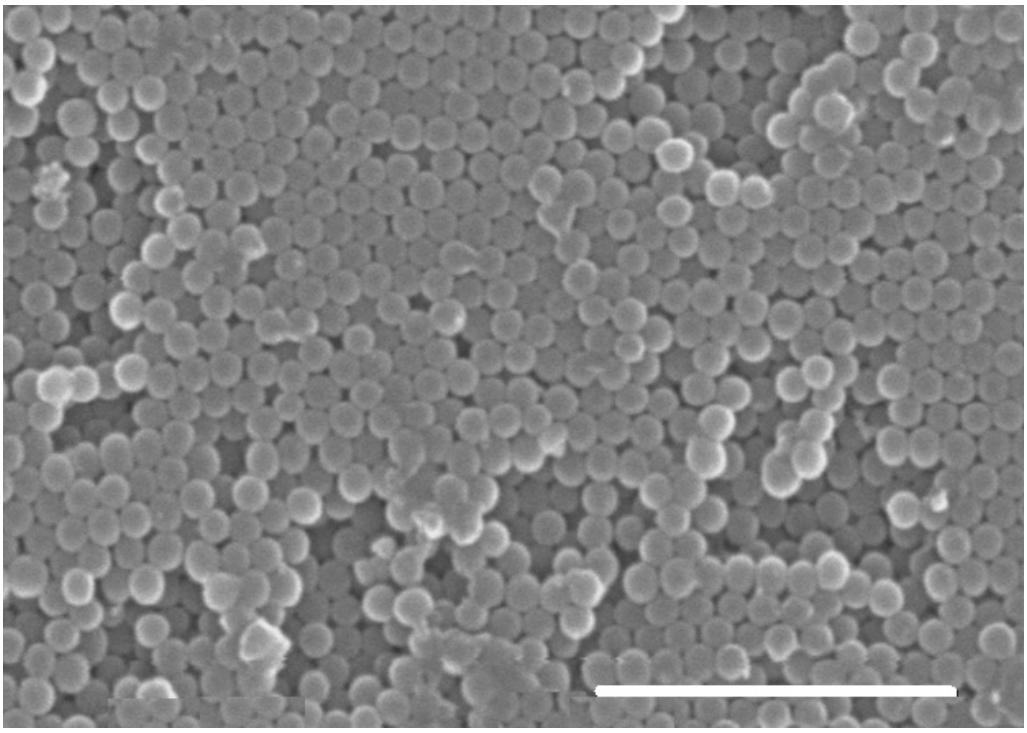

Figure 3.5. SEM image of silica nanofrit modified with poly (L-alanine) for 20 min (scale bar = 25 μm).

Table 3.1. Polymerization time with respect to nanoparticle growth for poly (L-alanine) modified nanofrits.

Nanofrit Modification	Size (SEM)	∆ Polymer length (radius)
Sintered	190 ± 16 nm	0 nm
Amine-modified	213 ± 21 nm	11.5 nm
Poly(L-alanine) 20 min	236 ± 18 nm	23 nm

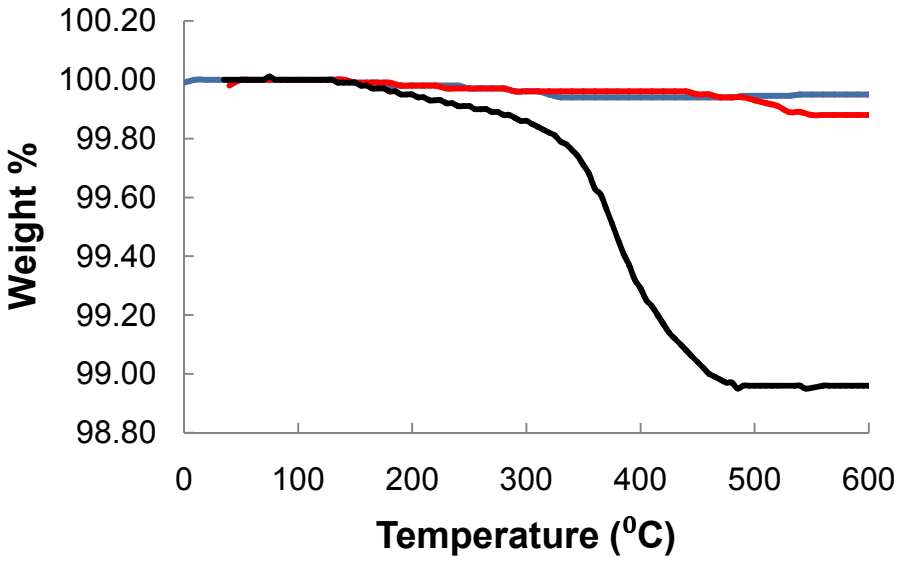

Figure 3.6. Thermogravimetric analysis (TGA) plots for unmodified (top line, blue), amine modified (second line from top, red), poly(L-alanine)-modified 20 minutes(bottom line, black), nanofrits.

initiators/nm^2 is used to calculate the length of the poly(L-alanine) chain as shown in Table 3.2. Chain length calculations are based on each initiator being a site of polymerization. Based on these results, we see that polymer is forming not only on silica nanoparticles on the surface of the nanofrit, but inside the nanopores as well.

pH selectivity of unmodified and poly(L-alanine)-modified colloidal frits. Diffusion through these membranes was measured spectrophotometrically for a 0.1 M aqueous solution of tannic acid (λ_{max} = 419 nm) at either pH 3.0 or 6.5 through poly(L-alanine)-modified colloidal frits by recording the absorbance of the diffusing dye molecule with respect to time, as in Chapter 5, Tannic acid was chosen because it is a neutral, water soluble dye molecule with a relatively high extinction coefficient (ε = 9.97 ± 1.94, calculated from a calibration curve). This probe molecule is neutral at pH 7 and will not experience any electrostatic interactions with the polymer-modified colloidal membrane. The structure of tannic acid is shown in Figure 3.7.

The diffusion apparatus is shown in, Figure 3.8. Table 3.3 shows the

Table 3.2. TGA unmodified and polymer-modified nanofrits showing percent weight loss and calculated amount of monomers/nm^2.

Nanofrit Modification	Total Weight Loss, %	weight loss above 150 ºC, %	Initiators per nm^2	Monomers/ Initiator
Unmodified	0.07	0.00	0.0	-
Amine-modified	0.13	0.09	0.46	-
Poly(L-alanine) 20 min	1.04	0.99	-	12.3

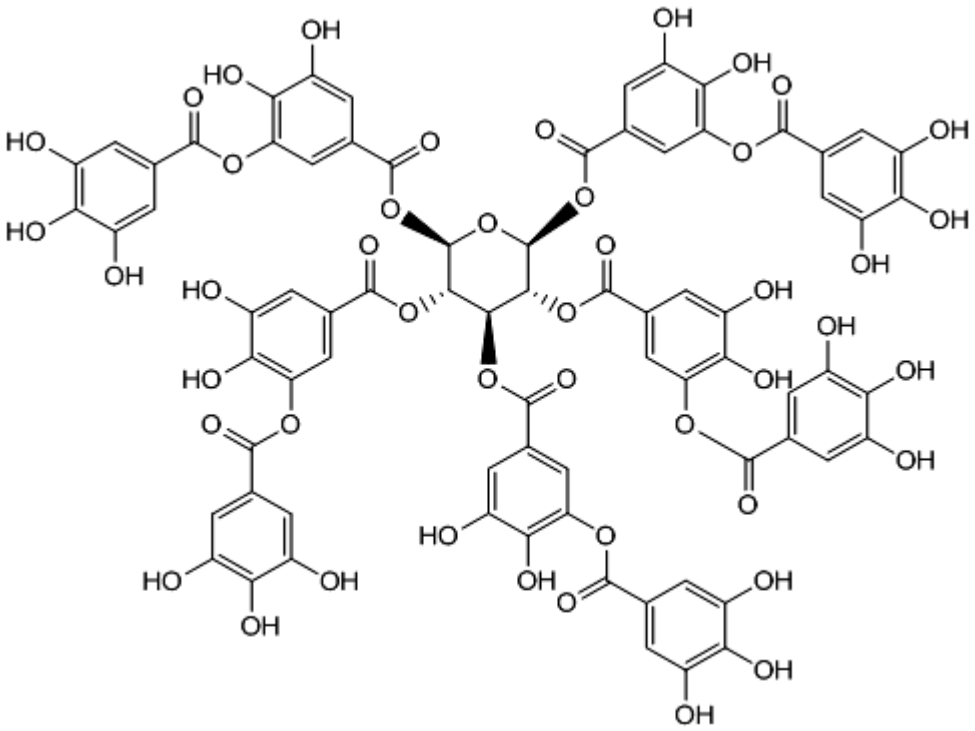

Figure 3.7. Structure of Tannic Acid.

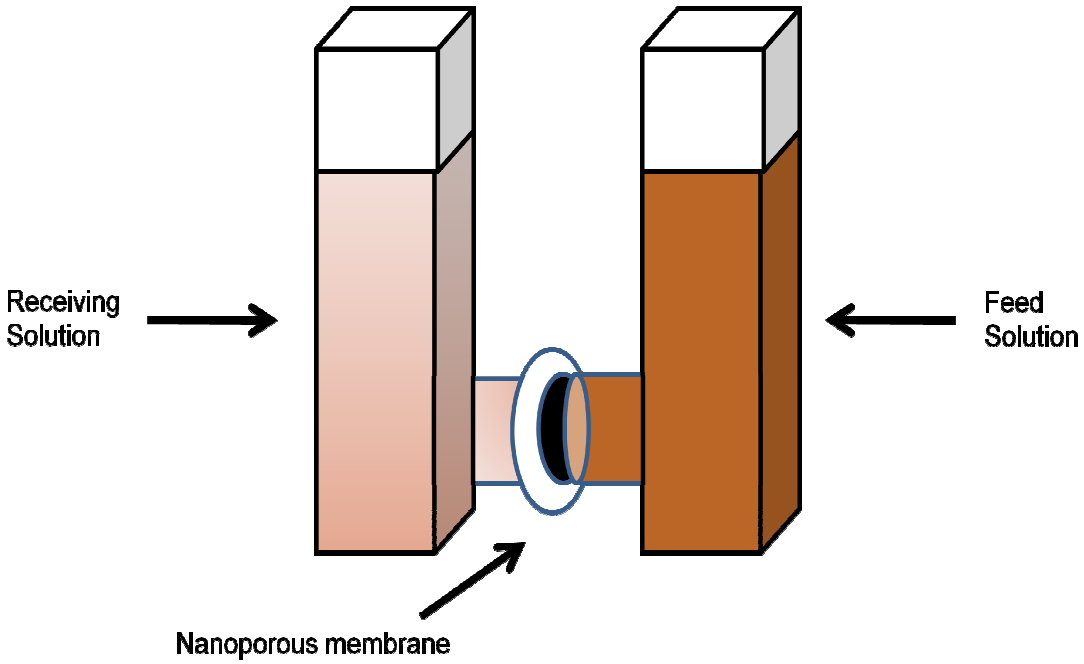

Figure 3.8. Illustration of the basic set-up used to conduct diffusion measurements through free-standing membranes.

Table 3.3. Diffusion rate of tannic acid through unmodified and modified colloidal membranes.

Diffusion Rate, mol/s × 10^{-12}			
Colloidal Frit	pH 6.5	pH 3.0	rate change , %
Amine-Modified	2.16 ± 0.33	2.06 ± 0.53	-4.63
Poly(L-alanine) 20 min	2.2 ± 0.03	1.4 ± 0.16	- 36.36

diffusion rate of tannic acid through unmodified and modified membranes. The results shown are reproducible regardless of previous membrane use; however, care must be taken to wash the membranes thoroughly with Millipore water after each diffusion experiment to avoid clogging the pores.

For amine-modified frits there is a 4.63 % drop in diffusion at pH 3.0. This is likely due to electrostatic interactions of the tannic acid with surface amines, causing the tannic acid to bind to the surface of the frit in acidic conditions.

For poly(L-alanine)-modified membranes, the diffusion of tannic acid decreased as pH decreased to a more acidic environment. Chapter 2 describes the behavior of poly(L-alanine) brushes on the surface of silica as pH is varied. Specifically, under acidic conditions, the poly(L-alanine) brush expands on the surface of silica compared to a more basic environment thus effectively reducing the nanopore size leading to hindered tranport.[11] We believe that this is the case here.

Future work on this system would involve varying the length of the poly (L-alanine) polymer to tune the selectivity by changing nanopore size. The polymer used in this study was found to be ca. 23 nm long, sufficiently blocking the nanopores. With shorter polymer chains, we may be able to observe a greater

change in the amount that the polymer brush expands and collapses due to having greater freedom inside the nanopore. This will allow for gated transport of a diffusing species when pH is changed from high to low.

Conclusion

We have prepared free-standing, polymer-modified nanofrits which exhibit permeability controlled by pH. The diffusion rate of a neutral dye, tannic acid is slower in acidic solutions than at neutral pH due to elongation of the polymer brush at low pH. These membranes show a proof of concept that polymer-modified nanofrits may be useful in applications where controlled transport is desirable. These results indicate that these free-standing membranes behave in a similar fashion as colloidal film pt electrodes. This is useful as these free-standing membranes can potentially be used for selective separations. Another advantage of these frits is their large surface area, relatively high molecular flux through the frit, and increased robustness from thin films formed using silica colloidal crystals.

References

1. Bohaty, A.; Smith, J.; Zharov, I. *Langmuir.* **2009**, *5*, 3096-3101.

2. Schepelina, O.; Poth, N.; Zharov, I. *Adv. Funct. Mater*. **2010**, *20*, 1962-1969.

3. Bogush, G. H.; Tracy, M. A.; Zukoski IV, C. F. *J. Non-Cryst. Solids*, **1988**, *104*, 95-106.

4. Lee, V. T.; Ross, E. E.; Velarde, T. R. C.; Legg, M. A.; Wirth, M. J. *Langmuir,* **2007**, *23,* 8554-8559.

5. Stober, W.; Fink, A.; Bohn, E. J. *Colloid. Interface Sci.* **1968***, 26*, 62-69.

6. Chabanov, A. A.; Jun, Y.; Norris, D. J. *Appl. Phys. Lett.* **2004**, *84*, 3573–3575.

7. Lee, T. V.; Ross, E. E.; Velarde, T. R. C.; Leg, M. A.; Wirth, M. J. *Langmuir*. **2007**, *23*, 8554-8559.

8. Zheng, S.; Ross, E.; Legg, M. A.; Wirth, M. J. *J. Am. Chem. Soc*. **2006**, *128*, 9016-9017.

9. Chabanov, A. A.; Jun, Y.; Norris, D. J. *Appl. Phys. Lett.* **2004**, *84*, 3573–3575.

10. Dijk-Wolthuis, W. N. E.; Water, L.; Wetering, P.; Steenbergen, M. J.; Bosch, J. J. K.; Schuyl, W. J. W.; Henninck, W. E. *Macromol. Chem. Phys*., **1997**, *198*, 3893–3906.

11. Abelow, A. E.; Zharov, I. *Soft Matter*, **2009**, *5*, 457-462.

CHAPTER 4

APTAMER-MODIFIED RESPONSIVE NANOPOROUS SILICA COLLOIDAL FILMS

Introduction

In Chapters 2 and 3, we demonstrated that supported and free-standing colloidal films can be modified with a polypeptide brush and showed that molecular transport can be controlled using pH and temperature. This chapter focuses on modifying the surface of silica nanoparticles and colloidal films with an oligonucleotide-based binder, or aptamer, which will impart permselectivity based on electrostatic interactions with a small molecule. The mechanism of this observed permselectivity will be elucidated by measuring the molecular flux of a neutral redox molecule through the bare, initiator modified, and aptamer-modified colloidal film in response to the binding of a small molecule.

Experimental Section

Materials

Chemicals. (3-Aminopropyl) triethoxysilane (99%) and tetraethoxysilane (TEOS, 99.999+%) were obtained from Aldrich and used as received. 1,1´-Ferrocenedimethanol, $Fc(CH_2OH)_2$ (98%, Aldrich), potassium chloride (99%,

Mallinckrodt) were used as received. Acetonitrile (Mallinckrodt) was distilled before using. 18 MΩ·cm water was obtained from a Barnsted "E-pure" water purification system. Mercaptohexanol was obtained from Aldrich and used as received. Diethyl ether was obtained from Mallinckrodt and used as received. Succinimidyl 4-[N-maleimidomethyl]cyclohexane-1-carboxylate, SMCC (>99%) and tris(2-carboxyethyl) phosphine hydrochloride, TCEP·HCl, were from Pierce (Rockford, IL) and used as received. *N*,*N*-Dimethylformamide (DMF, 99.9%) was obtained from Fisher Scientific and was dried over molecular sieves. 4-Dimethylaminopyridine, DMAP (>99%, Aldrich), was used as received. Tris-EDTA buffer solution (Sigma) was used as received. Cocaine hydrochloride was received from Sigma-Aldrich and stored at 2-8 ˚C until use. 3-amino-propyldimethylethoxysilane, $(EtO(Me)_2Si(CH_2)_3NH_2$, (Gelest, Inc.) was used as received.

The DNA aptamer was synthesized (Biosource International, Camarillo, CA) for the preparation of the electrochemical cocaine biosensor. The aptamer sequence was based on the oligonuclotide sequence developed by Stovanovic.[1] The sequence, AGACAAGGAAAATCCTTCAATGAAGTGGGTCG, was modified with a six-carbon disulfide group at the 5' terminus. The aptamer was purified by HPLC and PAGE, and its sequence was verified by mass spectrometry.

Methods

Preparation and modification of silica spheres in solution. 100 nm and 290 nm silica nanoparticles were prepared following the literature procedure

developed by Stöber and coworkers.[2] A solution of tetraethoxysilane (TEOS) in absolute ethanol was rapidly poured into a stirred mixture of ammonia and water in absolute ethanol at room temperature. The final concentrations of the reagents were 0.2 M TEOS, 0.4 M ammonia and 17 M water for 290 nm silica nanoparticles, and 0.2 M TEOS, 0.2 M ammonia and 17 M water for 100 nm nanoparticles. The reaction mixture was stirred for 18 hours. The silica spheres were isolated by repeated centrifugation and re-suspension in absolute ethanol. The diameter of the spheres was found to be 290 ± 2.5 nm and 93 ± 12 nm, respectively, using dynamic light scattering (DLS).

Amine functionalization of silica spheres was achieved by reacting the nanoparticles in a solution of 0.056 M 3-aminopropyl-triethoxysilane in dry acetonitrile at room temperature for 17 h followed by centrifugation and resuspension in acetonitrile. The presence of amino groups was confirmed by treating the silica spheres with dansyl chloride, followed by fluorescence measurements, as previously described.[3]

Preparation of colloidal film electrodes. Pt microdisk electrodes (25 μm in diameter) shrouded in glass were prepared as described in Chapter 2. First a 1.0-mm-diameter Cu wire (Alfa Aesar) is attached to a 25μm-diameter Pt wire using Ag paint (DuPont). The Pt wire was then flame sealed in a glass capillary which was then bent into a U-shape and cut orthogonal to the length of the capillary with a diamond saw to expose the Pt disk. The resulting electrodes were polished with Microcut Paper disks (Buehler), from 240 to 1200 grit in succession, until the surface was free from visible defects.

The colloidal films were deposited onto the Pt and the glass shroud by placing the electrodes vertically into 1.5 wt% colloidal solution of silica spheres in ethanol. The vials were placed under a crystallization dish and the solutions were allowed to evaporate for 3 days in a vibration-free environment.

Preparation of maleimide-activated silica spheres.[4] Amine-functionalized silica nanoparticles (1 mg) were first dried under vacuum for 24 h. SMCC (2.8 mg, 6.7 μmol) and DMAP (1.1 mg, 8.9 μmol) were added to the dried nanoparticles in DMF (5 mL) and the reaction mixture was stirred in the dark at room temperature for 24 h. The resulting maleimide-acitivated silica was collected by centrifugation and washed with DMF (×10), and 10 mM potassium phosphate buffer pH 7.0 (× 3) and used immediately.

Activation of the aptamer.[5] The activated aptamer was prepared by combining 0.2 mM aptamer stock solution in ×1 Tris buffer with 10 mM aqueous TCEP·HCl at a 1:1 (v/v) ratio and allowing to react for at least 2 h at 4 °C and used in the preparation of aptamer-modified silica nanoparticles without further purification.

Preparation of aptamer-modified silica nanoparticles.[6] The aptamer/TCEP solution (6.75 mL) was combined with 100mM NaCl/10mM potassium phosphate buffer pH 7.0 (18.9 mL) to make the aptamer solution. The maleimide-activated silica nanoparticles (~0.5 mg) were then dispersed into the solution and the reaction was allowed to stir in the dark for 25 min.

Passivation of silica surface.[5] Passivation of the area of the amine-modified silica surface still exposed after aptamer immobilization was achieved

by stirring the nanoparticles in 2 mM mercaptohexanol solution in 1 M NaCl/10 mM potassium phosphate buffer pH 7.0 for 3 h in the dark at room temperature. Upon completion of passivation, the nanoparticles were washed (× 3) with 1 M NaCl/10 mM potassium phosphate buffer pH 7.0 and collected by centrifugation.

Preparation of maleimide-activated silica colloidal film.[5] First, amine modification of the colloidal films was achieved by immersing the colloidal film electrode in a 0.056 M solution of 3-aminopropyltriethoxysilane in dry acetonitrile at room temperature for 17 h. The electrodes were then soaked in dry acetonitrile for 1 h.

Next, the surface of the colloidal film on the Pt electrodes was dried under vacuum for 24 h before immersing the electrodes vertically into a stirred solution of DMF containing DMAP (0.5 mg, 4.5 μmol) and SMCC (1.4 mg, 3.4 μmol). The solution was allowed to stir in the dark at room temperature for 24 h. The resulting maleimide-acitivated silica colloidal film was washed with DMF for 1 h in the dark and then 100 mM NaCl/10 mM potassium phosphate buffer pH 7.0 for 1 h in the dark and used immediately.

Preparation of aptamer-modified silica colloidal film.[5] Aptamer/TCEP solution (6.75 mL) was combined with 100 mM NaCl/10 mM potassium phosphate buffer pH 7.0 (18.9 mL) to prepare the aptamer solution. The maleimide-activated colloidal film electrode was then immersed vertically into the stirred solution for 25 min in the dark at room temperature.

Passivation of silica colloidal film.[5] Passivation of the area of the amine-modified silica surface still exposed after aptamer immobilization was achieved

by stirring the electrode in 2 mM mercaptohexanol solution in 1 M NaCl/10 mM potassium phosphate buffer pH 7.0 for 3 h in the dark at room temperature. Upon completion of the passivation, the electrode was washed with 1 M NaCl/10 mM potassium phosphate buffer pH 7.0.

Characterization. The molecular flux across the colloidal film was measured voltammetrically using a Par Model 175 Universal Programmer and Dagan Cornerstone Chem-Clamp potentiostat. The voltammetric responses of the bare, amine-modified, maleimide-modified, and aptamer-modified colloidal electrodes were measured in solutions of 10 mM monobasic/dibasic potassium phosphate buffer, pH 7 with 1.6 mM $Fc(CH_2OH)_2$ and 0.2 M KCl as supporting electrolyte with 1 mL methanol/5 mL redox solution at 0 ºC. The voltammetric response of aptamer-modified colloidal electrodes to cocaine was measured at 0 ºC in a solution of 10 mM monobasic/dibasic potassium phosphate buffer, pH 7 with 1.6 mM $Fc(CH_2OH)_2$ and 0.2 M KCl with 1.0 mg/ mL cocaine hydrochloride solution in methanol, 1 mL/5 mL redox solution. Aqueous solutions were prepared using 18 MΩ·cm water and purged with nitrogen to remove dissolved oxygen. Dynamic light scattering (Brookhaven ZetaPALS, measurements conducted in water at 25 °C) were employed to perform size characterization of aptamer-modified silica spheres. UV-visible spectra were measured in chloroform and recorded on an Agilent 8453 diode array spectrophotometer in order to determine the coverage of the aptamer on the surface of the colloidal nanoparticles.

Results and Discussion

Aptamer-Modified Silica Nanoparticles and Colloidal Films

Aptamer modification of silica spheres in colloidal solution. It has been shown that silica can be prepared with sulfhydryl-reactive functional groups for the immobilization of proteins for the use in high-performance affinity chromatography.[5] However, to our knowledge, there have been no reports on modification of silica nanoparticles with aptamer-based receptors. Thus, we developed the following procedure to attach the aptamers to the silica surface. Our approach was adapted from the previously reported work on the activation of silica with maleimide.[7]

First, the 290 nm and 100 nm silica nanoparticles were modified with maleimide by treatment with succinimidyl 4-[N-maleimidomethyl]cyclohexane-1-carboxylate (SMCC) in DMF in the presence of DMAP. The resulting sulfhydryl-reactive group activates the surface and allows it to react with the free thiol on the aptamer. In order to attach the aptamer to the maleimide-activated silica nanoparticles, the disulfide end group was cleaved with TCEP·HCl. The maleimie-activated silica nanoparticles were then subjected to the aptamer/TCEP solution (Scheme 4.1). In order to determine the surface coverage of the aptamer-modified silica nanoparticles, UV spectra were obtained. Based on the absorbance at 260 nm, the surface coverage was estimated using 2.07 g cm^{-3} density for silica spheres and extinction coefficient of the aptamer at 260 nm provided by the manufacturer. Surface coverage was calculated to be 0.5-2

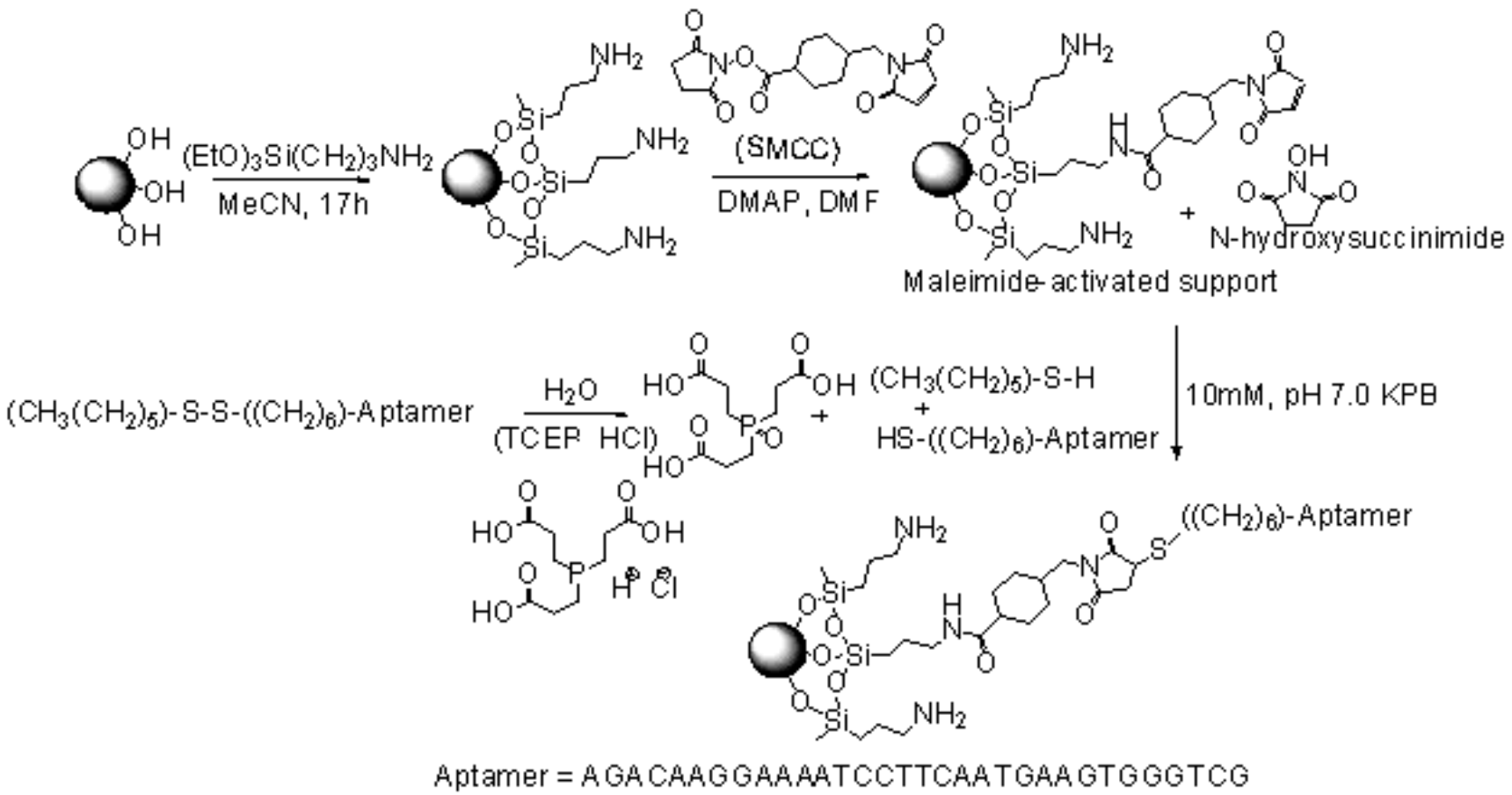

Scheme 4.1. Preparation of aptamer-modified silica spheres.

molecules nm^{-2}. We assume that similar surface coverage will be achieved for silica colloidal films.

Maleimide-activation and aptamer-modification of colloidal film electrodes. The colloidal films were assembled on the surface of Pt microelectrodes shrouded in glass using 1.5 wt% solution 290 nm silica spheres or 1.5 wt% solution of 100 nm silica spheres. The surfaces were modified with amines, and maleimide-activation was performed on the modified colloidal film electrodes in DMF solution. The electrodes were removed from solution and rinsed with DMF and potassium phosphate buffer solution. The aptamer was activated by the reducing agent tris(2-carboxyethyl)phosphine hydrochloride (TCEP) in order to cleave the disulfide group on the aptamer to generate a free thiol for reaction with the maleimide-functionalize colloidal film. The electrodes were then modified with the activated aptamer solution and washed again with potassium phosphate buffer. After the aptamer addition, the surface of the nanoparticles still exposed was passivated with mercaptohexanol to create an aptamer/mercaptohexanol monolayer on the surface of the nanoparticles.

The limiting current of ($Fc(CH_2OH)_2$), which is proportional to the amount of redox-active species that penetrates the colloidal film to the electrode surface in a given time, was measured for the electrodes after each modification, and compared to the initial limiting current, as shown in Figure 4.1. The limiting current measured for the electrodes decreases after each modification, as less of the redox-active species was able to reach the electrode surface in the given time, suggesting that an organic layer has been formed inside the nanopores,

thus partially blocking the nanopores. Calculated[8] nanopore sizes and the corresponding organic film thicknesses are given in Table 4.1. The increase in the organic film thickness for APTES and maleimide modification is consistent with the formation of one or two layers on the surface of the nanopores. This appears to be true also for the aptamer surface modification. While the size of unfolded aptamers can only be estimated, multiple NMR[9] and X-ray structures[10] have been reported for aptamers bound to small molecules, with the size ranging from 3.5 to 6.8 nm. In the case of the larger nanopores it appears that clearly more than a monolayer of the aptamer is introduced, based on the calculated thickness. This may result from the ability of the larger nanopores to accommodate more aptamer macromolecules.

We investigated the response of the aptamer-modified colloidal films to the presence of cocaine using cyclic voltammetry. To exclude the possibility that the observed changes in the molecular transport would result from electrostatic effects,[11,12] we examined the response of the colloidal film electrodes for a neutral redox probe, $Fc(CH_2OH)_2$. As can be seen in Figure 4.2, the limiting current for the aptamer-modified colloidal film electrodes is affected by the addition of cocaine to the solution. A 9.0 ± 3.5% change in the limiting current was observed as a result of the cocaine addition (measurements were performed in triplicate to ensure reproducibility), corresponding to 0.6 nm increase in effective nanopore radius (Table 4.2). The cocaine-dependent change in the limiting current is reversible and the nanoporous aptamer-modified colloidal films could be regenerated by immersing the electrode into a potassium phosphate

Table 4.1. Relative limiting current for colloidal film Pt electrodes as a function of the surface modification, the corresponding effective nanopore radius and organic film thickness inside the nanopore.

Initial radius, nm	22.5			7.8		
Surface modification	APTES	maleimide	aptamer	APTES	maleimide	aptamer
i_{lim} / $i_{lim}(0)$	0.93	0.91	0.32	0.69	0.68	0.28
Resulting radius, nm	21.0	20.2	14.3	6.0	5.9	3.4
Film thickness, nm	1.2	1.6	12.1	1.8	1.9	4.4

Table 4.2. Relative limiting current for colloidal film Pt electrodes in response to cocaine and the change in the organic film thickness inside the nanopore as a function of the nanopore size.

Nanopore radius, nm	Ave. % increase in i_{lim}	Film thickness change, nm
22.5	9.0 ± 3.5	-0.6
7.8	23.0 ± 8.0	-0.4

buffer. We attribute this behavior to the conformational change in the secondary structure where the aptamer changes from partially unfolded conformation with only one of the three junctions folded to a conformation with a three-way junction containing the cocaine molecule in the internal cavity (Figure 4.3). With the formation of the three-way junction, the space that the aptamer occupies inside the nanopores is reduced, allowing for increased transport through the nanopores.

To verify that the responsive behavior described above results from the nanopore surface modification, the limiting current for glass-shrouded platinum microelectrodes carrying the unmodified colloidal film was examined. The resulting electrodes did not exhibit any significant response to the presence or

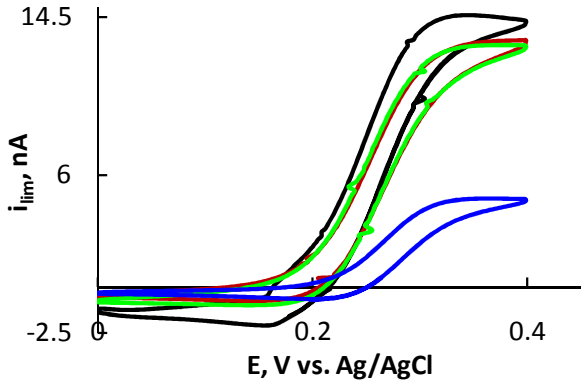

Figure 4.1. Representative $Fc(CH_2OH)_2$ voltammetric responses for unmodified colloidal film Pt electrode (black), amine-modified (brown), maleimide-modified (green), and aptamer-modified silica colloidal film Pt electrode (blue).

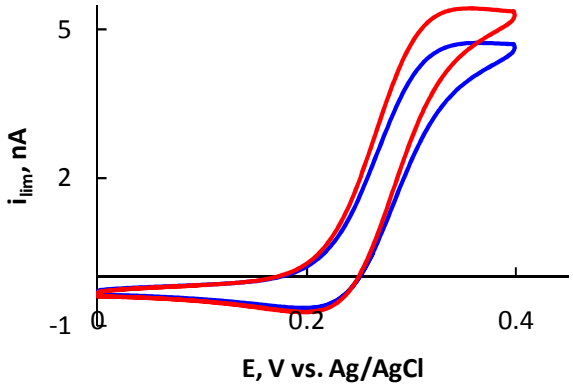

Figure 4.2. Representative $Fc(CH_2OH)_2$ voltammetric response for an aptamer-modified colloidal film Pt electrode in the absence (blue) and in the presence of cocaine (red).

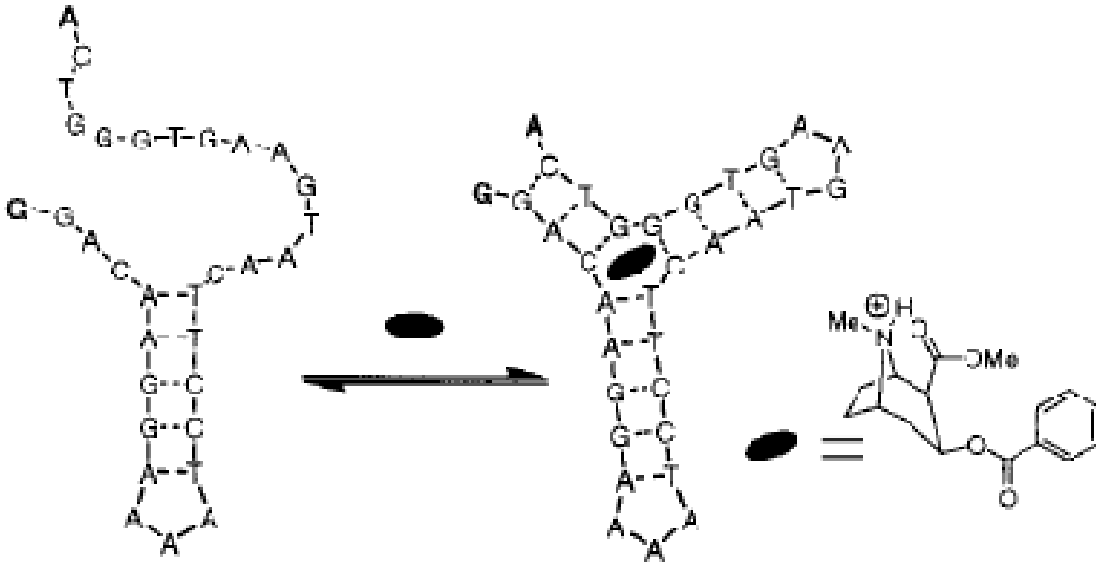

Figure 4.3. Cocaine-Response for Aptamer-Modified Colloidal Films.

absence of cocaine (data not shown). Previous studies with this aptamer have been conducted in order to assess the aptamer's ability to detect the cocaine molecule in complex, tainted samples. These studies conclude that in the presence of biological fluids and other contaminants, the conformational change of the aptamer remains selective to cocaine. [13]

In order to determine the effect of nanopore size on the aptamer-modified film response to cocaine, colloidal films were assembled using 100 nm silica spheres. The nanopore size of 100 nm silica nanoparticles is ca. 15 nm as described in Chapter 1, significantly smaller than those formed using 290 nm silica nanoparticles. The surfaces were then modified with amines, followed by modification with the maleimide linker and aptamer as well as passivated, as described above. The limiting current of $Fc(CH_2OH)_2$ was measured for the electrodes after each modification, and compared to the initial limiting current. The limiting current measured for the electrodes decreases after each

modification, suggesting that an organic layer has been formed inside the nanopores.

We investigated the response of the aptamer-modified colloidal films with smaller nanopores to the presence of cocaine using cyclic voltammetry, as described above. We found that the change in limiting current resulting from cocaine binding is indeed affected by the size of the nanopore, as shown in Table 4.2. For the nanopores that are ca. 2.9 times smaller the limiting current increase is ca. 2.6 times higher compared to the larger nanopores. This observation can be rationalized by assuming that the aptamer change in size as the result of cocaine binding remains constant regardless of the nanopore size, while having a greater effect for the smaller nanopores. Indeed, the calculated change in the organic layer thickness inside the nanopores resulting from cocaine binding is essentially identical for both nanopore sizes studied (0.4 nm for the smaller and 0.6 nm for the larger pores). This thickness change is presumably proportional to both the conformational change the aptamer undergoes in the process of the small molecule binding and its packing density on the nanopore surface.

The response for aptamer-modified colloidal films with respect to nanoparticle size was also measured. Colloidal films comprised of 290 nm diameter nanoparticles exhibited near saturated gating at ca. 235 μM cocaine, which, while significantly higher than the dissociation constant of 90 μM reported for this aptamer, is consistent with previous results published for nanopores modified with this aptamer.[14] Concentration response was also measured for

100 nm modified colloidal films with an observed near saturated gating of ca. 588 μM. This increased gating may be a result of the smaller nanopores formed from 100 nm nanoparticles, contributing to less efficient aptamer modification and thus, less efficient gating. This demonstrates the advantages of using silica colloidal crystals as a platform for a biomimetic pore in that the performance can be readily optimized by changing the sphere size.

Conclusions

We have prepared aptamer-modified silica colloidal nanopores using maleimide activation of amine-modified silica surfaces. Aptamer-modification of the colloidal films did not perturb the colloidal lattice. We then observed the response of the molecular flux through aptamer-modified colloidal films comprising 100 and 290 nm silica nanoparticles (7.8 and 22.5 nm radius nanopores, respectively) to cocaine using cyclic voltammetry. The molecular flux reversibly increases in the presence of cocaine indicating conformational changes (folding) of the aptamer as the result of the cocaine binding leading to ca. 0.5 nm increase in nanopore radius. This response is greater for colloidal films containing smaller nanopores. These results show that we are able to create gated channels that mimic biological ion channels.

References

1. Stojanovic, M.N.; Prada, P.; Landry, D. W. *J. Am. Chem. Soc*. **2001**, *123*, 4928-4931.

2. Stober, W.; Fink, A.; Bohn, E. *J. Colloid. Interface Sci*. **1968**, *26*, 62-69.

3. Newton, M. R.; Bohaty, A. K.; White, H. S.; Zharov, I. *J. Am. Chem. Soc*. **2005**, *127*, 7268-7269.

4. Mallik, R.; Wa, C.; Hage, D.S. *Anal. Chem*. **2007**, *79*, 1411-1424.

5. Baker, B. R.; Lai, R.; Wood, M. S.; Doctor, E. H.; Heeger, A. J.; Plaxco, K. W. *J. Am. Chem. Soc.* **2006**, *128*, 3138-3139.

6. Mallik, R.; Wa, C.; Hage, D.S. *Anal. Chem*. **2007**, *79*, 1411-1424.

7. Schepelina, O.; Zharov, I. *Langmuir*, **2006**, *22*, 10523-10527.

8. Schepelina, O.; Zharov, I. *Langmuir*, **2006**, *22*, 10523-10527.

9. (a) Flinders, J.; DeFina, S.C.; Brackett, D.M.; Baugh, C.; Wilson, C.; Dieckmann, T. *Chembiochem*, **2004**, *5,* 62-72. (b) Carothers, J.M.; Davis, J.H.; Chou, J.J.; Szostak, J.W. *Rna,* **2006**, *12*, 567-579. (c) Yang, Y.; Kochoyan, M.; Burgstaller, P.; Westhof, E.; Famulok, M. *Science*, **1996**, *272*, 1343-1347.

10. (a) Baugha, C.; Gratea, D.; Wilsona, C. *J. Mol. Biol*., **2000**, *301*, 117-128. (b) Spitale, R.C.; Torelli, A.T.; Krucinska, J.; Bandarian, V.; Wedekind, J.E. *J. Biol. Chem*. **2009**, *284*, 11012-11016. (c) Gilbert, S.D.; Love, C.E.; Edwards, A.L.; Batey, R.T. *Biochemistry*, **2007**, *46*, 13297-13309. (d) Serganov, A.; Yuan, Y.R.; Pikovskaya, O.; Polonskaia, A.; Malinina, L.; Phan, A.T.; Hobartner, C.; Micura, R.; Breaker, R.R.; Patel, D.*J. Chem. Biol*., **2004**, *11*, 1729-1741; (e) Lin, C.H.; Wang, W.; Jones, R.A.; Patel, D.*J. Chem. Biol*., **1998**, *5*, 555-572.

11. Newton, M. R.; Bohaty, A. K.; White, H. S.; Zharov, I. *J. Am. Chem. Soc.* **2005**, *127*, 7268-7269.

12. Newton, M. R.; Bohaty, A. K.; Zhang, Y.; White, H. S.; Zharov, I. *Langmuir* **2006**, *22*, 4429-4432.

13. Baker, B. R.; Lai, R.; Wood, M. S.; Doctor, E. H.; Heeger, A. J.; Plaxco, K. W. *J. Am. Chem. Soc.* **2006**, *128*, 3138-3139.

14. Abelow, A. E.; Schepelina, O.; White, R. J.; Valle´e-Be´ lisle, A.; Plaxco, K. W.; Zharov, I. *Chem. Commun*., **2010**, *46*, 7984–7986.

CHAPTER 5

BIOMIMETIC GLASS NANOPORES EMPLOYING APTAMER GATES RESPONSIVE TO A SMALL MOLECULE

Introduction

In Chapter 4, we demonstrated that colloidal films can be modified with the cocaine-sensing aptamer. This chapter focuses on modifying the surface of 40 and 130 nm diameter single glass nanopores with DNA aptamers which control the molecular transport through the nanopores in response to small molecule binding. The cocaine-induced folding of an aptamer in the nanopore orifice caused an increase in the rate of diffusion through the nanopore as a result of an increase in the free volume contained within. Thus, by covalently attaching cocaine-binding aptamers to the surface of the nanopores electrode we expected to create a nanopore that mimics a protein channel in which molecular transport is selectively controlled in response to small molecule binding. By using aptamers as stimuli-responsive components we will significantly broaden the range of molecular effectors that can be employed to control the gating of biological pore mimics. This work serves as a proof of principle that single glass nanopores can be used in conjunction with aptamers as a platform for creating small molecule-responsive biomimetic nanopores.

Experimental Section

Materials

Chemicals. (3-Aminopropyl) triethoxysilane (99%) and tetraethoxysilane (TEOS, 99.999+%) were obtained from Aldrich and used as received. Hexaammineruthenium (III) chloride, [Ru(NH3)6]Cl3 (99%, Strem Chemicals), 1,1´- ferro-cenedimethanol, Fc(CH2OH)2 (98%, Aldrich), potassium chloride (99%, Mallinckrodt) were used as received. Acetonitrile (Mallinckrodt) was distilled before using. 18 MΩ·cm water was obtained from a Barnsted "E-pure" water purification system. Mercaptohexanol was obtained from Aldrich and used as received. Diethyl ether was obtained from Mallinckrodt and used as received. Succinimidyl 4-[N-maleimidomethyl] cyclohexane-1-carboxylate, SMCC (>99%) and Tris(2-Carboxyethyl) phosphine Hydrochloride, TCEP·HCL were from Pierce (Rockford, IL) and used as received. *N*,*N*-Dimethylformamide (DMF, 99.9%) was obtained from Fisher Scientific and was dried over molecular sieves. 4-dimethylaminopyridine, DMAP (>99%, Aldrich), was used as received. Tris-EDTA buffer solution (Sigma) was used as received. Cocaine hydrochloride was received from Sigma - Aldrich and stored at 2-8 °C until use. 3-aminopropyldimethylethoxysilane (Gelest, Inc.) was used as received.

The DNA probes were synthesized (Biosource International, Camarillo, CA) for the preparation of the electrochemical cocaine biosensor. The aptamer sequence **A1** was based on the oligonuclotide sequence developed by Stojanovic *et al.*[1] The sequences used are listed in Table 5.1. Each of the

Table 5.1. Aptamer sequences (5' → 3')

A1	AGACAAGGAAAATCCTTCAATGAAGTGGGTCG
A2	AGACAAGGAAAA-T60-TCCTTCAATGAAGTGGGTCG-MB
A3	(AGACAAGGAAAATCCTTCAATGAAGTGTGGGTCG)3-MB

sequences was covalently modified during solid-phase synthesis with a six carbon disulfide group (CH3(CH2)5-S-S-(CH2)6-) at the 5' terminus. The aptamers were purified by HPLC and PAGE, and verified by mass spectrometry.

Methods

Fabrication and surface modification of glass nanopore electrodes. Figure 5.1 shows a schematic of the nanopore electrode surface. Preparation of the aptamer-modified electrodes is based on the procedures reported for covalent attachment of a propylamine silane[2] and spiropyran[3] monolayers to the interior surface of glass nanopore electrodes as well as the covalent attachment of aptamers to the surface of gold electrodes.[4] The preparation of aptamer-modified glass nanopore electrodes involved the following steps: (1) a 25-μm diameter platinum wire (Alfa-Aesar, 99.95%) was electrochemically etched to produce a sharp tip with ~10 nm radius of curvature; (2) the sharpened tip was sealed in a Corning 8161 lead glass capillary (Warner Instruments Inc., i.d. = 1.10 mm; o.d. = 1.50 mm); (3) the capillary was polished until a nanodisk of platinum is exposed; (4) the electrode was thoroughly cleaned by sonication in H_2O, EtOH, CH_3CN, and H_2O, soaking in 1 M KOH for 10 min, followed by rinsing in H2O and CH3CN; (5) the electrode is immersed overnight in an CH_3CN solution containing

~2% v/v $Cl(Me)_2Si(CH_2)_3CN$, resulting in covalent attachment of cyanopropyl silane to the exterior glass surface; (6) the exposed platinum disk was etched in a 15% $CaCl_2$ solution (pH 5.5) with 5 V ac voltage applied between the nanoelectrode and a platinum wire counter to produce a truncated cone-shaped nanopore in glass, the bottom of the pore defined by a platinum microdisk electrode; (7) the interior glass surface was modified in an CH3CN solution containing ~2% v/v $EtO(Me)_2Si(CH_2)_3NH_2$ using the above procedure; (8) the maleimide linker was attached to the surface by soaking the amine-modified nanopore electrode in a solution of DMF containing DMAP (0.5 mg, 4.5 μmol) and SMCC (1.4 mg, 3.4 μmol) with intervals of gentle sonication, in the dark at room temperature for 24 h, followed by soaking in DMF and then 100 mM NaCl/10 mM potassium phosphate buffer pH 7.0; (9) the maleimide-modified surface was immersed in a solution of activated-aptamer/TCEP solution (6.75 mL) with 100 mM NaCl/10 mM potassium phosphate buffer pH 7.0 (18.9 mL) 60 min in the dark at room temperature and sonicated gently three to four times; (10) the surface was passivated by stirring the electrode in 2 mM mercaptohexanol solution in 1 M NaCl/10 mM potassium phosphate buffer pH 7.0 for 3h in the dark at room temperature, and then washing with 1 M NaCl/10 mM potassium phosphate buffer pH 7.0. The radius of the nanopore orifice (*a*) was estimated by measuring the voltammetric limiting current at the nanodisk, prior to etching the platinum in the $CaCl_2$ solution. The diffusion-limited voltammetric current (i_d) for the oxidation of 5 mM ferrocene (Fc) in CH_3CN is

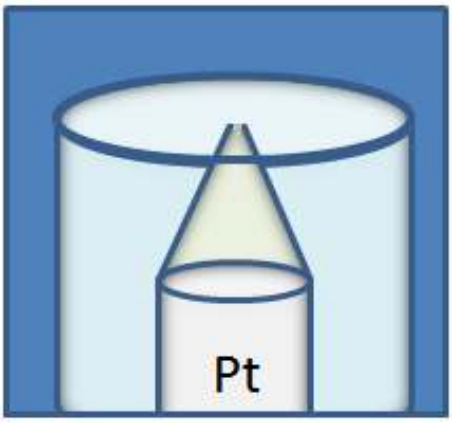

Figure 5.1. Schematic representation of the glass nanopore electrode.

given by i_d = 4*nFDC*a*, where *n* is the number of electrons transferred, *F* is Faraday's constant, and *D* isthe diffusion coefficient of Fc (2.4 × 10-5 cm2/s).[5] All radii reported here are based on the electrochemical response and thus are "apparent" radii.[6]

Cyclic voltammetry measurements. The molecular flux through the nanopore orifice was measured voltammetrically using a 2-electrode cell and an Ag/AgCl reference/counter electrode. A Par Model 175 Universal Programmer and Dagan Cornerstone Chem-Clamp potentiostat were used to conduct measurements. Data was recorded with a PC using LabView. All solutions were purged with N_2 to remove dissolved O_2 before use. The voltammetric response of the aptamer-modified glass nanopore electrodes to cocaine was measured by immersing the electrodes in a 10 mM monobasic/dibasic potassium phosphate buffer, pH 7, solution with 5 mM $Fc(CH_2OH)_2$ and 0.2 M KCl as supporting electrolyte with 1.0 mg/mL cocaine hydrochloride solution in methanol. Voltammetric studies comparing the aptamer-modified nanopore in the absence and presence of cocaine were carried out at 0 °C. Redox solutions were prepared using 18 MΩ·cm water and purged with nitrogen to remove dissolved oxygen.

Results and Discussion

Aptamer-Modified Single Nanopore Electrodes

Surface coverage of 290 nm aptamer-modified silica nanoparticles. In order to verify and optimize our surface modification procedure, we employed

silica nanoparticles as discussed in Chapter 4, as a proxy, assuming that their surface chemistry is similar to that of the glass nanopores. We modified 290 nm diameter silica spheres, prepared using the Stöber method,[7] with amines using $(EtO)_3Si(CH_2)_3NH_2$, followed by treatment with succinimidyl 4-[N-maleimidomethyl]-cyclohexane-1-carboxylate (SMCC) in DMF in the presence of DMAP.[8] Silica nanoparticles were then treated with the thiol-terminated **A1** (Scheme 5.1). UV/Vis spectroscopy of the aptamer-modified silica nanoparticles confirmed the surface modification with the aptamers and allowed their surface coverage to be calculated. Specifically, from the absorbance at 260 nm, the known extinction coefficient and 2.07 g cm^{-3} density of the silica spheres we estimated the surface coverage with **A1** to be 0.5 molecules nm^{-2}.

Aptamer modification of single nanopore electrodes. To attach the aptamers to the glass nanopores, we modified the nanopore surface with amines,[9] followed by a bisfunctional cross-linker containing maleimide and N-hydroxysuccinimide.[10] The sulfhydryl-reactive maleimide should activate the glass surface for reaction with a free thiol groups incorporated in the aptamer during its synthesis.

Initial studies of the small molecule responsive glass nanopores were performed using the 32-base **A1** aptamer immobilized on the surface of the nanopore. First, the surface of the glass nanopores was aminated using $EtO(Me)_2Si(CH_2)_3NH_2$.[11] Next, we attached the maleimide linker was attached to the surface by soaking the amine-modified nanopores in a DMF solution containing DMAP and SMCC. The electrodes were then treated with the thiol-

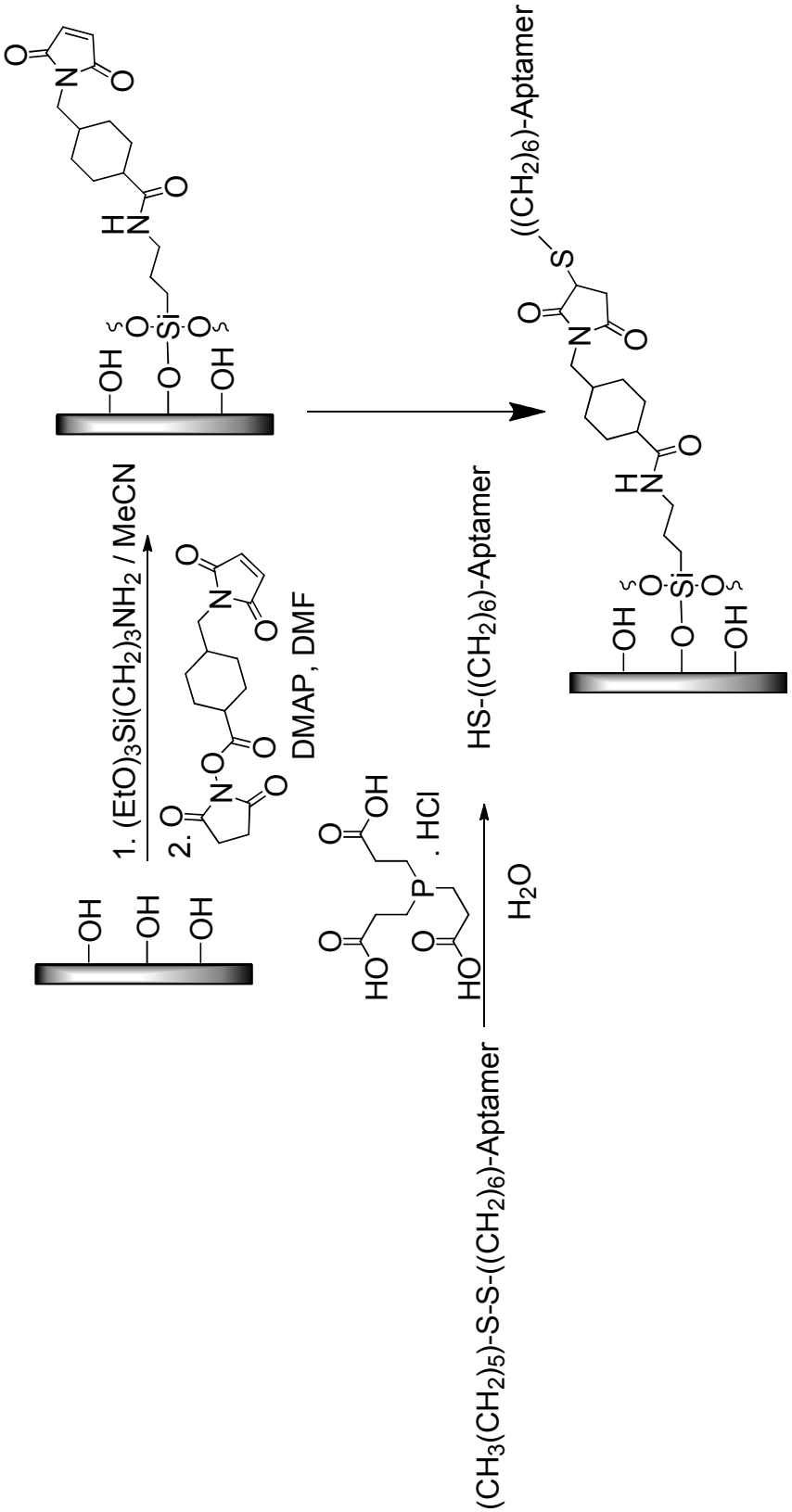

Scheme 5.1. Aptamer modification of single nanopores electrode surface.

terminated **A1** which had been reduced using tris-(2-carboxyethyl)phosphine hydrochloride (TCEP) (Scheme 5.1).

After the aptamer addition, the surface of the nanopore remaining unreacted was passivated with mercaptohexanol to create an aptamer/mercaptohexanol monolayer on the surface of the nanopore. The limiting current of a redox mediator, ferrocene dimethanol ($Fc(CH_2OH)_2$), was measured for the glass nanopores electrodes after each modification, and compared to the initial limiting current (Figure 5.2). The limiting current decreased after each modification, confirming that an organic layer has been formed inside the nanopores, reducing the size of the nanopore orifice and thus reducing the flux of ferrocene dimethanol.

Cocaine-response of the A1-modified single nanopore electrode. The response of the **A1**-modified single nanopore electrode was observed with respect to the addition of a small molecule, cocaine, by employing cyclic voltammetry to monitor the diffusion of $Fc(CH_2OH)_2$ in the presence and absence of cocaine. We employed ferrocene dimethanol, a small, neutral molecule as our redox mediator in order to exclude the possibility that the observed changes in the molecular transport would result from electrostatic effects arising due to the high charge density of the aptamers.[12,13] As expected, the voltammetric limiting current through the **A1**-modified nanopores responds to cocaine: nanopore electrodes of both 40 and 130 nm diameter exhibited increased $Fe(CH_2OH)_2$ transport upon cocaine addition, with the 40 nm nanopores producing a relatively greater change than the larger, 130 nm nanopores (Figure 5.3). Removal of the

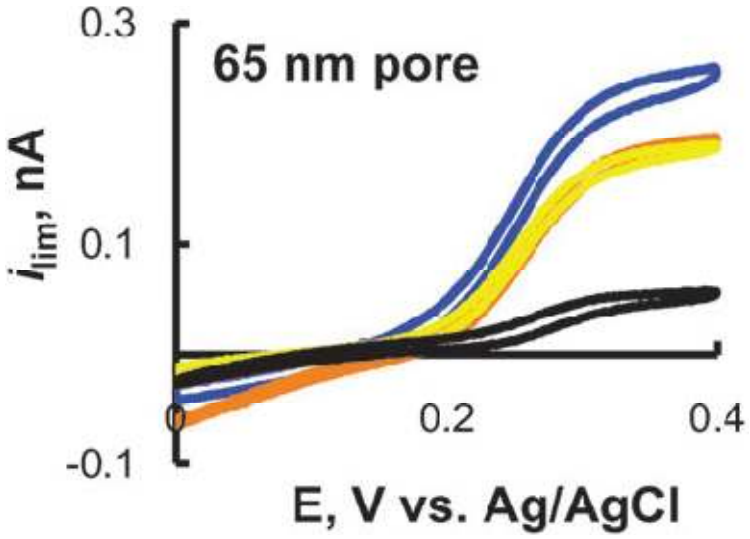

Figure 5.2. Representative voltammetric responses of a single nanopores platinum electrode in ($Fc(CH_2OH)_2$) unmodified (blue), aminemodified (orange), maleimide-modified (yellow) and A1-aptamer modified (black). Nanopore orifice radius is shown on the figure.

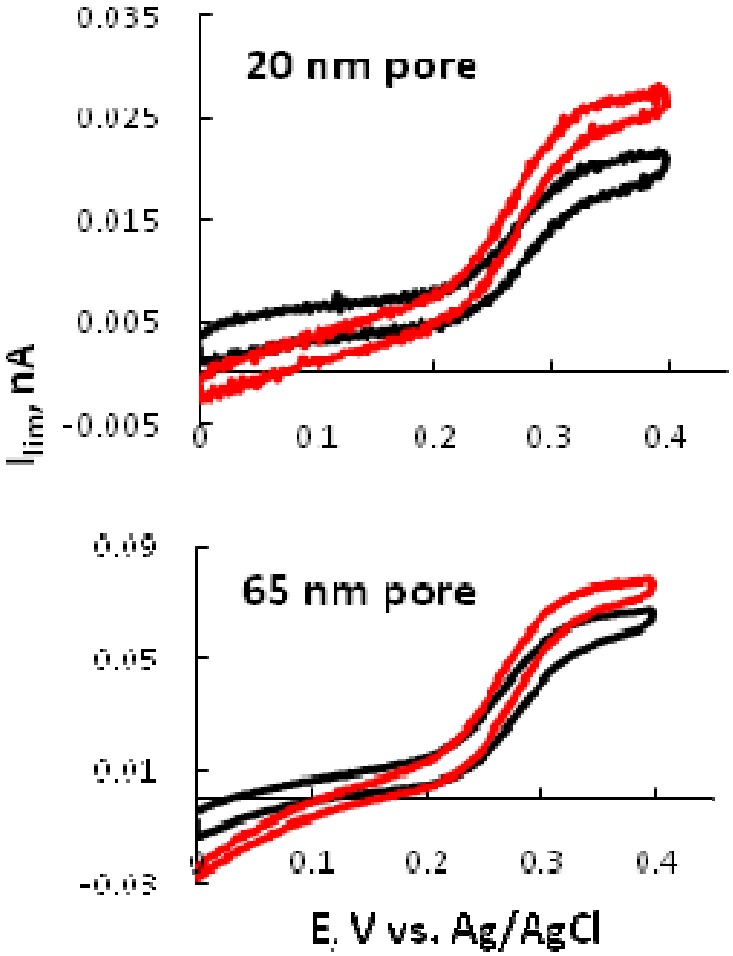

Figure 5.3. Representative voltammetric responses of the 32-base A1 aptamer-modified single nanopore on a platinum electrode in $Fc(CH_2OH)_2$ (black) and in $Fc(CH_2OH)_2$ with 530 mM cocaine (red). Nanopore orifice radii are shown on the figures.

cocaine by washing in potassium phosphate buffer recovered the original current, allowing the nanopore to be reused multiple times (Figure 5.4). The cocaine-modulated gating of the glass nanopores presumably arises due to a conformational change in the aptamer where it is converted from partially unfolded conformation with only one of the three junctions formed to a conformation with a fully formed three-way junction containing the cocaine molecule in the internal cavity (Figure 5.5 and Figure 5.6). With the formation of the three way junction, the space that the aptamer occupies inside the nanopores is reduced, allowing for increased transport.

Although analytes other than cocaine were not tested in our work, previous studies have shown[14] that their presence does not affect the folding of the **A1** aptamer immobilized on a solid support in the presence of cocaine. In order to verify that the responsive behavior described above results from a change in the conformation of the cocaine-sensing aptamer, the limiting current for a bare single nanopore electrode was examined for pure redox solution and in the presence of cocaine. This bare nanopore electrode did not exhibit any measurable response to cocaine.

Characteristics of the nanopore response with alternate aptamer constructs. In order to study how the nanopore works, two other aptamer constructs (**A2**, **A3**, Table 5.1.) were immobilized onto the surface of 130 nm diameter single nanopore electrode orifices. By observing the effect of cocaine addition using different aptamer constructs we are able to study how changing aptamer size effects gating efficiency. The gating efficiencies of these longer

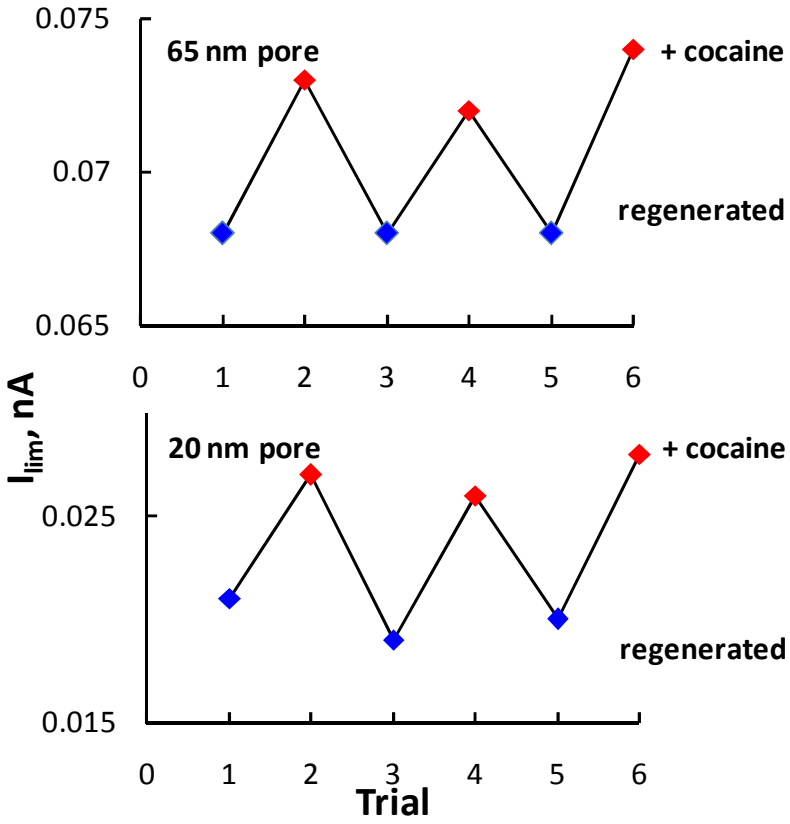

Figure 5.4. The regeneration of the **A1** aptamer-modified single nanopore platinum electrode signal ($Fc(CH_2OH)_2$) without cocaine (red), with cocaine (blue). Nanopore orifice radii are shown on the figures.

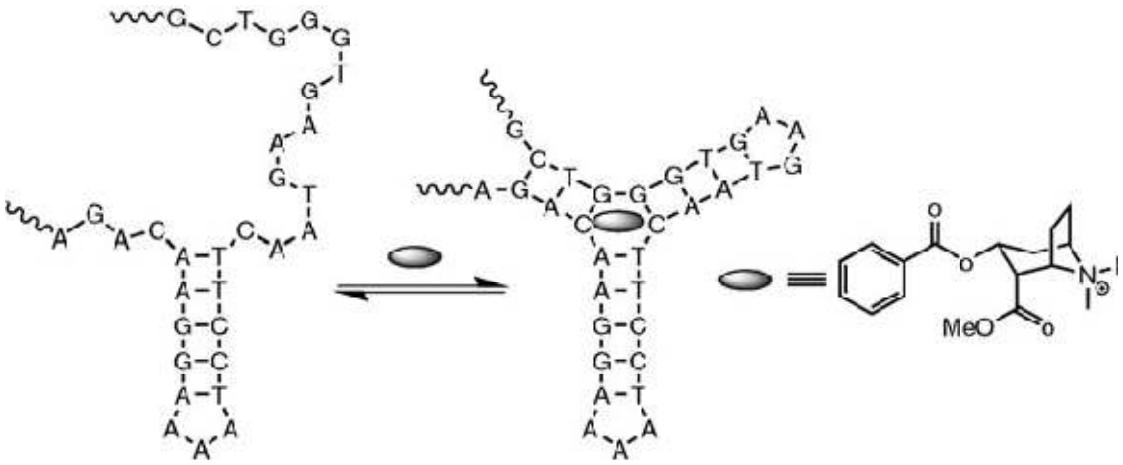

Figure 5.5. Conformational change of aptamer in response to cocaine binding.

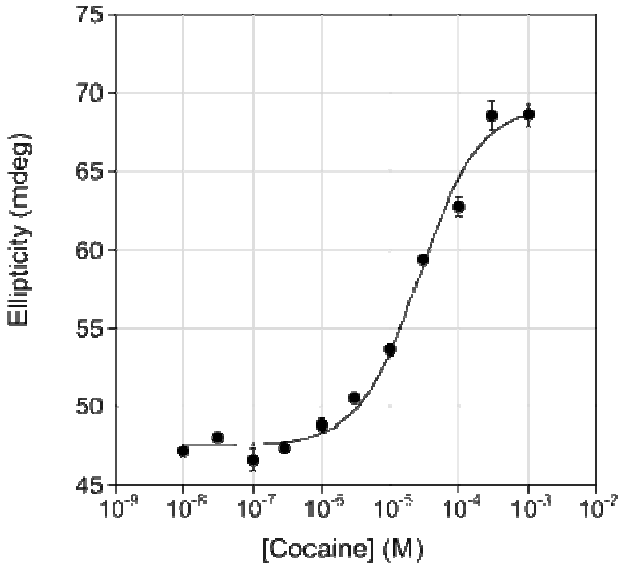

Figure 5.6. Circular dichroism data of the **A3** aptamer incurring a structural change as it folds in the presence of cocaine.

constructs were approximately twice that of the shorter parent aptamer when employed in nanopores of the same size (Table 5.2), suggesting a more efficient blocking of the nanopores by the larger biomacromolecules.

In order to gain insight into the gating mechanism of the aptamer-modified nanopores, we measured the concentration response for single nanopore electrodes with orifice diameter of 130 nm modified with aptamers **A2** and **A3** (Figure 5.7, A). The **A2**-modified nanopore electrodes produce near saturated gating at ca. 150 μM cocaine, which is just below the ~165 μM dissociation constant reported for this aptamer.[15] The **A3**-modified nanopore electrodes produce near saturated gating at ca. 230 μM cocaine, similar to the reported dissociation constant (~230 μM) for this aptamer.[15] Below these concentration, no gating was observed for either aptamer. This observation and the somewhat non-hyperbolic concentration response curves (Figure 5.7) are consistent with the suggestion that a large fraction of the aptamers must be bound and folded before a significant change in transport is observed.

We also measured the response for single nanopore electrodes with orifice diameter of both 40 nm and 130 nm modified with aptamer **A1** as a

Table 5.2. Percent signal change in response to cocaine binding for aptamers **A1**-**A3**.

aptamer	nanopore radius (nm)	% signal change
A1	40	28.6 ± 1.8
A1	130	15.5 ± 10.7
A2	130	31.8 ± 15.1
A3	130	30.8 ± 11.9

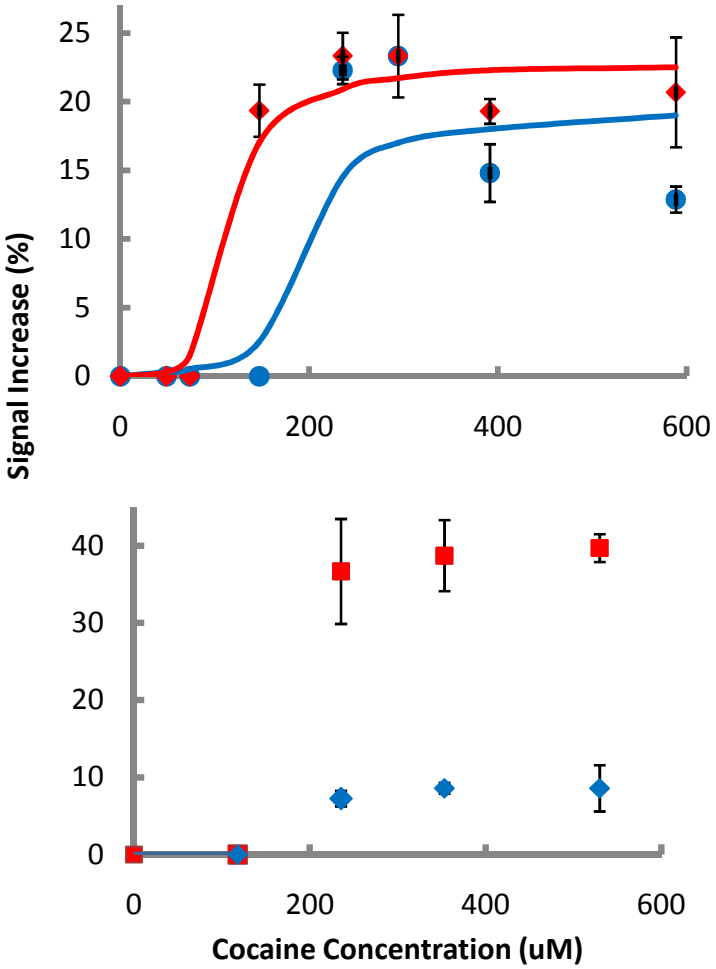

Figure 5.7. (A) Percent change in signal for cocaine-sensing aptamers **A2** (red) and **A3** (blue) on single nanopore electrodes with 65 nm nanopores. (B) Percent change in signal for cocaine-sensing aptamer **A1** on single nanopore electrode for 20 nm (red) and 65 nm (blue) nanopore.

function of cocaine concentration and found near saturated gating at ca. 235 μM cocaine, which is significantly higher than the dissociation constant of ca. 90 μM reported for this aptamer.[15] This may be the result of the smaller size of the **A1** aptamer leading to less efficient gating. Thus, we are able to study the change in signal as nanopore size and cocaine concentration are varied. We expect that further increases in gating efficiency will lead to improved detection limits for the gated nanopores. This optimization will involve fine-tuning not only the nanopore size but also the aptamer as aptamer length is a significant factor in gating efficiency.

Conclusion

We have shown that single glass nanopores surface-modified with aptamers that fold in response to cocaine binding are a ready means of producing cocaine-responsive nanopores. Specifically, the binding of cocaine to each of three aptamers used to modify our nanopores triggers a large-scale change in the conformation of the aptamer that, in turn, allows the orifice of the nanopore to be reversibly switched from a more blocked to a more opened state. Consistent with the proposed mechanism, the observed gating efficiency is a strong function of the relative size of the gating aptamer and the orifice diameter. These findings demonstrate the possibility of creating biomimetic nanopores with molecular gating driven by a specific recognition of a small molecule by a biomacromolecule. This work also demonstrates that it is possible to modify the surface of a single nanopore electrode with aptamers, a process that is useful in

the future development of sensors or biomimetic pores responsive to other small molecules using single nanopore electrodes.

References

1. Stojanovic, M. N.; Prada, P.; Landry, D. W. *J. Am. Chem. Soc.* **2001**, *123*, 4928.

2. Wang, G.; Zhang, B.; Wayment, J. R.; Harris, J. M.; White, H. S. *J. Am. Chem. Soc.* **2006**, *128*, 7679.

3. Wang, G.; Bohaty, A. K.; Zharov, I. Z.; White, H. S. *J. Am. Chem. Soc.* **2006**, *128*, 13553.

4. Baker, B. R.; Lai, R. Y.; Wood, M. S.; Doctor, E. H.; Heeger, A. J.; Plaxco, K. W. *J. Am. Chem. Soc*. **2006**, *128*, 3138.

5. Kuwana, T.; Bubitz, D. E.; Hoh, G. *J. Am. Chem. Soc*. **1960**, *82*, 5811.

6. (a) Zhang, B.; Zhang, Y.; White, H. S. *Anal. Chem.* **2004**, *76*, 6229; (b) Zhang, B.; Zhang, Y.; White, H. S. *J. Phys. Chem. B* **2006,** *110*, 1768.

7. Stöber, W.; Fink, A.; Bohn, E. J. *J. Colloid Interface Sci.,* **1968**, *26*, 62.

8. Malik, R.; Wa, C.; Hage, D. S.; *Anal. Chem*., **2007**, *79*, 1411.

9. (a) Zhang, B.; Zhang, Y.; White, H. S. *Anal. Chem*., **2004**, *76*, 6229; (b) Zhang, B.; Zhang, Y.; White, H. S. *Anal. Chem.,* **2006**, *78*, 477; (c) Zhang, B.; Zhang, Y.; White, H. S. *J. Phys. Chem. B,* **2006**, *110*, 1768.

10. Whitmann, C. *Immobilization of DNA on Chips I and II*, Springer, Berlin/Heidelberg, **2005**.

11. Wang, G.; Bohaty, A. K.; Zharov, I.; White, H. S. *J. Am. Chem. Soc.,* **2006**, *128*, 13553.

12. Newton, M. R.; Bohaty, A. K.; White, H. S.; Zharov, I. *J. Am. Chem. Soc.* **2005**, *127*, 7268-7269.

13. Newton, M. R.; Bohaty, A. K.; Zhang, Y.; White, H. S.; Zharov, I. *Langmuir* **2006**, *22*, 4429-4432.

14. Baker, B. R.; Lai, R. Y.; Wood, M. S.; Doctor, E. H.; Heeger, A. J.; Plaxco, K. W. *J. Am. Chem. Soc*., **2006**, *128*, 3138.

15. (a) Baker, B. R.; Lai, R. Y.; Wood, M. S.; Doctor, E. H.; Heeger, A. J.; Plaxco, K. W. *J. Am. Chem. Soc*., **2006**, *128*, 3138. (b) Swensen, J. S.;

Xiao, Y.; Ferguson, B. S.; Lubin, A. A.; Lai, R. Y.; Heeger, A. J.; Plaxco, K. W.; Soh, H. T. *J. Am. Chem. Soc*., **2009**, *131,* 4262. (c) White, R. J.; Plaxco, K. W. *Proc. Soc. Photo-Opt*. *Instrum*. *Eng*., **2009**, *7321*, 732105.

CHAPTER 6

ELECTRICALLY RESPONSIVE NANOPOROUS MEMBRANES

Introduction

This chapter focuses on the preparation of electrically active, free-standing, nanoporous membranes. The surface of commercially available electrochemically etched alumina anodiscs were uniformly coated with either polypyrrole (PPy) or poly(3,4-ethylene-dioxythiophene) (PEDOT) doped with either tosylate or $FeCl_3$ via vapor phase polymerization. These polymers include: poly(3,4-ethylenedioxythiophone) doped with tosylate (PEDOT:Ts), poly(3,4-ethylenedioxythiophone) doped with $FeCl_3$ (PEDOT:$FeCl_3$), polypyrrole doped with tosylate (PPy:Ts), and polypyrrole doped with $FeCl_3$ (PPy:$FeCl_3$). These polymers are electrically active in that they undergo a reversible 3-fold increase in molecular flux of a neutral dye molecule, tannic acid, for membranes in their oxidized state compared to the flux for the membranes in their reduced state.

Experimental Section

Materials

Chemicals. Tannic acid and silver conductive paste were purchased from Alfa Aesar, Inc., and used as received. Potassium Chloride (99%) was

purchased from Mallinckrodt and used as received. Tungsten rods (0.010" x 3") were purchased from FHC and used as received. Baytron C (iron(III)toluene sulphonate in butanol) was purchased from Merck. $FeCl_3$, ethylene-dioxythiophene (EDOT) and pyrrol were purchased from Sigma Aldrich. The pyrrol monomer was distilled prior to use. All water used was 18 MΩ·cm water and was obtained from a Barnstead "E-pure" water purification system. All ethanol used was 200 proof.

Instrumentation. Scanning electron microscopy was carried out (FEI NanoNova: 630, University of Utah, Salt Lake City), to image bare Anodiscs and polymer-modified Anodiscs. Unmodified samples were coated with gold for use with SEM. Pore size and polymer depth was determined by the side view SEM images of the polymer-modified Anodiscs. Thermogravimetric analysis of polymer-modified Anodiscs was performed using TGA Q500 (TA Instruments). A Branson 1510 sonicator (50-60 Hz) was used for all sonications. Cyclic voltammetry was performed to test the electrochemical activity of the membrane using a μAutolab potentiostat (Ecochemie). UV/Vis measurements were performed using an Ocean Optics USB2000 or USB4000 instrument.

Anopore inorganic membranes (Anodisc^{TM}). Aluminum oxide membranes (Anodisc^{TM}) 60-μm-thick with a diameter of 43 mm and a pore size of 200 nm were purchased from Whatman.

Methods

Coating of oxidant onto anodisc.[i] Anodiscs were dipped in either oxidant, Baytron C diluted 1:4 with butanol or 0.5 M $FeCl_3$ (aq), until completely soaked on both sides. After coating, the Anodiscs were dried at 40°C using a hot plate. During drying the Anodiscs were placed between two Petri dishes using the plastic ring surrounding the membranes to avoid the oxidant coating coming in contact with the hotplate surface, which could potentially damage the coating, and ensured an even oxidant coating.

Vapour phase polymerization.[1,i] The oxidant-coated membranes were placed in the lid of a Petri dish and held in place by a paper mask which was glued to the Petri dish. The paper mask contained holes matching the size of the membranes, enabling exposure of selected regions of the Anodisc (namely the membranes, not the plastic rings) to the monomer vapour. To start the polymerisation, 200 μl of monomer were put in a glass beaker and the Petri dish lid with the membranes was placed on top of it. Polymerisation of pyrrole was performed at room temperature. Polymerisation of EDOT required heating and the glass beaker with monomer was placed on top of a hot plate set to 40°C. The polymerization was stopped when even polymer films had been formed on the membranes, approximately two h.

After polymerization, the membranes were washed in butanol and water to remove any oxidant that had not reacted with monomer. After washing, the membranes were dried at room temperature.

---

[i] Prepared by Kristin Persson, Linköpings University, Sweden

Cyclic voltammetry. The Anodisc membranes coated with conducting polymer were placed in 0.1 M NaCl (aq) and connected to the potentiostat by means of conducting copper tape. A platinum counter electrode and an Ag/AgCl reference electrode were also included in the set up.

Diffusion measurements through unmodified and polymer-modified anodiscs. A tungsten wire was attached to all unmodified or polymer-modified Anodisc membranes using silver conductive paste and allowed to cure for 24 h before further modification. The unmodified and polymer-modified Anodiscs were then placed between two PTFE flat washers (5.16 mm inner diameter, 14.27 mm outer diameter and 1.02 mm thickness (Small Parts, Inc.) coated with Loctite Hysol 0151 Epoxy so that the epoxy came in contact with the Anodisc. This produces a frit with a surface area of 19.63 cm^2. The newly constructed membranes were allowed to cure for 24 h before any diffusion measurements were performed. Diffusion measurements through the membranes were conducted by placing the membrane between two connected 1.0 cm quartz cuvettes as shown in Figure 6.1. One of the cuvettes contained 4 mL of 0.2 M KCl in water, and the other cuvette contained 4 mL of 0.2 M KCl and 0.1 M tannic acid in water. The extinction coefficient of tannic acid ($\varepsilon = 9.97 \pm 1.94$ m^{-1} cm^{-1}) was determined by taking the slope of the line as absorbance vs. concentration is plotted for at least five tannic acid solutions, ranging in concentration from 0.1 - 0.025 M. The membrane was placed between two Kalrez o-rings to prevent leaking and a clamp was used to hold the cuvettes, o-rings and colloidal membrane in place. Each cuvette contained a stir bar and was covered with

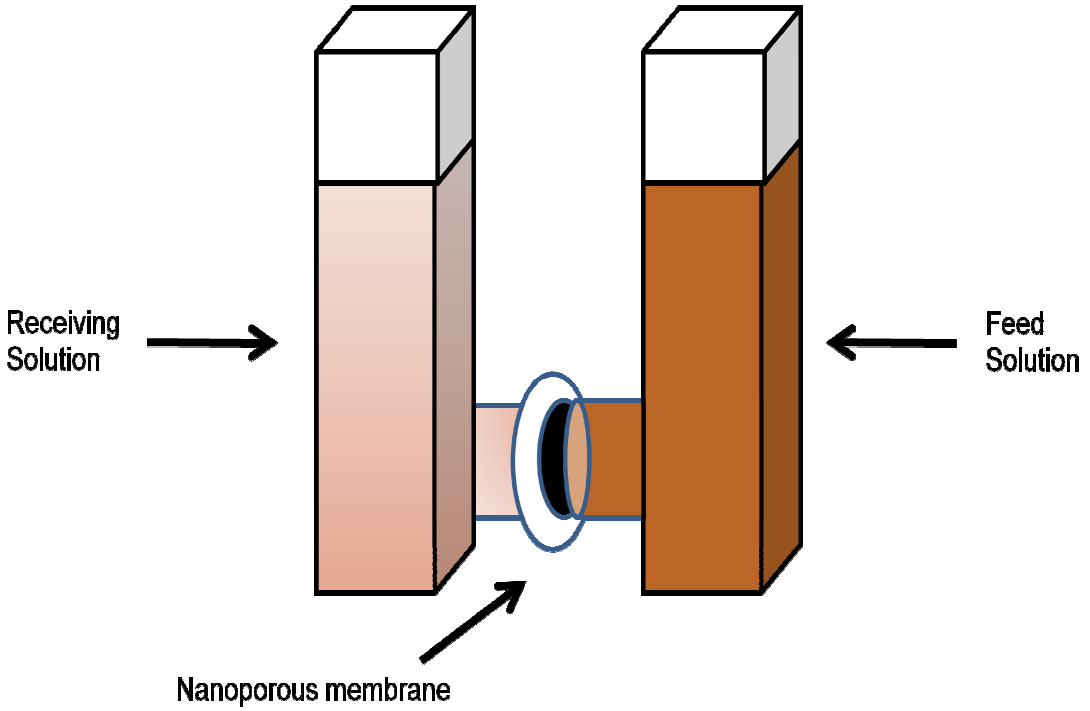

Figue 6.1. Illustration of the basic set-up used to conduct diffusion measurements through Anodisc membranes.

Parafilm to prevent evaporation. The cuvette containing the receiving solution was then placed in the cuvette holder between two fiber optics cables and the solution was blanked. Both solutions were stirred and the dye diffusion rate was measured by recording the absorbance in the receiving cuvette at a wavelength of 419 nm for at least 6 h while stirring both solutions as either a zero, positive, or negative voltage was applied. Electrochemical reduction or oxidation of the membrane was undertaken by applying a negative or a positive potential using a Princeton Applied Research VersaSTAT3to the samples (-1 and +1 V for all PPy-modified membranes and -0.8 and +0.8 V for all PEDOT-modified membranes) versus the Ag^{+}/AgCl reference electrode held in the feed solution with a Pt plate counter electrode also held in the feed solution. The unmodified or polymer-modified Anodisc was used as the working electrode. Each electrochemical reduction-oxidation switch was performed by applying a constant voltage for 6 h. The change in diffusion rate as a potential is applied was measured by measuring the absorbance of the analyte using Ocean Optics USB2000 or USB4000 spectrometer. Data points were recorded every 150 s. All measurements were repeated in duplicate or triplicate for each type of membrane.

Results and Discussion

Electrically Active Polymer-Modified Anodiscs

Vapor phase polymerization of anodiscs. Figure 6.2 shows SEM images of unmodified Anodisc membranes from the top (6.2 (a)) and side (6.2 (b)) showing a continuous pore structure throughout the membrane. Figure 6.3

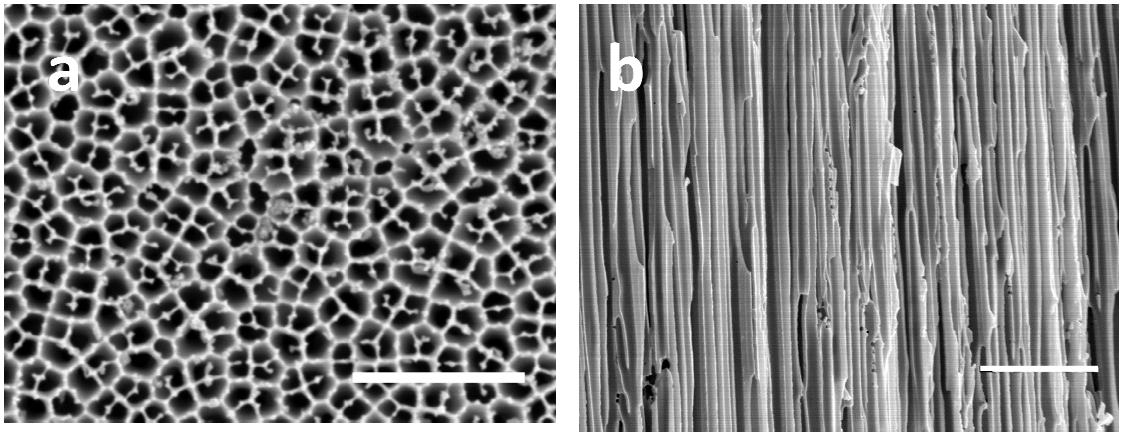

Figure 6.2. Unmodified Anodisc viewed from (a) top and (b) side. Scale bars represent 1 μm, and 3 μm, respectively.

shows SEM images polymer-modified Anodiscs from the top. The images demonstrate the formation of a polymer layer on each of the Anodiscs. For PPy prepared using $FeCl_3$ as the oxidant the polymer layer appears to cover the top portion of alumina nanopores almost completely (Figure 6.3 c). For PEDOT prepared using $FeCl_3$ and $FeTs_3$ and for PPy prepared using $FeTs_3$ the polymer layer does not block the top of alumina nanopores, which are clearly visible (Figure 6.3 a, b, and d). Thus, the morphology of the polymer-modified Anodisc membranes varies depending on the monomer and the oxidant used.

In order to estimate the thickness of the polymer layer on top of Anosdiscs and polymer penetration inside the nanopore we obtained side view images of the membranes (Figure 6.4). It appears that the polymer thickness on top of the membranes is minimal and the majority of the polymer is formed inside the nanopores. The diameters of the pores (d_1) and depth of polymer penetration (h_1) as observed by SEM are listed in Table 6.1. For comparison, we use 197

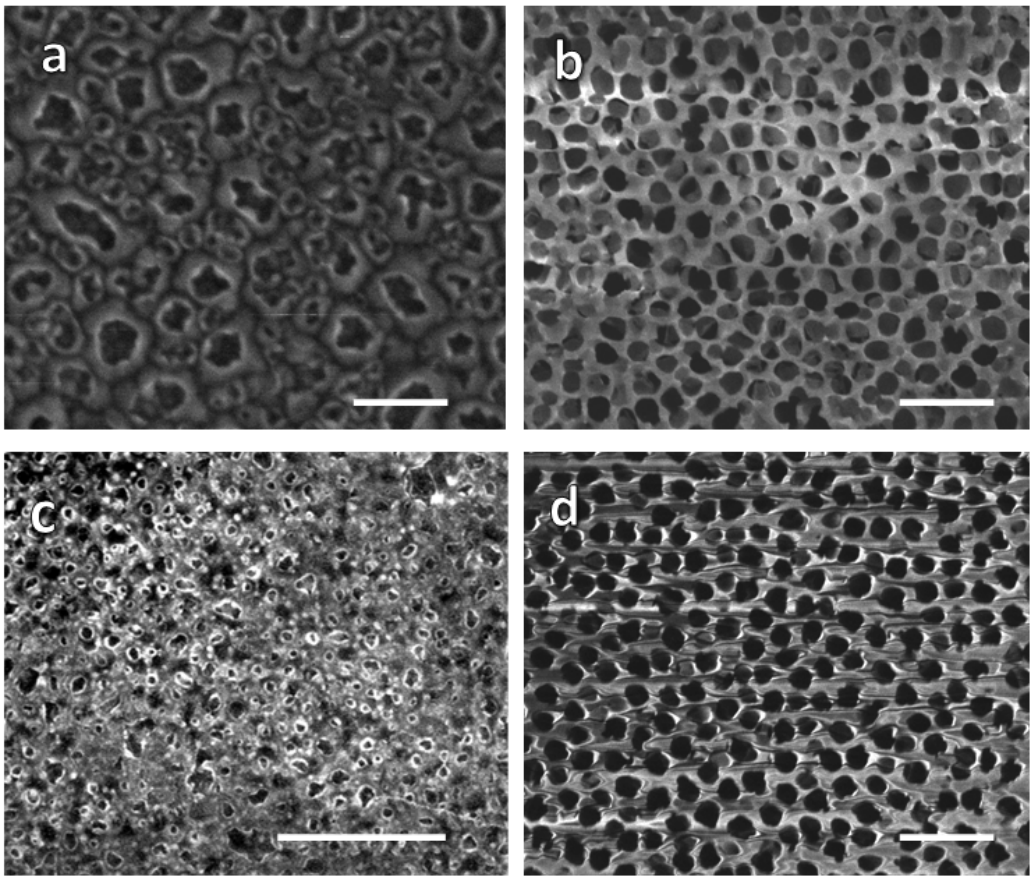

Figure 6.3. Top view of polymer-modified Anodiscs: (a) PEDOT prepared using $FeCl_3$, (b) PEDOT prepared using $FeTs_3$, (c) PPy prepared using $FeCl_3$, and (d) PPy prepared using $FeTs_3$. Scale bars = 1 μm.

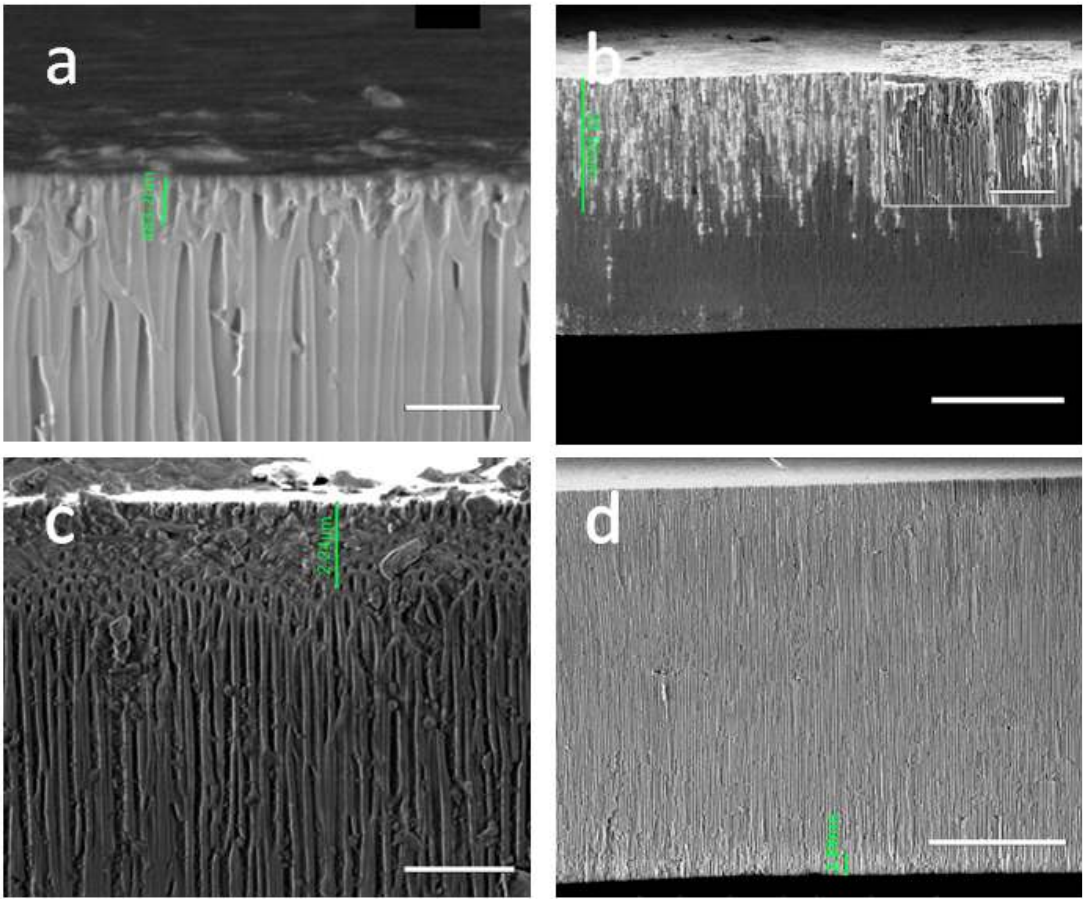

Figure 6.4. Side view of polymer-modified Anodiscs: (a) PEDOT prepared using $FeCl_3$, scale bar = 1 µm; (b) PEDOT prepared using $FeTs_3$, scale bar = 30 µm, scale bar of inset = 5 µm; (c) PPy prepared using $FeCl_3$, scale bar = 3 µm; and (d) PPy prepared using $FeTs_3$, scale bar = 20 µm. Green bars represent the polymer penetration depth (h_1) in each membrane.

Table 6.1. Pore diameter (d_1), polymer penetration (h_1) for polymer-modified Anodiscs based on SEM, and pore diameter calculated for oxidized membranes (d_2).

Anodisc	d_1, nm	d_2, nm	h_1, μm	monomer units/chain
unmodified	197 ± 38	197	-	-
PEDOT:Cl	85 ± 26	66	0.42 ± 0.11	103
PEDOT:Ts	162 ± 54	160	24.6 ± 7.0	32
PPy:Cl	90 ±24	76	2.71 ± 2.70	105
PPy:Ts	121 ± 43	92	1.98 ±7.90	75

nm nanopore diameter for unmodified membranes based on our SEM images, comparable to the diameter reported by the manufacturer. None of the polymers penetrate the entire Anodisc nanopore length (60 μm). Polymer depth ranges from 0.4 μm to 27 μm and appears to be independent of the oxidant used. For PEDOT:Cl, the polymer layer is quite thick at the nanopore entrance, reducing the nanopore size from 197 nm to 85 nm. However, the polymer layer only penetrates the pores to the depth of 0.4 μm. For PEDOT:Ts modified Anodiscs, the pore size remains quite large after polymerization (162 nm) with deep penetration (25 μm). This is the highest polymer penetration observed. For PPy, a much higher amount of the polymer is found for the membrane prepared using $FeCl_3$, in which the nanopores are coated with a relatively thick polymer layer (pore diameter 90 nm) penetrating the nanopores to 2.7 μm. For PPy:Ts membranes the pores remain quite large after the polymerization (121 nm), with polymer penetration of 2.0 μm. Based on the pore diameter of polymer-modified Anodiscs (d_1) and estimated monomer length, the number of monomer units in

each polymer chain can be calculated assuming fully extended polymer chains. For PEDOT:Cl and PEDOT:Ts the number of PEDOT monomers is 103 and 32, respectively. For PPy:Cl and PPy:Ts membranes the number of PPy monomers is 105 and 75, respectively.

TGA of polymer modified anodiscs. To further characterize the nanopore coverage with the polymer we used thermogravimetric analysis (TGA) of the Anodiscs (Figure 6.5, Table 6.2). For bare Anodiscs, we observed a smooth weight loss of ~0.23 % continuing to 500 ºC, likely due to surface water. For polymer-modified Anodiscs, a more significant weight loss was observed. For PEDOT:Cl and PEDOT:Ts modified Anodiscs, the weight loss was 0.64 and 0.71 wt%, respectively. For the PPy:Cl and the PPy:Ts modified Anodiscs, the polymer weight loss was 0.81 and 0.52 wt %, respectively. This weight loss was used to calculate the polymer content based on Anodisc surface area of 6.4 ± 0.6 $m^2\ g^{-1}$, which accounts for the porosity of the membrane,[2,3] and assuming that the top surface area of the membrane is negligible compared to the nanopore surface. A correction factor was used when calculating for the amount of monomers/nm^2, which takes into account the polymer penetration of the nanopores. The coverage calculated for the entire membrane surface was divided by the percent height that the polymer penetrated the membrane from the total thickness (60 μm). For PEDOT:Cl and PEDOT:Ts modified Anodiscs, we calculated 603 and 11 monomer units/nm^2, respectively, while for the PPy:Cl and the PPy:Ts modified Anodiscs we calculated 253 and 172 monomer units/nm^2, respectively. These numbers, when compared to the estimated polymer chain

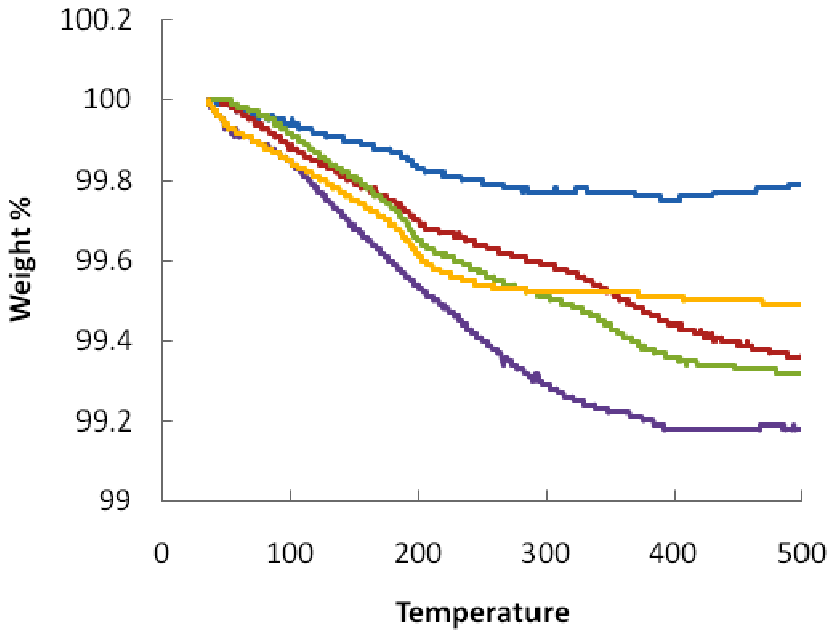

Figure 6.5. Thermogravimetric analysis (TGA) plots for unmodified (top line, blue), PEDOT : $FeCl_3$ modified (second line from top, red), PEDOT : $FeTs_3$ modified (third line from the top, green), PPy : $FeTs_3$ modified (fourth line from the top, yellow), and PPy : $FeCl_3$ (bottom line, purple) Anodiscs.

Table 6.2. TGA data for unmodified and polymer-modified Anodiscs.

Anodisc	total weight loss, wt%	monomer units per nm^2
unmodified	0.23	0
PEDOT:Cl	0.64	603
PEDOT:Ts	0.71	11
PPy:Cl	0.81	253
PPy:Ts	0.52	172

length (Table 6.1) suggest that for PEDOT:$FeCl_3$, PPy:$FeTs_3$ and PPy:$FeCl_3$ more than one polymer chain is present per nm^2. It is important to note that all of the above calculations provide only rough estimates of the polymer size due to the multiple assumptions used to arrive at these numbers.

Diffusion of tannic acid dye through unmodified and polymer-modified anodiscs. To insure that the polymer-modified Anodiscs are conducting and can be oxidized and reduced, we performed cyclic voltammetry experiments. All membranes were conducting and we observed reversible CV curves for all membranes, as expected for PEDOT[4] and PPy.[5]

In order to perform diffusion measurements for the membranes, the following set-up was used. A tungsten wire was attached to unmodified and polymer-modified anodiscs with silver conductive paste before the membrane was sandwiched between two PTFE washers (Figure 6.6).

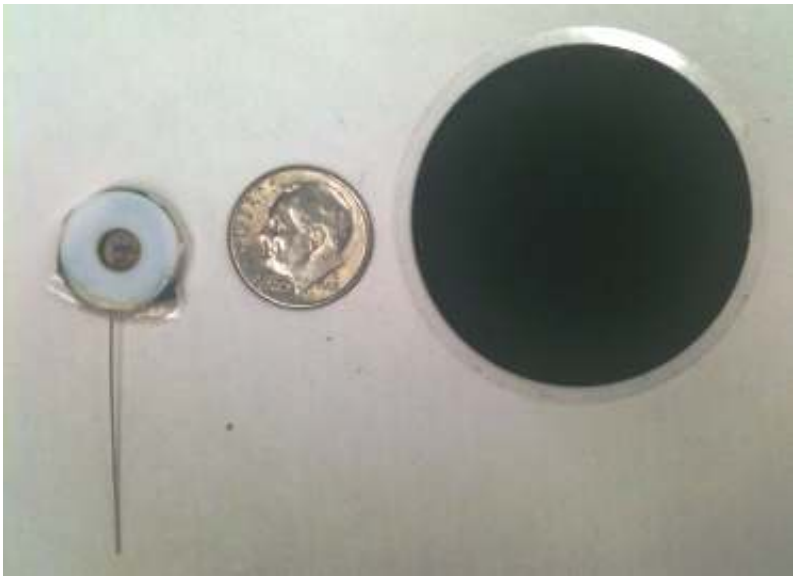

Figure 6.6. Photograph of PEDOT-modified Anodisc piece "sandwiched" between a Teflon washer (Left), and whole PEDOT-modified Anodisc (Right). The figures are shown next to a dime for size comparison.

Diffusion through these membranes was measured spectrophotometrically for a 0.1 M aqueous solution of tannic acid (λ_{max} = 419 nm) with 0.2 M KCl as electric potential was applied to the membranes. Tannic acid was chosen as the diffusion probe due to its water solubility, a relatively high extinction coefficient (ε of ca. 10) and the fact that it is a neutral molecule at pH 7[6] that will not experience any electrostatic interactions with PEDOT and PPy as charges are generated through redox reactions. Finally, tannic acid does react with Fe(III), present in the polymers, to form the corresponding tannate.[7]

Figures 6.7 and 6.8 show the diffusion rate of tannic acid through the PEDOT- and PPy- modified membranes at positive and negative potentials. The diffusion rates are listed in Table 6.3. The results shown were reproducible regardless of the previous oxidation or reduction state of the membrane. In all but one case we observed a substantially increased diffusion rate of tannic acid at the positive potential. This implies that the polymers inside alumina nanopores

Table 6.3. Diffusion rates of tannic acid across polymer-modified and unmodified Anodiscs as a function of applied potential.

Anodisc	diffusion rate, mol/s × 10^{-9}		rate increase factor
	at (-) potential	at (+) potential	
PEDOT:Cl	0.08 ± 0.01	0.3 ± 0.001	3.75
PEDOT:Ts	5.0 ± 0.01	5.0 ± 0.02	1.0
PPy:Cl	0.05 ± 0.002	0.1 ± 0.002	2.0
PPy:Ts	2.0 ± 0.05	6.0 ± 0.01	3.0
unmodified	10 ± 0.10	10 ± 0.01	1.0

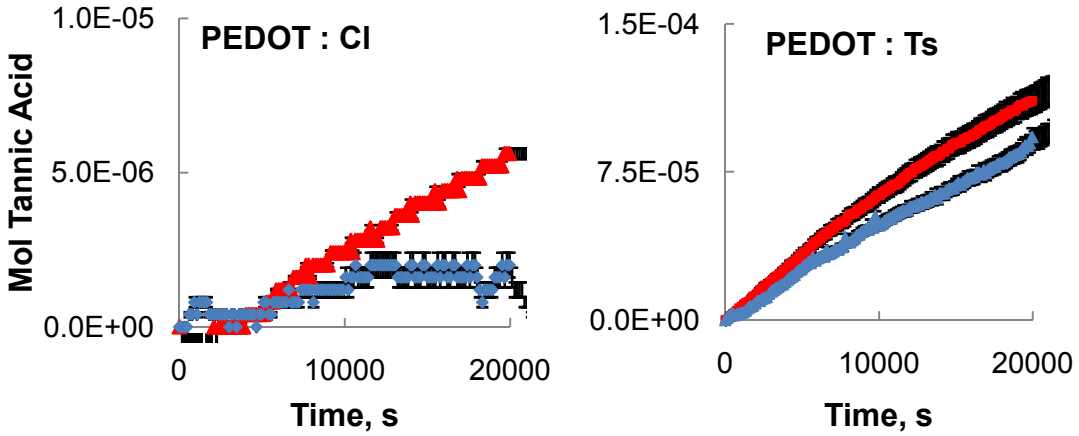

Figure. 6.7. Representative diffusion plots for PEDOT-Anodisc membranes doped with either Cl^- or Ts^- at +0.8 V (red) and -0.8 V (blue) potential applied. Measurements were done in triplicate and similar results were observed for two additional membranes.

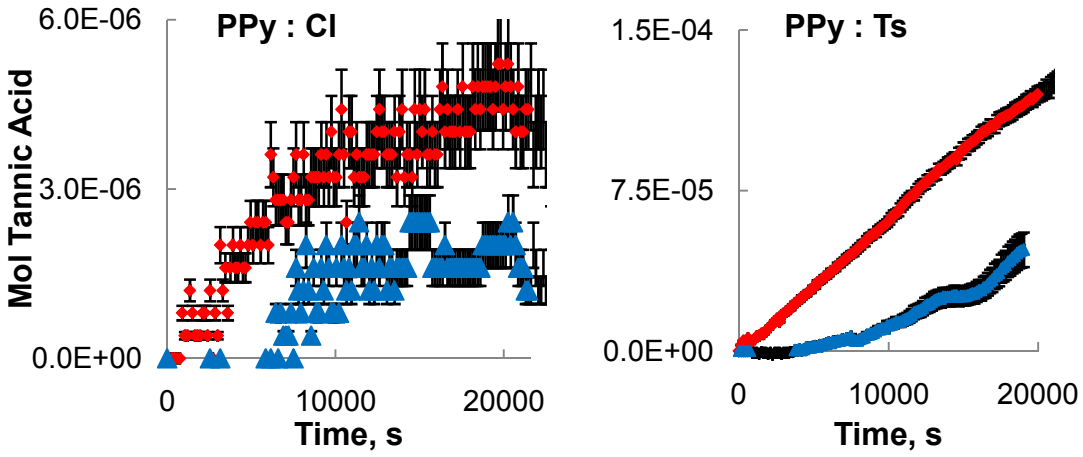

Figure 6.8. Representative diffusion plots for PPy-Anodisc membranes doped with either Cl^- or Ts^- at +1 V (red) and -1 V (blue) potential applied. Measurements were done in triplicate and similar results were observed for two additional membranes.

expand in the reduced state and contract in the oxidized state. When the potential was set at 0 V, intermediate diffusion rates were observed, suggesting that under these conditions the polymers contained a mixture of oxidized and reduced chains.

It has been shown[8] that volume changes in conjugated polymers result from ionic movement into and out of the polymer due to oxidation and reduction. For the films of such polymers, expansion in the reduced state was observed for the polymers doped with large immobile anions in contact with an electrolyte containing small mobile cations. In this case, cations are inserted upon reduction to maintain electroneutrality and thus the polymers expand when a negative potential is applied. However, the polymers utilized in our membranes contain relatively small anions. Thus, we speculate that the observed behavior results from the fact that the polymers are confined inside the nanopores, and the anions cannot freely de-insert upon reduction, which would cause the polymers to shrink when a negative potential is applied, opposite to our observations.

Our results also show that the exact response and diffusion rates are the function of the polymer structure and the dopant used along with polymer coverage inside the nanopores. We observed the highest diffusion rate increase upon oxidation for PEDOT:Cl membranes, but they had a relatively low diffusion rate. The latter can be explained by the high thickness of the polymer inside the nanopores, as measured by SEM and TGA. On the other hand, PPy:Ts membranes showed a similar diffusion rate increase upon oxidation yet maintained the diffusion rate 20 times higher than that of PEDOT:Cl membranes

and only 1.7 times lower than that of unmodified Anodiscs. This results from the smaller polymer thickness inside the nanopores in this case, as shown by SEM and TGA. PPy:Cl membranes showed a smaller, 2-fold increase in diffusion rate upon oxidation, and possessed the slowest diffusion rate due to thicker polymer layer inside the nanopores. Finally, PEDOT:Ts showed almost no change in the diffusion rate upon oxidation, probably caused by the low coverage of the polymer inside the nanopores.

Flux (J, moles sec^{-1} cm^{-2}) through the alumina anodisc membranes is related to the pore diameter (d). We calculated fluxes and their ratios (Table 6.4) using the experimentally found diffusion rates using Equations (6.1) and (6.2), where R_D is the molecular diffusion rate in mol s^{-1}, D is the diffusion rate, ε is the extinction coefficient (9.97 L mol^{-1} cm^{-1}), V is the volume used (0.004 mL), L is the length of the cuvette, and S is surface area of the membrane (0.196 cm^2).

$$R_D = \frac{D}{\varepsilon}\frac{V}{L} \tag{6.1}$$

Table 6.4 Polymer volume change with respect to flux (J).

Anodisc	J_2/J_1	Volume Change (%)
PEDOT:Cl	0.36	22.0
PEDOT:Ts	0.95	1.25
PPy:Cl	0.50	16.0
PPy:Ts	0.33	24.0
unmodified	0.00	0.0

$$J = \frac{R_D}{S} \tag{6.2}$$

According to the Hagen-Poiseuille equation[9] for cylindrical straight pores:

$$J = \frac{d_{pore}^2 \varepsilon}{32\eta\tau} \frac{\Delta P}{h} \tag{6.3}$$

where d_{pore} is the diameter of pores, ε is the porosity of the film, ΔP is the pressure difference, η is the viscosity of water, τ is the tortuosity of the pore, and h is the thickness of the membrane. Although the Anodiscs used have long cylindrical pores (60 μm), we are only interested in the thickness of the polymer layer inside the pores (h_1 in Table 6.1) because the flux is mainly affected by the smaller pores. At a constant ΔP, the ratio of the flux at different electrochemical states is given by:

$$\frac{J_2}{J_1} = \frac{h_1 d_2^4}{h_2 d_1^4} = \frac{h_1 d_2^4}{\left[h_1 + \frac{d_1 - d_2}{2}\right] d_1^4} \tag{6.4}$$

where the subscripts 1 and 2 correspond to the oxidized and reduced states of the polymer inside the pore, respectively, h_1 and d_1 are measured using SEM. The change in the nanopore diameter (d_2, Table 6.1) and volume change between both states can be calculated using Equation 6.4. The volume change calculated for PEDOT:Cl and PEDOT:Ts is 22 and 1.25%, respectively (Table 6.4). We believe that the small change in volume for PEDOT:Ts is the result of its low polymer coverage of the Anodisc pores. The volume change calculated for PPy:Cl and PPy:Ts is 16 and 24%, respectively (Table 6.4), in good

agreement with values reported for the PPy volume change between two oxidation states (0.5-35%).[10]

To confirm that the change in molecular flux was due to the presence of the polymer on the Anodisc, we measured the diffusion rate of tannic acid through unmodified Anodisc. Applying either positive or negative potential to these membranes caused no change in the flux.

Optimization of conductive polymer-modified Anodiscs would involve varying the counter ions used in the hopes of creating both membranes that exhibit higher transport as the polymer is oxidized as shown in the above work, and those where transport is increased as the membrane is reduced. We would also like to study the effect of pore size on the rate of transport with the intent that decreasing the pore size will increase the selectivity, as with each oxidation and reduction the effect of expansion and contraction will be magnified with decreasing pore size.

Conclusion

We have prepared a supported, conductive, polymer-modified anodized alumina nanoporous membranes which exhibit permeability controlled by the applied electric potential. In these membranes, the diffusion of a neutral dye is faster when the polymer is in the oxidized state (positive applied potential) than when they are in the reduced state (negative applied potential) as a result contraction and expansion of the polymer, respectively. These membranes may

be used in applications where controlled molecular transport is needed, such as in drug release and separations devices.

References

1. Bolin, M. H.; Svennersten, K.; Wang, X.; Chronakis, L. S.; Richter-Dahlfors, A.; Jagera, E.; Berggren, M., *Sensors and Actuators B*. **2009,** *142*, 451.

2 . (a) Crawford, G. P.; Steele, L. M.; Ondris-Crawford, R.; Iannacchione, G. S.; Yeager, C. J.; Doanne, J. W.; Finotello, D. *J. Chem. Phys.* **1992**, *96*, 7788-7796. (b) Marchal, D.; Bourdillon, C.; Deme, B. *Langmuir* **2001**, *17*, 8313-8320.

3. Aasmundtveit, K. E.; Samuelsen, E. J.; Pettersson, L. A. A.; Inganäs, O.; Johansson, T.; Feidenh, R.; *Synth. Metals*, **1999,** *101*, 561-564.

4. (a) Syritski, V.; Idla, K.; Opik, A. *Synth. Metals*, **2004**, *144*, 235. (b) Lock, J. P.; Lutkenhaus, J. L; Zacharia, N. S.; Im, S. G.; Hammond, P. T.; Gleason, K. K**.** *Synth. Metals* ,**2007**, *157*, 894. (c) Tonzola, C. J.; Alam ,M. M.: Kaminsky, W.; Jenekhe, S.A. *J. Am. Chem. Soc.* **2003**, *125*, 13548.

5. (a) Syritski, V.; Idla, K.; Opik, A. *Synth. Metals*, **2004**, *144*, 235. (b) Pihel, K.; Walker, D.; Wightman, R. M. Anal. Chem. **1996,** *68*, 2084. (c) Levi, M. D.; Lopez, C.; Vieil, E.; Vorotyntsev, M. A. *Electrochimica Acta*, **1997**, *42*, 757. (d) Otero, T. F.; Tejada, R.; Elola, A. S. *Polymer,* **1987**, *28*, 651.

6. Kozlovskaya, V.; kharlampieva, E.; Drachuk, I.; Cheng, D.; Tsukruk, V. V. *Soft Matter.* **2010**, *6,* 3596-3608.

7. Gaffney, S.; Williams, V.; Flynn, P.; Carlino, R.; Mowry, C.; Dierenfild, E.; Babb, C.; Fan, J.; Tramontano, W. A. *Bios.* **2004,** *75,* 43-52.
8. Jager, E. W. H.; Smela, E.; Inganas, O. *Science*, **2000,** *290*, 1540.

9. (a) Viscosicty and Flow Measurement (Ed: Lyons, K.; Colwell), Intersicience, New York, **1963**. (d) Polymer Processing Fundamentals. Osswald, T. A. Cincinnatti: Hanser/Gardner, **1998**. (c) Wiegmann, R.; Zhang, Y.; Yarin A. *J. Undergrad. Research*, **2010**, *3*, 1-5.

10. (a) Smela, E.; Gadegaard, N. *Adv. Mater*. **1999**, *11*, 953-957. (b) Smela, E. J. *Micromech. Microeng*. **1999**, *9*, 1-18.

CHAPTER 7

SUMMARY

In this thesis, we focused on the preparation and investigation of new stimuli-responsive membrane materials, using nanoporous membranes.

First, the surface of colloidal films was modified with poly(L-alanine), with the goal of creating a temperature and pH responsive membrane. We found that the flux through polymer-modified colloidal films on the surface of 25 μm-diameter Pt microdisk electrodes increased with increasing temperature with a transition temperature of 65-75 ºC, depending on the thickness of the polymer brush. We also observed change in thickness of the polymer brush as pH was changed, with the polymer extending at low pH and contracting at high pH.

Next, we prepared sintered, free-standing, colloidal film membranes (nanofrits) which are modified with poly(L-alanine). The diffusion of a neutral dye molecule through these membranes is slower as pH is decreased, most likely caused by an expansion of the polymer brush in acidic conditions as demonstrated in Chapter 2.

Next, we studied the transport through colloidal film electrodes modified with an oligonucleotide-based binder in response to the binding of a small molecule. The silica surface was modified with a maleimide activator followed by

a cocaine sensing aptamer. We demonstrated that upon binding to cocaine, the molecular flux through the film increases as a result of a conformational change in the aptamer.

This work was followed by preparation of single nanopore electrodes modified with the cocaine-sensing aptamer which mimics a protein channel by selectively controlling molecular transport via small molecule binding.

Finally, we prepared free-standing, electroacitve, nanoporous membranes by vapor phase polymerizing either polypyrrole (PPy) or poly(3,4-ethylene-dioxythiophene) (PEDOT) on the surface of an anodized aluminum oxide Anodisc. These membranes undergo an increase in molecular flux of a dye molecule in their oxidized state compared to their reduced state which is caused by a contraction and swelling, respectively.

Overall, this work describes and demonstrates that we are able to mimic transport through biological channels with the appropriate choice of surface modifiers according to the desired stimulus used to trigger the response. This thesis has illustrated that external stimuli can include temperature, pH, response to small molecule binding, and the application of a positive or negative potential.

Future Directions

Electrically Responsive Nanoporous Membranes

The work outlined in Chapter 6 represents a preliminary study of an electrically-active polymer modified nanopourous membrane. Future work on this project will involve studying the diffusion across free-standing colloidal films

or opal “frits” modified with a conducting polymer, either PPy or PEDOT as a positive, negative, or zero potential is applied. These free-standing colloidal membranes are mechanically robust and possess a large surface area, similar to the Anodiscs used previously. These membranes however, contain the ordered arrays of three-dimensional interconnected pores which have been utilized in Chapters 2 and 3. To prepare such membranes, the silica spheres used to create the colloidal membrane need to be physically bonded together. This is accomplished by sintering, which is a process where the film is heated to a temperature of >1000 °C , causing the silica to flow at the surface and flow, fusing the silica spheres to one another.[1,2,3] We hypothesize that, because of this pore structure, electrically active membranes made from sintered colloidal films will exhibit increased selectivity from those prepared using porous Aluminum oxide membranes previously discussed in Chapter 5.

References

1. Chabanov, A. A.; Jun, Y.; Norris, D. J. *Appl. Phys. Lett.* **2004**, *84*, 3573–3575.

2. Lee, T. V.; Ross, E. E.; Velarde, T. R. C.; Leg, M. A.; Wirth, M. J. *Langmuir*. **2007**, *23*, 8554.

3. Zheng, S.; Ross, E.; Legg, M. A.; Wirth, M. J. *J. Am. Chem. Soc*. **2006**, *128*, 9016.

APPENDIX

L-ALANINE N-CARBOXY ANHYDRIDE

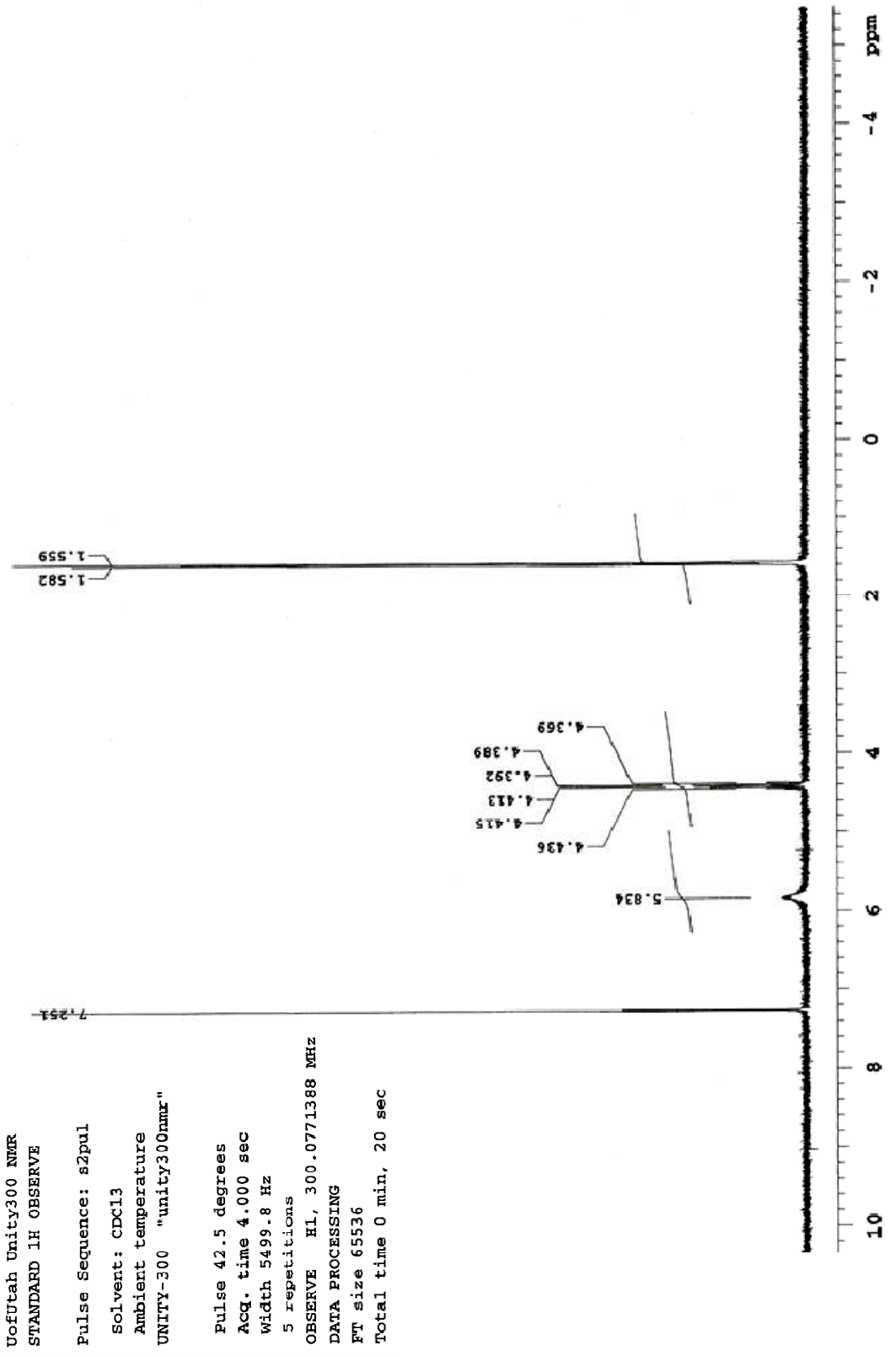
UofUtah Unity300 NMR
STANDARD 1H OBSERVE
Pulse Sequence: s2pul
Solvent: CDCl3
Ambient temperature
UNITY-300 "unity300nmr"
Pulse 42.5 degrees
Acq. time 4.000 sec
Width 5499.8 Hz
5 repetitions
OBSERVE H1, 300.0771388 MHz
DATA PROCESSING
FT size 65536
Total time 0 min, 20 sec
7.254
5.834
4.436
4.415
4.413
4.392
4.389
4.369
1.582
1.559
10
8
6
4
2
0
-2
-4
ppm